

Fabrication of oxide film on AZ91D
magnesium alloy by environmentally friendly
plasma anodization method

March 2020

Department Frontier Materials and Functional Engineering
Graduate School of Engineering
Iwate University

Sung Hyung LEE

DECLARATION OF CO-AUTHORSHIP / PREVIOUS PUBLICATION

This thesis includes 6 original papers that have been previously published in peer reviewed journals and conference proceedings, as follows:

Chapter	Publication title / full citation	status
Chapter III.	1. S.H. Lee, H. Yashiro and S.-Z. Kure-Chu, Fabrication of Plasma Electrolytic Oxidation Coatings on Magnesium AZ91D Casting Alloys, <i>J. Korean Inst. Surf. Eng.</i> , 50(6) (2017) 432-438.	Published
	2. S.H. Lee, H. Yashiro and S.-Z. Kure-Chu, Effect of Power Mode of Plasma Anodization on the Properties of formed Oxide Films on AZ91D Magnesium Alloy. <i>Korean Journal of Materials Research</i> , 28(10) (2018) 544-550.	Published
Chapter IV	1. S.H. Lee, H. Yashiro and S.-Z. Kure-Chu, Electrolyte Temperature Dependence on the Properties of Plasma Anodized Oxide Films Formed on AZ91D Magnesium Alloy. <i>Korean Journal of Materials Research</i> , 29(5) (2019) 288-296.	Published
	2. S.H. Lee, H. Yashiro and S.-Z. Kure-Chu, Effect of sodium hydroxide concentration of Plasma Anodic Oxidation on the properties of oxide film formed on AZ91D Magnesium Alloy, <i>IJARSET volume.6(4)</i> (2019) ISSN: 2350-0328.	Published
Chapter V.	1. Sung-Hyung Lee, Hitoshi Yashiro, Kazuki Aoki, Hidetaka Nanao, Song-Zhu Kure-Chu, Physical Properties of Oxide Films on Mg Alloy Formed by Plasma Anodization. <i>Korean Journal of Materials Research</i> , (11) 2019.	In print
Chapter VI	1. Lee, Sung-Hyung, Hitoshi Yashiro, and Song-Zhu Kure-Chu. "Comparative Evaluation of Surface Treatment Effect of AZ91D Alloy Material." <i>Ijasre</i> 5(5) (2019) DOI: 10.31695/IJASRE.2019.33213.	Published

POSTER / ORAL PRESENTATION

1. Anodize it ! 2017 Conference.
Development of Environment Friendly Plasma Anodizing Method for AZ91D Alloys.
LEE Sung Hyung, Kure-Chu Song-Zhu , Li Xiaopei , Hitoshi Yashiro,
Toulouse, France, 2017 年 07 月
2. The 11th Asian-European International Conference on Plasma Surface Engineering.
Fabrication and Characterization of Plasma Electrolytic Oxidation Coatings on Magnesium Alloys.
Sung-Hvung Lee, Song-Zhu Kure-Chu, Yashiro Hitoshi,
JEJU, SOUTH KOREA, 2017 年 9 月
3. 第 34 回金属のアノード酸化皮膜の機能化部会 (ARS) 松島コンファレンス
Fabrication and Characterization of Plasma Electrolytic Oxidation Coatings on AZ91D Alloys.
Sung-Hvung Lee, Hitoshi Yashiro, Song-Zhu Kure-Chu.
松島, JAPAN 2017 年 10 月.
4. Korean Institute of Surface Engineering Conference.
Fabrication and Characterization of Plasma Electrolytic Oxidation Coatings on Magnesium Alloys.
SH Lee, H Yashiro, SZ Kure-Chu.
GYUNG JU, SOUTH KOREA 2018 年 11 月
5. Effect of electrolyte condition on the characteristics of oxide film for AZ91D magnesium alloy formed by plasma anodization.
The 3rd International Symposium on Anodizing Science and Technology (AST2019).
Sung-Hvung Lee, Song-Zhu Kure-Chu, Hitoshi Yashiro,
Awaji Island, Hyogo, Japan. 2019 年 06 月
6. 化学系学協会東北大会/Joint Meeting of the Tohoku Area Chemistry Societies.
Electrolyte Temperature Dependence of the Properties of Plasma Anodized Oxide Films Formed on Magnesium Alloy.
Sung-Hvung Lee, Hitoshi Yashiro, Song-Zhu Kure-Chu,
山形大学, Japan 2019 年 09 月

PATENT

1. 黒色酸化被膜を備えるマグネシウム鋳造合金とアルミ鋳造合金その製造方法,
2018-041892, PCT/JP2018/042730, Sung-Hvung Lee

ABSTRACT

The use of magnesium, a common material on the earth, is gradually increasing because of growing demand for light material in mobile phones, auto mobiles aircraft, etc. However, magnesium is the most chemically active among the commercial structural metals. Its standard electrode potential is as low as - 2.363 V vs. SHE, and without surface treatment, it generally undergoes corrosion very quickly in air or aqueous solutions. Therefore, in order to put magnesium products into wide practical use, the surface must be treated chemically, electrochemically, or physically to improve the corrosion resistance. In this study, a relatively new technique of plasma anodization was introduced to improve the corrosion resistance of magnesium alloys by forming a dense oxide film on the surface. Among several kinds of magnesium alloys, AZ91D is the most widely used die cast alloy because it has an excellent combination of mechanical properties and castability. However, AZ91D requires an advanced plasma anodizing process because a large number of defects can be generated during anodization. But no systematic study of plasma anodization of AZ91D has been reported so far.

Chapter 1 describes the background of this study, in which the industrial importance of magnesium alloy is emphasized. Although magnesium alloy is an attractive material because of its extremely low density, its high chemical activity hinders it from industrial application without surface treatment. In this chapter, conventional surface treatment methods as well as latest plasma anodizing in literature are reviewed.

Chapter 2 describes the setting up of plasma anodizing equipment and experimental procedures. The electrolyte for plasma anodization contains sodium aluminate, sodium hydroxide, and sodium silicate but no chromate.

Abstract

Chapter 3 examines the effect of power mode on the properties of oxide film formed by plasma anodizing treatment on AZ91D magnesium alloy and the power mode is optimized in respect of corrosion resistance. In the DC plasma anodization mode, the thickness of the electrolytic oxide film of the AZ91D alloy was uneven. In the pulse mode, the thickness was relatively uniform with formation of a three-layer structure. The pulse mode caused less roughness, uniform thickness and improved corrosion resistance. The change in power mode from DC to pulse decreased the surface roughness and increased the corrosion resistance.

Chapter 4 examines the corrosion resistance of plasma anodized AZ91D magnesium alloy together with the change in surface morphology and chemical composition of the oxide films as functions of electrolyte temperature and NaOH concentration. The higher electrolyte temperature resulted in the lower surface roughness, the smaller oxide film thickness, and the better corrosion resistance. As the concentration of NaOH increased, the thickness and the surface roughness (R_a) of the oxide layer decreased and corrosion resistance increased.

Chapter 5 describes the physical properties of oxide films formed on AZ91D magnesium alloy by plasma anodizing treatment in the electrolyte at different temperature, i.e. breakdown voltage, heat conducting property, and wear resistance. The higher the electrolyte temperature for the formation of oxide films by the plasma anodization, the lower the breakdown voltage, probably because the films formed at higher temperatures were thinner and denser. The friction test against steel ball indicated that the wear scar became narrower for the films formed at higher temperatures because the films became harder. The thinner and denser nature of the oxide film formed at higher temperatures would be also advantageous for heat transfer in use as a heat sink. A laser flash test showed faster heat transfer for AZ91D with plasma anodized oxide layer formed at higher temperatures.

Abstract

Chapter 6 describes the result of comparative examination of surface treatment methods of AZ91D alloy including non-chromate, anodization and plasma anodization in terms of physical and chemical properties of the oxide films. The least thermal barrier of the formed layer is recognized in non-chromate, and the breakdown voltage and Vickers hardness are the highest in the case of plasma anodization. In the salt spray test, the corrosion resistance rating number was lowest for the non-chromate test, middle for the anodizing test, and the highest for the plasma anodizing. Thus, the plasma anodization treatment has a remarkable advantage over conventional process.

Chapter 7 summarizes the main conclusions drawn from this study and provides suggestions for further studies.

Thus, this study has developed a surface treatment method for magnesium alloy of AZ91D in an environmentally friendly manner using reagents with less environmental load.

LIST OF TABLES

Chapter 2

Table 2-1. Chemical composition of the AZ91D Mg alloy cast (mass %).

Table 2-2. Friction and wear testing conditions.

Chapter 6

Table 6-1. Comparison of surface treatment processes of AZ91D alloy materials.

Table 6-2. Comparison of characteristics of surface treatment process of AZ91D alloy materials.

LIST OF FIGURES

Chapter 2

Figure 2-1. Pretreatment of AZ91D magnesium alloy for plasma anodization.

Figure 2-2. Experiment apparatus for plasma anodizing test of magnesium alloy.

Figure 2-3. Schematic of the pulsed unipolar output of a plasma anodizing power supply.

Chapter 3

Figure 3-1. Cross-sectional view and EDS mapping of AZ91D after plasma anodization using (a) DC and (b) pulse at 150 V.

Figure 3-2. XRD patterns of AZ91D (a) before and (b) after plasma anodizing at (a) AZ91D (b) 150 V.

Figure 3-3. Surface morphologies of AZ91D after plasma anodizing using DC (a) and pulse (b) at (a, b) 50 V, (a-1, b-1) 100 V, (a-2, b-2) 150 V and (a-3, b-3) 200 V.

Figure 3-4. Cross sections of AZ91D after plasma anodizing using DC (a) and pulse (b) at (a, b) 50 V, (a-1, b-1) 100 V, (a-2, b-2) 150 V and (a-3, b-3) 200 V.

Figure 3-5. Digital microscope surface photographs (1000× magnification) of AZ91D after plasma anodizing using DC (a) and pulse (b) at (a, b) 50 V, (a-1, b-1) 100 V, (a-2, b-2) 150 V and (a-3, b-3) 200 V.

Figure 3-6. Effect of voltage on the surface roughness of the oxide film on the AZ91D surface after plasma anodization. DC (a) and pulse (b).

Figure 3-7. Effect of applied DC and pulse voltage for plasma anodizing on the corrosion resistance of AZ91D as evaluated by EIS in a 3 mol dm⁻³ NaCl solution at 25 ° C.

Figure 3-8. Effect of DC and pulse voltage for plasma anodizing of AZ91D on the corrosion behavior by 72 hours salt spray test.

Figure 3-9. Cross-sectional micrograph of the corrosion site of pulse plasma anodized AZ91D at 150 V after the salt spray test.

List of figures

Figure 3-10. Surface micrograph and EDS analysis data for the pulse plasma anodized material at 150 V after the salt spray test.

Figure 3- 11. Cross sectional view of AZ91D after plasma anodizing using pulse for at 150 V, 10 min.

Figure 3-12. Surface morphologies of AZ91D before (a) and after pulse plasma anodizing for 30 min under (b) voltage control of 150 V and (c) current control of 10 A dm^{-2} .

Figure 3-13. The structure of oxide film formed on AZ91D by the pulse plasma anodizing for 10 min under current control of 10 A dm^{-2} .

Figure 3-14. Surface roughness of AZ91D after pulsed plasma anodization for 10 min: (a) Raw material (b) Voltage control 150 V (c) Current control 10 A dm^{-2} .

Figure 3-15. Anodic polarization curves of AZ91D in a 3.5 wt.% NaCl solution at 25 ° C (a) raw material, (b) plasma anodized under current control of 10 A dm^{-2} , (c) plasma anodized under voltage control of 150 V.

Figure 3-16. Surface images of specimens after 72 hours salt spray test.

Figure 3-17. EDS elemental maps of the plasma anodizing films formed on AZ91D Mg alloy at 150 V for 30 min.

Chapter 4

Figure 4-1. Effect of electrolyte temperature on the variation of current density in different stages of plasma anodization.

Figure 4-2. Digital microscope surface photographs of plasma anodized AZ91D under the electrolyte temperatures of (a) 10 °C, (b) 20 °C, (c) 30 °C, (d) 40 °C and (e) 50°C.

Figure 4-3. Effect of electrolyte temperature on the surface roughness of the AZ91D after plasma anodization.

Figure 4-4. Surface morphologies of the AZ91D after pulse plasma anodization at (a) 10 °C and (b) 50 °C.

Figure 4-5. Cross-sectional view and EDS mapping of the AZ91D after plasma anodization at (a) 10 °C and (b) 50°C.

List of figures

Figure 4-6. Effect of electrolyte temperature on the thickness of oxide film formed by plasma anodization of AZ91D.

Figure 4-7. Effect of electrolyte temperature on the composition of oxide film formed by plasma anodization of AZ91D.

Figure 4-8. Effect of electrolyte temperature for plasma anodization on the corrosion resistance of the treated AZ91D. (Corrosion test solution: 3 mol dm^{-3} NaCl, temperature: $25 \text{ }^{\circ}\text{C}$).

Figure 4-9. Effect of electrolyte temperature for plasma anodization of AZ91D on the surface images after the salt spray test (72 h).

Figure 4-10. Cross-sectional micrographs of the corrosion site of the AZ91D after the salt spray test for 72 h. The oxide layer was formed by the plasma anodization for 15 min with electrolyte temperature of (a) $10 \text{ }^{\circ}\text{C}$ and (b) 50°C .

Figure 4-11. Surface micrographs of the corrosion area and EDS component analyses of the AZ91D after the salt spray test for 72 h. The specimens were plasma anodized with electrolyte temperature of (a) $10 \text{ }^{\circ}\text{C}$ and (b) 50°C .

Figure 4-12. Effect of NaOH concentration on the variation of current density in different stages of plasma anodization at $50 \text{ }^{\circ}\text{C}$.

Figure 4-13. Digital microscope surface photographs of AZ91D plasma-anodized in electrolytes with NaOH concentrations of (a) 0.06 M, (b) 0.13 M, (c) 0.25 M.

Figure 4-14. Surface roughness of the oxide film formed on AZ91D by the plasma anodization in electrolytes with NaOH concentrations of (a) 0.06 M, (b) 0.13 M, (c) 0.25 M.

Figure 4-15. Surface morphologies of AZ91D after plasma anodization in electrolytes with NaOH concentration of (a) 0.06 M, (b) 0.13 M, (c) 0.25 M.

Figure 4-16. Thickness of oxide films formed on AZ91D by plasma anodization in electrolytes with NaOH concentrations of (a) 0.06 M, (b) 0.13 M, (c) 0.25 M.

Figure 4-17. Cross-sectional views of AZ91D after plasma anodization in electrolytes with NaOH concentrations of (a) 0.06 M, (b) 0.13 M, (c) 0.25 M.

Figure 4-18. Cross sectional views of AZ91D after plasma anodizing in electrolytes with NaOH concentrations of (a) 0.06 M, (b) 0.13 M, (c) 0.25 M.

Figure 4-19. Effect of NaOH concentration for plasma anodization on the corrosion resistance of the treated AZ91D (Corrosion test solution: 3 mol dm^{-3} NaCl, temperature: $25 \text{ }^{\circ}\text{C}$).

List of figures

Figure 4-20. Surface images and RN values after the salt spray test (72 h) for the AZ91D plasma anodized in electrolytes with NaOH concentrations of (a) 0.06 M, (b) 0.13 M, (c) 0.25 M.

Figure 4-21. Surface micrograph of the corrosion area of AZ91 and EDS component analysis after the salt spray test (72 h) for the AZ91D plasma-anodized in electrolytes with NaOH concentration of (a) 0.06 M, (b) 0.13 M, (c) 0.25 M.

Chapter 5

Figure 5-1. Surface and cross-section morphologies and EDS element mapping of the AZ91D after plasma anodization at (a) 20 °C, (b) 30 °C, (c) 40 °C and (d) 50°C.

Figure 5-2. Effect of electrolyte temperature on the breakdown voltage of the AZ91D after plasma anodization.

Figure 5-3. Thermal diffusion measurement by laser flash method on AZ91D magnesium alloy material.

Figure 5-4. The half time ($t_{1/2}$) determined from the laser flash method for the AZ91D after plasma anodization in the electrolyte of different temperatures.

Figure 5-5. Effect of electrolyte temperature on the Vickers hardness of the AZ91D after plasma anodization.

Figure 5-6. Digital microscope surface photograph of AZ91D magnesium alloy after the surface friction test under the applied load of (a) 50 N, (b) 10 N and (c) 1 N. Specimens were plasma anodized by pulsed voltage of 150 V for 15 min at 50 °C.

Figure 5-7. Digital microscope surface photographs of AZ91D and SUJ2 steel ball after surface friction test after plasma anodization of AZ91D at (a) 20 °C, (b) 30 °C, (c) 40 °C and (d) 50 °C.

Figure 5-8. Surface comparison of AZ91D before (left) and after (right) the surface friction test. Specimens were plasma anodized under the electrolyte temperature of (a) 20 °C and (b) 50 °C.

Figure 5-9. Comparison of wear diameter of SUJ2 steel balls after friction test with AZ91D plasma anodized at different electrolyte temperatures.

Chapter 6

Figure 6-1. Typical variation of current density showing different stages of AZ91D surface treatment.

Figure 6-2. Surface morphologies and composition of AZ91D alloy materials after Non-chromate (b) Anodizing (c) Plasma anodizing.

Figure 6-3. Cross sections of AZ91D alloy materials after Non-chromate (b) Anodizing (c) Plasma anodizing.

Figure 6-4. Effect of AZ91D alloy materials surface treatment method on the $t_{1/2}$ value in the laser flash test.

Figure 6-5. Effect of AZ91D alloy materials surface treatment method on breakdown voltage.

Figure 6-6. Effect of AZ91D alloy materials surface treatment method on the Vickers hardness.

Figure 6-7. Effect of surface treatment method on the corrosion resistance of the treated AZ91D alloy materials (solution: 3 mol dm⁻³ NaCl, temperature: 25 °C).

Figure 6-8. Surface images of the AZ91D alloy materials surface treatment method after the salt spray test (72 h).

Contents

Chapter I. Introduction	1
1.1 Background	1
1.2 Literature overview	2
1.2.1 General feature of magnesium and its alloys	2
1.2.2 Corrosion properties of magnesium alloys	3
1.2.3 Conventional surface treatment of magnesium alloys	4
1.2.3.1 Chromate conversion coatings	4
1.2.3.2 Phosphate-permanganate conversion coatings	7
1.2.3.3 Fluorozirconate conversion coatings	9
1.2.3.4 Stannate treatments	10
1.2.4 Anodization	11
1.2.5 Plasma anodization	12
1.3 Research objective	14
1.4 Overview of thesis	14
1.5 References	15
Chapter II. Experimental	19
2.1 Specimen	19
2.2 Apparatus	19
2.3 Electrolyte	20
2.4 Characterization	20
2.5 Corrosion test	20
2.6 Wear test	21
2.7 Conventional anodizing	21
2.8 Non-chromate treatment	21
2.9 References	25
Chapter III. Effect of power mode of plasma anodization on the properties of formed oxide films on AZ91D magnesium alloy.....	26
3.1 Introduction	26

Contents

3.2	Results and Discussion	27
3.2.1	Evaluation of oxide films formed under DC and pulse voltage mode conditions	27
3.2.2	Evaluation of oxide films formed under pulse current and pulse voltage mode conditions	40
3.3	Conclusion.....	42
3.4	References	48
Chapter IV. Effect of electrolyte parameters on the corrosion resistance of plasma anodized AZ91D magnesium alloy.....		49
4.1	Introduction	49
4.2	Results and Discussion	50
4.2.1	Effect of electrolyte temperature on the characteristics of oxide film for AZ91D magnesium alloy formed by plasma anodization	50
4.2.2	Effect of sodium hydroxide concentration of Plasma Anodic Oxidation on the properties of oxide film formed on AZ91D Magnesium Alloy	65
4.3	Conclusion.....	68
4.4	References	78
Chapter V. Physical properties of oxide films on AZ91D magnesium alloy formed by plasma anodization		79
5.1	Introduction	79
5.2	Results and Discussion	80
5.2.1	Film morphology	80
5.2.2	Dielectric breakdown voltage	80
5.2.3	Heat conducting property	80
5.2.4	Tribological property	82
5.3	Conclusion.....	84
5.4	References	94
Chapter VI. Comparative evaluation of the surface treatment effect of AZ91D alloy material		95
6.1	Introduction	95
6.2	Results and Discussion	96

Contents

6.3	Conclusion	99
6.4	References	109
Chapter VII. General Conclusion		110

Chapter I. Introduction

1.1 Background

Among the commercial metallic structural materials, magnesium alloys have the lowest density and an excellent strength/weight ratio. Therefore, they are being used extensively in lightweight engineering applications to improve fuel efficiency and thereby to satisfy economic and environmental requirements [REF 1,2]. Their use is also expanding to the field of mobile terminals lately. Despite the attractive properties, the poor corrosion resistance of magnesium alloys impedes their use in wide applications, especially in corrosive environments [REF 3,4]. Therefore, many surface treatment techniques such as electrochemical plating, conversion coating, gas-phase deposition, and anodization and plasma anodizing processes have been developed to improve the resistance against corrosion and wear. [REF 5].

The creation of a chemical-conversion surface layer on magnesium and magnesium alloys is extremely important in order for improving corrosion resistance and as a pretreatment for painting. Many methods have been proposed for the chemical conversion processing of magnesium and its alloys, and each has different layer characteristics. In practice, manufacturers used to use baths containing chromium(VI) oxide or dichromate. However, chromium has been recognized as being harmful to human health with risk of ulceration and even carcinogenicity. The volume of chromium emitted into the atmosphere from factories has been strictly restricted in the interests of protecting work environments and for pollution control. In response to this movement, the chemical conversion layer containing manganese phosphate or stannate have been proposed for magnesium and its alloys. However, chromium-free surface treatment methods were not satisfactory in that they had low corrosion resistance, complicated manufacturing processes, low productivity, and wastewater problems. Plasma anodization is a new surface treatment method to form oxide layers on magnesium alloys in a suitable electrolyte, owing to its ability to produce a relatively thick, dense, and hard film to improve surface properties [REF 6]. In general, the plasma anodizing process has been used to improve metal surfaces such as Mg, Al, Ti, and Zr in the anodic regime, but can

also be used in the cathodic regime, and it combines cleaning and coating of metals [REF 7,8]. This process primarily involves the anodic polarization of magnesium alloys in aqueous electrolyte solutions and has advantages that it improves corrosion resistance significantly and does not produce strong odors. In addition, it involves simple manufacturing and a heavy metal-free environment. An important feature of the plasma anodizing process is a plasma discharge that occurs at the metal/electrolyte interface when the applied voltage exceeds a certain critical breakdown value. The constituents of the surface oxide are from the substrate and the anodic complexes from the electrolyte.

1.2 Literature overview

1.2.1 General feature of magnesium and its alloys

Magnesium is the 8th most abundant element on the earth comprising approximately 1.93% of the mass of the earth's crust and 0.13% of the mass of the oceans [REF 9]. It also has some advantageous properties that make it an excellent choice for a number of applications. Magnesium has a high strength-to-weight ratio with a density that is only 2/3 that of aluminum and 1/4 that of iron. Magnesium also has high thermal conductivity, high dimensional stability, good electromagnetic shielding characteristics, high damping characteristics, and good machinability; further, it is easily recycled [REF 9-13]. These properties make it valuable in a number of applications, including in automobile and computer parts, aerospace components, mobile phones, sporting goods, handheld tools, and household equipment. Magnesium has even been suggested for use as an implant metal due to its low weight and inherent biocompatibility [REF 14]. Due to limited fossil fuel storage and environmental problems associated with fuel emission products, there is a push in the automotive industry to make cars lighter in order to decrease fuel consumption. The use of magnesium alloys can significantly decrease the weight of automobiles without sacrificing structural strength. Unfortunately, magnesium has a number of undesirable properties including poor corrosion and wear resistance, poor creep resistance, and high chemical reactivity that have hindered its widespread use in many applications. One of the main challenges in the use of magnesium, particularly for outdoor applications, is its poor corrosion resistance. Magnesium and its alloys are extremely susceptible to galvanic corrosion, which can cause severe pitting in the metal, resulting in decreased mechanical

stability and an unattractive appearance. Corrosion can be minimized by the use of high purity alloys that maintain heavy metal impurities such as iron, nickel and copper below a threshold value. The elimination of bad design, flux inclusions, surface contamination, galvanic couples and inadequate or incorrectly applied surface protection schemes can also significantly decrease the corrosion rate of magnesium alloys in service [REF 15].

1.2.2 Corrosion properties of magnesium alloys

Magnesium usage has been limited due to the poor corrosion properties. Corrosion resistance is especially poor when a magnesium alloy contains specific metallic impurities or when the magnesium alloy is exposed to aggressive electrolyte species such as Cl^- ions. However, the oxide film on magnesium can usually offer considerable protection to magnesium susceptible to atmospheric corrosion in rural, industrial, and marine environments. As a result, the atmospheric corrosion resistance of magnesium alloys is better than that of mild steel, even for exposure to marine atmospheres [REF 16,17]. Generally, the corrosion rate of magnesium alloys lies between that of aluminum and mild steel. In some cases, magnesium may have better resistance than some aluminum alloys. Nevertheless, magnesium is also susceptible to corrosion in chloride-containing solutions in practical applications. Die cast alloy AZ91 can give a salt spray corrosion performance that ranges from good to excellent and is superior to that of steel and aluminum [REF 18]. The high purity alloy, for example, AZ91E, has salt water corrosion resistance 10–100 times better than the standard purity alloy, and equal to or better than that of mild steel and the die cast aluminum alloy 380 [REF 19,20]. In most cases, the corrosion of magnesium and magnesium alloys initiates from localized corrosion, but sometimes the localized corrosion is shallow and widespread. The corrosion morphology of magnesium and magnesium alloys depends on the alloy chemistry and environmental conditions. For example, atmospheric corrosion is uniform in typical industrial atmospheres, whereas corrosion is usually localized in immersed conditions. Turnold et al. [REF 18] found that the corrosion of commercial-purity magnesium was usually transgranular, while the corrosion of alloys was more uniform. There are two main reasons for the poor corrosion resistance of many magnesium alloys [REF 10]. First, there is internal galvanic corrosion caused by second phases or impurities [REF 19]. Second, the quasi-passive hydroxide film on magnesium is much less stable than the passive films that form on metals such as aluminum and stainless steels. This quasi-passivity provides only

poor pitting resistance for magnesium and magnesium alloys. The early magnesium alloys suffered rapid attack in moist conditions due mainly to the presence of impurities, notably iron, nickel, and copper. These impurities or their compounds act as miniature cathodes in the presence of a corroding medium. They form micro-cells with the anodic magnesium matrix. High-purity alloys are a relatively recent development. In high-purity alloys, the concentrations of these impurities are controlled to below critical concentrations, and, as a consequence, high purity alloys exhibit a resistance to salt water markedly better than that of alloys of normal purity.

1.2.3 Conventional surface treatment of magnesium alloys

Conversion coatings are produced by chemical or electrochemical treatments of a metal surface to produce a superficial layer of substrate metal oxides, chromates, phosphates or other compounds that are chemically bonded to the surface [REF 24-26]. On magnesium, these coatings are typically used to provide corrosion protection and good paint-base properties to the metal [REF 25,26]. Conversion coatings protect the substrate from corrosion by acting as an insulating barrier of low solubility between the metal surface and the environment [REF 20-23] and/or by containing corrosion-inhibiting compounds. There are a number of different types of conversion coatings, including those formed by chromate, phosphate/permanganate and fluorozirconate treatments. As with all surface treatments, cleaning and pretreatment of the sample is crucial to obtaining a good conversion coating.

One of the main disadvantages of conversion coatings is the toxicity of the treatment solutions. The conventional conversion coatings are based on chromium compounds that have been shown to be highly toxic carcinogens [REF 26]. The development of an environmentally friendly process is a necessity due to the more stringent environmental protection laws currently in effect or being proposed. The coating of alloys also represents a significant challenge due to their non-uniform surface composition. The conversion coating must therefore be capable of coating all the elements present in the alloy uniformly [REF 26].

1.2.3.1 Chromate conversion coatings

Chromate conversion coatings can be used as pretreatments prior to a final sealing process or as 'post-treatments' after a plating process to improve corrosion resistance, paint or adhesive bonding properties, or provide a decorative finish [REF 26]. There are a few general rules that should be followed when applying a conversion coating, these include [REF 20]

1. Substrates with fine grained microstructure respond best to chromating,
2. Co-deposition of other metals is detrimental to the coating process,
3. Proper cleaning and pretreatment of the surface is necessary to ensure optimum coating,
4. After chromating, the substrate should be properly rinsed to remove any residual acid or base which could react with the coating,

The coating should be air dried at relatively low temperature (70 °C) for a maximum of 10 min. The mechanism of formation of chromate conversion coatings [REF 28-32] is believed to be the dissolution of the metal surface, with a corresponding reduction of water or oxygen to form hydroxyl ions, which causes an increase in pH at the liquid–metal interface. This in turn causes precipitation of a thin complex of chromium–metal gel on the surface that contains both hexavalent and trivalent chromium compounds [REF 27]. Pure chromic acid solutions are not used to form conversion coatings because the deposition rate is too slow [REF 32]. Other anions in solution that can act as a catalyst for deposition are required [REF 33]; some of these include acetate, formate, sulfate, chloride, fluoride, nitrate, phosphate and sulfamate ions [REF 34]. The pH of the solution is the most important factor in controlling the formation of chromate films [REF 34]. The as-deposited gel is very soft but hardens upon drying to become hydrophobic, less soluble, and more abrasion resistant [REF 34]. These coatings provide corrosion protection by presenting a non-reactive barrier to the environment, through their self-healing properties and by the inhibiting effect of Cr (VI) that is slowly leachable in contact with moisture [REF 28,34]. The hexavalent chromium is reduced during corrosion to form an insoluble trivalent chromium species that terminates the oxidative attack [REF 32]. The protection afforded by the coating is proportional to the coating thickness [REF 34]. In order to maintain its protective properties, the coating cannot be subjected to high temperatures (>68 °C) since this would decrease the coating thickness and eradicate the self-healing ability of the coating [REF 28,34]. The coating retains its self-healing characteristics as long as it remains in its hydrated form. The stability of the films at higher

temperature can be improved by sealing or painting on top of the conversion layer [REF 28,34]. Chromate conversion coatings on magnesium have been shown to have the following structure: a dense layer of Mg(II) and Cr(III) hydroxides covers the magnesium surface with a porous overlayer of Cr(OH)₃. This over layer results from selective dissolution of Mg(OH)₂ from the dense layer. Increasing the thickness of the dense layer has been shown to inhibit the corrosion of magnesium in chloride solutions [REF 35]. It has been suggested [REF 36] that the rate of formation of the coating is controlled by the diffusion of Cr(VI) through the deposited coating. The protective properties of the coating can be increased by reducing the porosity of the over layer through the precipitation of coating components that are insoluble in alkali solutions [REF 36]. Simaranov et al. [REF 36] also suggest that the deposition rate of chromate conversion coatings on pure magnesium can be increased by introducing copper ions into the bath. These metal ions are inert to magnesium but precipitate on the deposited Cr species and act as cathodic sites to enhance deposition. These coatings have been shown to provide good corrosion protection for magnesium and its alloys in mild service conditions. However, due to the significant environmental hazards associated with the use of chromate compounds, there is a push to find alternative coating processes. The application of chromate conversion coatings for magnesium is discussed below. Chromate conversion coatings have been shown to significantly reduce corrosion on AZ31C, AZ63A and AZ91C magnesium alloys in salt spray tests [REF 31]. However, the coatings are thin and are generally not suitable as a final coating for outdoor use. A study on the composition and protective properties of chromate conversion coatings on magnesium [REF 35] has demonstrated that the protective properties of these coatings are due to the presence of Cr(OH)₃ in their structure. An increase in the amount of Cr(OH)₃ in the dense layer through an increase in chromate concentration in the bath leads to improved protective properties of the coating. The addition of zinc cations to the chromating solution have also been shown to improve the properties of the chromate coatings.

The structures of chromate conversion coatings formed using the commercial processes, MX1, MX3 and MX7 on AZ91D have been reported [REF 37]. The MX1 process was found to produce a magnesium chromate film while MX7 was shown to produce magnesium phosphate at the surface. The MX3 process produced an amorphous chromium oxide film containing some oxides and fluorides of magnesium and aluminum. Corrosion studies showed that conversion films with a significant amount of oxygen and chrome, such as MX3, gave the best corrosion protection. Another study [REF 37] investigated the

structure of surface films formed by the Dow 7 commercial conversion coating process on die cast AZ91D and pure magnesium. On AZ91D, the structure of the film was granular, while on pure magnesium a porous cell structure was observed which was separated from the substrate by a thin barrier layer at the interface. This structure resembles the structure of films formed by anodizing. The films produced in both cases were composed of MgF_2 , $MgO_x(OH)_y$, $NaMgF_3$, Cr_2O_3 and NH_4^+ . Additional compounds such as $AlO_x(OH)_y$, $FeO_x(OH)_y$ and $Mn(IV)$ were also found in the film formed on AZ91D. A chromate conversion coating has been developed for magnesium–lithium alloys [REF 36]. The coatings were found to be around 8-11 μm in thickness with excellent adhesion, even under humidity and thermal cycling tests. The optical and paint-base properties of the coating were also unaffected by humidity and thermal cycling tests. A number of patents that discuss chromate conversion coatings are also available for review [REF 38,39]. These are all based on the technology discussed above with various coating baths. One novel variation involves the deposition of a chromium–silicon coating from a chromite bath that contains a soluble silicate [REF 39]. The coating produced is porous which renders it suitable for further processing such as painting. However, the corrosion resistance of the initial conversion coating is poor.

1.2.3.2 Phosphate-permanganate conversion coatings

Phosphate–permanganate treatments are being explored as an alternative to conventional chromate conversion coatings [REF 40]. These treatments are more environmentally friendly and have been shown to have corrosion resistance comparable to chromate treatments. A systematic study on phosphate–permanganate treatment of AZ91D and WE43A alloys [REF 40] using a bath containing potassium permanganate and sodium phosphate has shown that homogeneous, non-powdery and uniform coatings can be achieved. The phosphate concentration and pH of the conversion bath were found to have the most significant effect on the quality of the final coating. The corrosion resistance observed was comparable to chromate coatings. For AZ91 alloys a filiform corrosion morphology with phosphate–permanganate was observed which minimized the depth of pitting. For WE43, the corrosion behavior was the same for both chromate and phosphate–permanganate coatings. Another study investigated the use of phosphate–permanganate treatments for the conversion coating of AM60B die cast magnesium alloys [REF 41]. After appropriate pretreatment, the samples were treated with a phosphate permanganate process and E-coated (cathodic epoxy

electrocoated). It was shown that the treatment provides good paint adhesion. The most important factor in producing the best quality conversion coatings was found to be the control of the pH.

Another study with the same magnesium alloy [REF 42] demonstrated that with proper sample pretreatment, i.e. sufficient cleaning and acid pickling, magnesium samples with good paint-base performance could be achieved with a phosphate–permanganate bath. The permanganate is said to contribute manganese to the coating and acts as an accelerator without depositing metallic manganese on the magnesium surface. The coatings were shown to have a good corrosion resistance and paint base performance, and were composed of agglomerates of well-formed crystalline phosphate compound particles.

In a subsequent study [REF 43], the authors tested this treatment on the AZ91D magnesium alloy. They determined that the phosphate–permanganate treatment can be operated over a wide range of conditions without affecting the corrosion inhibition of the coating produced when pretreatment included either grinding or phosphoric acid pickling. Samples that had been alkaline cleaned showed extremely high corrosion rates perhaps due to non-uniform deoxidation of the magnesium surface. It was found that samples pretreated with a phosphoric acid pickle and then phosphate permanganate gave excellent corrosion resistance and paint base properties. Another study [REF 40] examined the possibility of producing manganese type conversion coatings on the surface of the magnesium alloy AZ91D. After cleaning and surface activation, the samples were immersed in a solution containing potassium permanganate and either nitric or hydrofluoric acid. The coating formed in the HF-containing bath was very thin and was shown to be amorphous in structure. It contained magnesium fluoride, hydroxides and manganese oxides. The coatings formed in the bath containing nitric acid were substantially thicker and crystalline manganese oxide was observed. The corrosion resistance of these coatings was equivalent to the protection afforded by a standard chromate treatment.

A number of phosphate-based conversion coatings can be found in the patent literature. One of these involves treating a magnesium-based sample with an aqueous bath containing diammonium hydrogen phosphate [REF 44]. The inventors suggest that this results in the formation of magnesium phosphate, its hydrate and magnesium hydrogen phosphate on the surface without any prior pretreatment. This coating was found to have good adhesive properties for subsequent powder coatings. Another patent [REF 45]

recommends treatment of magnesium with a solution containing sodium ions, condensed phosphate ions, and borate ions as a treatment prior to powder coating.

Magnesium phosphate conversion coatings have also been shown to protect the internal surface of a magnesium-based combustion engine pistons [REF 46]. A thin layer of magnesium phosphate is formed on the surface of the piston upon dipping in a solution of iron phosphate. This layer then acts as an adhesive for the combustion products of fuel and lubricants in the engine, which, in turn, form a protective coating on the piston surface.

Conversion coatings composed of zinc phosphate have also been shown to have adhesion and corrosion resistance comparable to coatings formed by conventional anodic oxidation or chromating [REF 47,48]. These films are formed in a solution containing zinc, manganese, phosphate, and hydrofluoric acid.

Paint-adherent and corrosion-resistant coatings composed of magnesium phosphate and magnesium fluoride have also been developed [REF 49]. These are formed from phosphate ion and fluoride ion containing solutions at neutral pH. The development of coatings made up of P-Mn, Mn-N and other nitrogen containing species have been described [REF 50,51]. These coatings are formed from a slightly acidic bath containing a phosphorous containing acid, divalent manganese ions and an amine compound. The amine component is believed to prevent excessive etching of the substrate in the acidic media [REF 50]. These films were shown to be corrosion-resistant, highly rust inhibiting, and strongly paint-adherent [REF 51].

1.2.3.3 Fluorozirconate conversion coatings

Fluorozirconate treatments have also shown promise as potential pretreatments for magnesium and magnesium alloy materials. The group IV-A elements such as titanium, hafnium and zirconium are believed to form continuous three-dimensional polymeric metal or metalloid-oxide matrices, from aqueous solutions, in a similar manner as chromium [REF 52]. This makes them an attractive alternative for environmentally friendly conversion coatings. These coatings may provide corrosion protection through a galvanic setting or may act as a physical barrier to the environment [REF 52]. This has been exploited to produce corrosion resistant coatings, by exposing a metal substrate to an aqueous acidic solution of zirconium ions, stabilized in solution by organic or inorganic oxy-anion compounds [REF 52].

Upon drying, a continuous polymeric zirconium oxide layer becomes fixed on the surface. In a related patent, a conversion coating system composed of mixtures of group IV-A and group III-A elements was proposed [REF 6]. It is believed that these coatings provide enhanced corrosion resistance over simple zirconium oxide systems due to a redox component in the coating that mimics the chromate redox model.

The preferred embodiment of this patent uses cerium and zirconium in combination. One difficulty with this type of treatment is its higher sensitivity to contamination with hard water or constituents of the pretreatment baths that necessitates the use of demineralized water rinsing prior to the fluorozirconate treatment [REF 53].

In a recent study [REF 54], samples of magnesium alloys AZ91D and AM50A were treated with a commercial fluorozirconate solution followed by powder coating with an epoxy-polyester powder. This treatment was shown to have similar paint adhesion properties as chrome conversion coatings. The samples showed reasonable corrosion resistance in mild corrosive environments but extremely poor resistance to stone chipping, which limits its use in more severe service conditions.

Another study on fluorozirconate treatment of magnesium alloy AZ91 HP [REF 53] has shown that the coating contains predominantly Zr-Mg-Al oxides and hydroxides. Morphological studies concluded that the coating is composed of two layers. The first layer covers the metal surface continuously and is porous and amorphous. The second layer consists of individual crystalline particles rich in MgO/Mg(OH)₂. Good corrosion resistance was observed and drying temperatures up to 200 °C were shown to have no effect on the quality of the coating. A recent article concluded that fluorozirconate treatments were not suitable for use in severe corrosive environments [REF 54]. The use of fluorotitanate treatments was investigated for this purpose. It was found that the fluorotitanate treatment alone did not provide adequate protection against corrosion in severe corrosive environments. However, a combination of fluorotitanate + E-coat + powder paint was shown to be effective in mildly corrosive environments.

1.2.3.4 Stannate treatments

A process for creating stannate and zincate-based conversion coatings on magnesium alloy AZ91B+0.5% Si has been developed [REF 55]. Following pickling and activation, the

samples were treated with one of a variety of immersion tinning solutions or a zincate solution. The coatings showed some corrosion resistance, but in both cases, only thin layers were formed. Details on the corrosion resistance of these coatings were not given, and further studies are warranted.

A study on stannate treatment of ZC71 and a metal matrix composite of ZC71+12% SiC particles has been undertaken [REF 56]. After mechanical finishing and pickling, the samples were immersed in a stannate bath for selected periods of time. The treatment resulted in the formation of a 2- 3 μm thick, continuous and adherent, crystalline coating of MgSnO_3 on both materials. The nucleation and growth of the coating was completed in about 20 min. The initial nucleation was found to occur at cathodic sites on the surface with crystal growth to a grain size of about 2- 5 μm until they coalesced. There was an increase in the corrosion potential of the magnesium surface as the film formation proceeded indicating that the coating does have a passivating effect on the surface. Further corrosion studies are warranted. In a more recent study [REF 57], the authors examined this process on magnesium, ZC71 alloy, WE43 alloy, and a metal matrix composite with a ZC71 alloy matrix and 12% (v/v) silicon carbide particles. They found that crystalline MgSnO_3 was formed on all four substrates by a similar mechanism as discussed above.

1.2.4 Anodization

Anodization is an electrolytic process for producing a thick, stable oxide film on metals and alloys. Anodization technique has been developed in order for structure treatment of aluminum but extended to so called value metals and even for magnesium alloys and steel. These films may be used to improve paint adhesion to the metal, as a key for dyeing or as a passivation treatment. The stages for processing include: mechanical pretreatment, degreasing, cleaning and pickling, electrobrightening or polishing, anodizing using DC or AC current, dyeing or post-treatment, and sealing. The films have a thin barrier layer at the metal-coating interface followed by a layer that has a cellular structure. Each cell contains a pore whose size is determined by the type of electrolyte and its concentration, temperature, current density, and applied voltage. Their size and density determine the extent and quality of sealing of the anodized film. Coloring of anodized films can be achieved by absorbing organic dyes or inorganic pigments into the film immediately after anodizing, by a second-

step electrolytic deposition of inorganic metal oxides and hydroxides into the pores of the film or by a process called integral color anodizing. The latter is achieved by adding organic constituents to the anodizing electrolyte that decompose during the process and form particles which become trapped in the film as it grows. The color may also be controlled by a process called interference coloring. Interference coloring involves control of the pore structure to produce color by interference of the light reflected from the top and bottom of the pores [REF 29]. This process is difficult to control in production. Sealing of the anodized film is necessary in order to achieve an abrasion and corrosion resistant film. In this step, the porous oxide film is sealed off by the precipitation of hydrated base metal species inside the pores. This can be accomplished by boiling in hot water, steam treatment, dichromate sealing, and lacquer sealing [REF 29]. These films are often inadequate as the only surface treatment, but they provide an excellent paint base for a corrosion protection system. The wear resistance and hardness of anodized films can be improved by operating at a decreased electrolyte temperature and an increased current density. The process is referred to as hard anodizing [REF 29]. The properties of the hard-anodized coatings can be further improved through the incorporation of solid film lubricants such as PTFE or molybdenum disulfide [REF 29].

One of the main challenges for producing adherent, corrosion resistant, anodic coatings on magnesium results from the electrochemical inhomogeneity due to the phase separation in the alloy. The presence of flaws, porosity, and inclusions from mechanical pretreatment can also result in uneven deposition. It can also be difficult to achieve uniform throwing power over all areas of shapes featuring deep recesses, narrow cavities or sharp corners. Enhanced corrosion can occur if the coating contains defects [REF 30]. Another disadvantage of this technique is that the fatigue strength of the base metal can be affected by localized heating at the surface during the treatment, especially in thicker films. Yet another disadvantage is that the coatings produced are a brittle ceramic material that may not have appropriate mechanical properties for all applications. On the other hand, incorporation of PTFE type particles in hard anodized coatings may result in coatings with some technically superior functional properties.

1.2.5 Plasma anodization

In the 1960s and 70s scientists in the former Soviet Union investigated the anodizing process at potentials of over 200 volts for developing parts for the submarine sector and for military purposes. This led to plasma anodizing technology. The process for depositing an oxide coating on aluminum using the plasma anodizing process was first reported by Markov and co-workers in the 1970s [REF 58,59], and Yerokhin et al. [REF 6] identify Markov as the ‘father’ of the plasma anodizing process. Many other researchers worked with the plasma anodizing process throughout the 1980s [REF 60,61]. It wasn’t until the 1990s that the plasma anodizing process gained worldwide recognition as an eco-friendly technology for depositing the tribologically superior ceramic coatings on aluminum and magnesium alloys [REF 6]. Plasma anodizing technique has been developed quickly in recent years and is attracting increased attention from both academic institutions and many industries [REF 62]. To date, there are thousands of scientific publications dealing with a plasma anodizing technology that are distributed in a wide variety of journals and conference proceedings. Plasma anodizing is a novel surface engineering technology, considered as one of the most cost-effective and environmentally friendly ways to improve the corrosion and wear resistance of magnesium and magnesium alloys [REF 63, 64]. A driving force for these developments is the avoidance of expensive equipment required for competing vacuum-based plasma technologies. The plasma anodizing method can be used to form a thick, hard and adherent ceramic-like coating on the surface of magnesium alloys as well as of lightweight metals (Al and Ti) and their alloys [REF 6]. The substrate is immersed in an alkaline electrolyte (containing neither the concentrated sulfuric acid nor the chromate ions used for hard anodizing) and a high potential is applied to it. Different current modes have been utilized in the plasma anodizing treatment including, DC, AC, unipolar and bipolar current modes [REF 6, 65]. The formation mechanisms of the coating layer by plasma anodizing are complex due to the involvement of electro-, thermal-, and plasma- chemical reactions in the electrolyte [REF 66]. Plasma anodizing is certainly one of the most promising surface treatments for magnesium and magnesium alloys since it can provide both corrosion protection, and wear resistance.

1.3 Research objectives

Among several types of magnesium alloy, AZ91D is the most widely used die cast alloy because it has an excellent combination of mechanical properties and castability. Therefore,

this study focuses on the processing of plasma anodization of AZ91D magnesium alloy. The purpose of this study is to improve the understanding of plasma anodizing, which can be affected by several processing parameters with a wide range of values, e.g. power mode, electrolyte composition, electrolyte temperature, etc. The main theme of this study is to clarify the effect of these processing parameters on the structure and chemical and physical properties of plasma anodizing oxide film formed on AZ91D magnesium alloy substrate.

1.4 Overview of thesis

Chapter 1 describes the background of this study, in which the industrial importance of magnesium alloy is emphasized. Although magnesium alloy is an attractive material because of its extremely low density, its high chemical activity hinders it from industrial application without surface treatment. In this chapter, conventional surface treatment methods as well as latest plasma anodizing in literature are reviewed.

Chapter 2 describes the setting up of plasma anodizing equipment and experimental procedures.

Chapter 3 examines the effect of power mode on the properties of oxide film formed by plasma anodizing treatment on AZ91D magnesium alloy and the power mode is optimized in respect of corrosion resistance of the formed films.

Chapter 4 examines the corrosion resistance of plasma anodized AZ91D magnesium alloy together with the change in surface morphology and chemical composition of the oxide films as functions of electrolyte temperature and NaOH concentration.

Chapter 5 describes the physical properties of oxide films formed on AZ91D magnesium alloy by plasma anodizing treatment in the electrolyte at different temperature, i.e. breakdown voltage, heat conducting property, and wear resistance.

Chapter 6 describes the result of comparative examination of surface treatment methods of AZ91D alloy including non-chromate, anodization and plasma anodization in terms of physical and chemical properties of the oxide films.

Chapter 7 summarizes the main conclusions drawn from this study and provides suggestions for further studies.

1.5 References

1. G. L. Maker and J. Kruger, *J. Electrochem. Soc.*, **137** (1990) 414.
2. E. Aghion, B. Bronfin and D. Elezer, *J. Mater. Process Technol.*, **117** (2001) 381.
3. A. L. Rudd, C. B. Breslin and F. Mansfeld, *Corros. Sci.*, **42** (2000) 275.
4. G. Song, A. Atrens and D. ST John, X. Wu and J. Nairn, *Corros. Sci.*, **39** (1997) 1981.
5. J. E. Gray and B. Luan: *J. Alloys Compd.*, **336** (2002) 88.
6. A. L. Yerokin, X. Nie, A. Leyand, A. Matthews and S. J. Dowey, *Surf. Coat. Technol.*, **122** (1999) 73.
7. P. Gupta, G. Tenhundfeld, E. O. Daigle, D. Ryabkov, *Surf. Coat. Technol.*, **201** (2007) 8746.
8. P. Gupta, G. Tenhundfeld, E. O. Daigle, P. J. Schilling, *Surf. Coat. Technol.*, **200** (2005) 1587.
9. J. E. Gray and B. Luan: *J. Alloys Compd.*, **336** (2002) 88.
10. G. L. Maker and K. Kruger, *J. Electrochem. Soc.*, **137** (1990) 414.
11. E. Aghion, B. Bronfin and D. Elezer, *J. Mater. Process Technol.*, **117** (2001) 381.
12. Y. Kojima, *Mater. Sci. Forum*, **3** (2000) 350–351.
13. H. Kuwahara, Y. Al-Abdullat, M. Ohta, S. Tsutsumi, K. Ikeuchi, N. Mazaki and T. Aizauta, *Mater. Sci. Forum*, **349** (2000) 350–351.
14. D. S. Tawil, *Corrosion and surface protection developments, magnesium technology, in: Proceedings of the Conference*, (1986) 66.
15. G. L. Makar and J. Kruger, *Int. Mater. Rev.*, **38(3)** (1993) 138.
16. O. Linder, J. E. Lein, T. K. Aune and K. Nisancioglu, *Corrosion*, **45(9)** (1989) 741.
17. E. Hillis, *The Effects of Heavy Metal Contamination on Magnesium Corrosion Performance*, *SAE Technical Paper*, #830, Detroit (1983) 523.
18. R. Tunold, H. Holtan, M.-B. Hagg Berfe, A. Lasson, R. Steen-Hansen, *Corr. Sci.*, **17** (1977), 353.
19. E. F. Emley, *Principles of Magnesium Technology*, Ch. XX, Pergamon Press New York 1966.
20. G. Song, C. Blawert, W. Dietzel and A. Atrens, *Mat. Sci. Eng. A*, **A399** (2005) 308.
21. G. Song, A. Atrens, X. Wu, Z. Bo and B. Zhang, *Corr. Sci.*, **40** (1998) 1769.
22. S. K. Das and C. F. Chang, *US Patent No. 4765954* (1988).
23. C. K. Mittal, *Transactions of the Metal Finishers Association of India*, **4** (1995) 227

24. A. Brace, *Transactions*, **75** (1997) B101.
25. A. K. Sharma, R. Uma Rani and K. Giri, *Metal Finishing*, **95** (1997) 43.
26. F. A. Lowenheim, *Modern Electroplating*, Wiley, New York, 1974.
27. J. B. Mohler, *Metal Finishing*, **73** (1974) 30.
28. P. L. Hagans, C.M. Haas, *Chromate conversion coatings*, in: *ASM Handbook, Surface Engineering*, **Vol. 5**, ASM International, (1994) 405.
29. J. Horner, *Metal Finishing* **88** (1990) 76.
30. F. W. Eppensteiner, M.R. Jenkins, *Metal Finishing Guidebook and Directory* **90** (1992) 413.
31. A. U. Simaranov, S.L. Marshakov, Yu.N. Mikhailovskii, *Protection of Metals*, **28** (1992) 576.
32. A. U. Simaranov, S.L. Marshakov, Yu.N. Mikhailovskii, *Protection of Metals*, **25** (1990) 611
33. S. Ono, K. Asami, T. Osaka, *Characterization of chemical conversion coating films grown on magnesium*, in: *International Corrosion Congress Proceedings*, 13th, Clayton, Australia, (1996) 1.
34. J. M. Leuzinger, *Conversion coating of magnesium alloy surfaces*, **CA726661** (1966).
35. P. L. Hagans, *Method for providing a corrosion resistant coating for magnesium containing materials*, **US4569699** (1986).
36. I. Azkarate, P. Cano, A. Del Barrio, M. Insausti, *P. Santa Coloma Alternatives to Cr(VI) conversion coatings for magnesium alloys*, in: *International Congress Magnesium Alloys and their Applications*, 2000.
37. J. I. Skar, D. Albright, *Phosphate permanganate: a chrome free alternative for magnesium pretreatment*, in: *International Congress Magnesium Alloys and their Applications*, 2000.
38. D. Hawke, D.L. Albright, *Metal Finishing*, **93** (1995) 34.
39. J. I. Skar, M. Water, D. Albright, *Non-chromate conversion coatings for magnesium die castings*, in: *Society of Automotive Engineers, International Congress and Exposition*, (1997) 7.
40. U. Naohiro, K. Yoshiaki, N. Yukio, S. Kenichi, *Surface treated magnesium or magnesium alloy product, method of surface treatment and coating method*, **JP11029874A2** (1999).
41. U. Naohiro, K. Yoshiaki, N. Yukio, N. Yoshihiko, S. Yoshinori, F. Takeshi, *Surface treated magnesium or magnesium alloy product, primary treatment for coating and coating method*, **JP11323571A2** (1999).

42. J. D. Santi, *Magnesium piston coated with a fuel ignition products adhesive*, **US5014605** (1991).
43. M. Naoharu, *Formation of corrosion resistant coating film on magnesium alloy member*, **JP9031664A2** (1997).
44. L. S. Joesten, *Process for applying a coating to a magnesium alloy product*, **US5683522** (1997).
45. S. Ishizaki, M. Nishida, Y. Sato, *Composition and process for treating magnesium-containing metals and product therefrom*, **US5900074** (1999).
46. C. E. Tomlinson, *Conversion coatings for metals using group IV-Z metals in the presence of little or no fluoride and little or no chromium*, **US5952049** (1999).
47. C. E. Tomlinson, *Protective coatings for metals and other surfaces*, **US5964928** (1999).
48. H. Gehmecker, in: *International Magnesium Association*, (1994) 32.
49. J. I. Skar, M. Walter, D. Albright, *Non-chromate conversion coatings for magnesium die-castings*, in: *Proceedings of Society of Automotive Engineers*, (1997) 7.
50. G. Bech-Nielson, P. Leisner, *American Electroplaters and Surface Finishers Society*, (1991) 743.
51. M. A. Gonzalez-Nunez, C.A. Nunez-Lopez, P. Skeldon, G.E. Thompson, H. Karimzadeh, P. Lyon, T.E. Wilks, *Corrosion Sci.* **37** (1995) 1763.
52. M. A. Gonzalez-Nunez, P. Lkeldon, G.E. Thompson, H. Karimzadeh, *Corrosion*, **55** (1999) 1136.
53. P. Gupta, G. Tenhundfeld, E. O. Daigle, D. Ryabkov, *Surf. Coat. Technol.*, **201** (2007) 8746
54. P. Gupta, G. Tenhundfeld, E. O. Daigle, P. J. Schilling, *Surf. Coat. Technol.*, **200** (2005) 1587
55. N. P. Sluginov, J. Russ. *Phys. Chem. Soc.*, 12 1–2 Phys. (1880) **193**, in Russian.
56. A. Günterschultze, H. Betz, *Electrolytkondensatoren*, Krayn, Berlin, 1937.
57. W. McNiell, G. F. Nordbloom, *US Patent 2 854 390*, September 30, 1958.
58. [Markov G A, Markova G V: *USSR patent 526961*, 1976.
59. Markov G A, Tatarchuk V V, Mirnova M K: *Izvest. SO AN SSSR, Ser. Khim. Nauk*, **3** (1977) 32 (in Russian).
60. Snezhko L A and Tchernenko V I: *USSR patent 973583*, 1982.
61. Kurze P, Schreckenbach J, Schwarz Th, *Krysmann W Beschichten durch anodische oxidation unter Funkenentladung (ANOF)// Metalloberflaeche*, **B.40** (1986 S.539-540).

62. Li Q, Liang J, Wang Q, Plasma Electrolytic Oxidation Coatings on Lightweight Metals, 'In: Modern Surface Engineering Treatments, (Aliofkhazraei M., Ed), *InTech Open Publisher*. 2013 ISBN 978-953-51-1149-8.
63. Ghasemi A, Raja VS, Blawert C, Dietzel W and Kainer KU, Study of the structure and corrosion behavior of PEO coatings on AM50 magnesium alloy by electrochemical impedance spectroscopy. *Surface & Coatings Technology*, **202** (2008) 3513-3518.
64. Nie X, Wang L, Konca E and Alpas AT, Tribological behavior of oxide/graphite composite coatings deposited using electrolytic plasma process, *Surface & Coatings Technology*. 188–189 (2004) 207-213.
65. Curran J A and Clyne W T, Thermo-physical properties of plasma electrolytic oxide coatings on aluminum. *Surface & Coatings Technology*, **199** (2005) 177–183.
66. Duan H, Yan C, Wang F, Effect of electrolyte additives on performance of plasma electrolytic oxidation films formed on magnesium alloy AZ91D, *Electrochimica Acta*, **52** (2007) 3785-3793.

Chapter II. Experimental

2.1 Specimen

AZ91D specimens with chemical composition shown in Table 2-1 were machined into 12 x 40 mm with 3 mm thickness and used as an anode. As shown in Figure 2-1, distilled water and ethanol were used to remove impurities adhering to the surface of the raw material.

2.2 Apparatus

The plasma anodizing system is comprised of the electrolytic component, a high-voltage, high-current, 50 Hz pulse-reverse rectifier (NF, BP4650), a cooler (Lab Companion, RW-1025G), stainless steel (type 316) heat exchanger, and an air bubble system. Figure 2-2 shows the schematic of this plasma anodizing system.

Figure 2-3 shows a schematic of the pulsed unipolar output. There is a pause between pulses, and voltage is constant in the unipolar type. An insulated gate bipolar transistor (IGBT) type multimeter was used in this study to control the pulse width. In the pulse mode, the cycle consists of 500 ms of positive (+) time (on-time) and 500 ms (off-time). Meanwhile, the graphite plates were used as a cathode. Since the current density varies depending on the interelectrode distance and their size, graphite plates having a size of 10 x 30 mm were placed each side of specimen to form a uniform oxide film layer.

When the micro-arc occurs on the surface of the specimen by the electric pulse, the surface material melts at a momentarily high temperature, and the molten material is then quenched by the surrounding water forming craters and then cooled. A circulation system with a stainless steel heat exchange was used control of the temperature of the electrolyte solution. Oxygen gas generated on the anode during the plasma anodizing was effectively eliminated using strong pump flow without any additional vortex equipment. The system was designed to align the direction of the cold electrolyte solution being supplied to the position of the specimen. By positioning the specimen parallel to the direction of the electrolyte supply, the oxygen gas adsorbed on the surface was eliminated by the force of the flow of the electrolyte solution.

2.3 Electrolyte

A mixture of 0.024 M (2.0 g dm^{-3}) of sodium aluminate, 0.13 M (5.0 g dm^{-3}) of sodium hydroxide, and 0.082 M (10 g dm^{-3}) of sodium silicate was used as an electrolyte solution. In some experiments, the concentration of sodium hydroxide was changed from 0.06 to 0.25 M (chapter 4). Electrolyte temperature was changed from 10 to 50 °C. But it was set 50 °C unless otherwise mentioned.

2.4 Characterization

The plasma anodized specimens were cut, cold mounted, and polished with silicon carbide (SiC) paper in order to observe their cross-sections. EDS analysis was carried out to obtain their elemental mapping. Surface and morphology of the plasma anodized samples were observed using a digital optical microscope and field emission scanning electron microscopy (FE SEM). To observe the crystalline phase appearing in the oxide film, X-ray diffraction (XRD) patterns were recorded over a range of 10-90° at $1.2^\circ \text{ min}^{-1}$.

Surface roughness was measured using surface roughness tester (MITUTOYO, SJ-400) and the roughness average (R_a) was used. The measurement was made over the surface of 0.8 mm for 3 times for each specimen. The R_a represents an average surface roughness value from the measurement center line to the surface contour.

To measure the dielectric breakdown voltage and the thermal diffusivity, a withstanding voltage tester (model TOS5051A, KIKUSUI) and a laser flash analyzer (model LFA 457, Netzsch) were used, respectively.

The hardness of the samples were tested with a nanoindenter (model ENT-1100b, Elionix).

2.5 Corrosion test

Anodic polarization curve and electrochemical impedance spectroscopy (EIS) was measured using a potentiostat/galvanostat (10 V/2 A, ZIVE SP2, WonATech, Co., Ltd) to evaluate the corrosion resistance of the treated specimens. A frequency response analyzer (FRA) was used to evaluate the EIS. In addition, a saltwater spray tester was used to perform

a salt spray test according to the American Society for Testing and Materials (ASTM) - B117 standard test using a 5wt% NaCl solution maintained at 35 °C for 72 h. Corrosion characteristics were quantified by assessing the corrosion resistance by average rating number (RN).

2.6 Wear test

The wear test was carried out using an abrasion tester (Shinko zoki-sei, SSWT). Table 2-2 shows the test conditions. In this test, SUJ2 steel ball (\emptyset 10mm) was used as an upper specimen with a normal load of 1 ~ 50 N. The plasma anodized AZ91D specimen was subjected to abrasion in a manner of reciprocation with slip distance of 6 mm and frequency of 1 Hz for 100 s. The test was conducted in air at ambient temperature.

2.7 Conventional anodizing

The HAE method was used as the treatment process [REF 1]. A mixture of 2.7 M (150 g dm^{-3}) of KOH, 0.38 M (30 g dm^{-3}) of $\text{Al}(\text{OH})_3$ was used as an electrolyte solution. Anodizing was conducted under the condition of temperature of 30 °C, applied voltage of 50 V, and treatment time of 10 min. The power was supplied using a DC rectifier. The whole process is as follows: Degrease -> Acid Pickle -> Anodizing -> Sealing.

2.8 Non-chromate treatment

A phosphate process was used as the non-chromate treatment [REF 2]. The whole process is as follows: alkali wash (60% NaOH)-> distilled water bath-> acid activation (75% H_3PO_4)-> distilled water bath-> surface conditioning-> phosphating-> drying (120 °C, 20min).

A mixture of 0.2 M (20 g dm^{-3}) of phosphoric acid and 0.25 M (30 g dm^{-3}) of manganese sulfate was used as a phosphating solution. The pH of the phosphate solution was adjusted to 2.8 with H_3PO_4 and NaOH.

Table 2-1. Chemical composition of the AZ91D Mg alloy cast (mass %).

Element	Aluminum	Zinc	Copper	Manganese	Nickel	Silicon	Iron	Magnesium
Mass %	8.5-9.5	0.45-0.90	<0.025	0.17-0.40	<0.001	<0.03	<0.004	Balance

Table 2-2. Friction and wear testing conditions.

Upper spherical specimen (\varnothing 10mm)	SUJ2: HV 810
Reciprocating slip (mm)	6
Reciprocating frequency (Hz)	1
Normal load (N)	50 ~ 1
Cycle number	200
Temperature (°C)	21 - 25
Relative humidity (%)	45 - 57

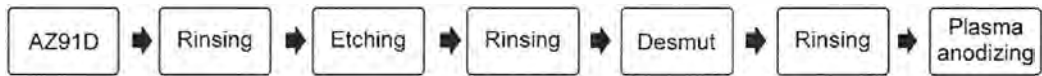


Figure 2-1. Pretreatment of AZ91D magnesium alloy for plasma anodization.

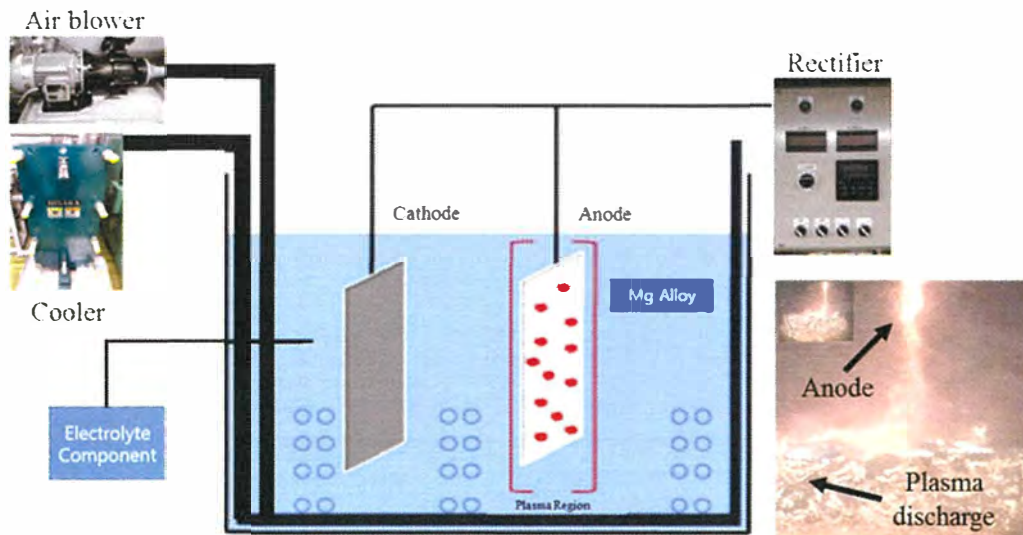


Figure 2-2. Experiment apparatus for plasma anodizing test of magnesium alloy.

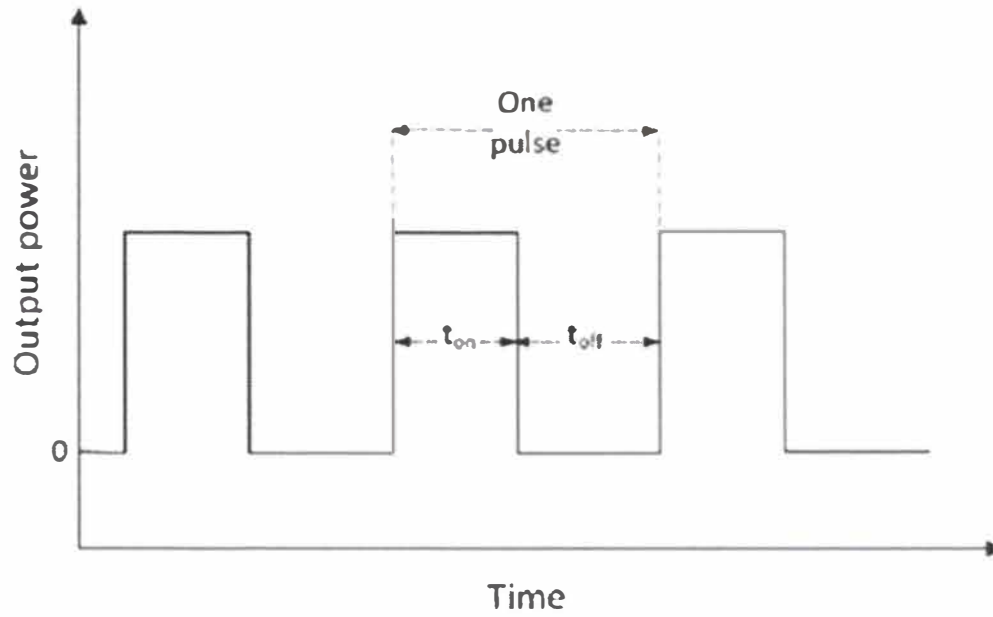


Figure 2-3. Schematic of the pulsed unipolar output of a plasma anodizing power supply.

2.9 References

1. De, L. H. K. U.S. Patent No. 2,901,409. Washington, DC: *U.S. Patent and Trademark Office*. (1959).
2. X.J. Cui, X.C. Wang, J.F. Lu. A chromium-free phosphate solution and process for magnesium alloy. *China Patent 201010123677.6* (2010).

Chapter III. Effect of power mode of plasma anodization on the properties of formed oxide films on AZ91D magnesium alloy

Published in:

- S.H. Lee, H. Yashiro and S.-Z. Kure-Chu, Fabrication of Plasma Electrolytic Oxidation Coatings on Magnesium AZ91D Casting Alloys, *J. Korean Inst. Surf. Eng.*, **50(6)** (2017) 432-438.
- S.H. Lee, H. Yashiro and S.-Z. Kure-Chu, Effect of Power Mode of Plasma Anodization on the Properties of formed Oxide Films on AZ91D Magnesium Alloy. *Korean Journal of Materials Research*, **28(10)** (2018) 544-550.

3.1 Introduction

Various anodizing methods can be used to grow porous oxide films on magnesium surfaces, but these films do not usually possess sufficient thickness, hardness, or corrosion resistance for practical applications [Ref 1-8]. Plasma anodization is a type of surface treatment that forms more protective oxide films electrochemically through the generation of plasma in an aqueous solution. This method uses low-concentration neutral/alkaline electrolytes and does not require harmful substances such as sulfuric acid or chromic acid.

Plasma anodization involves a series of complex processes, including the formation of an oxidation layer, dielectric breakdown, dissolution of the formed oxidation layer, and evolution of gases [Ref 9-10]. When the voltage applied during the treatment becomes higher than the dielectric breakdown voltage, the oxide film layer breaks, and plasma is generated. Furthermore, metal ions produced via the electrolysis of substrate react with hydroxide ions at the surface to form a strong oxide film [Ref 11]. Several parameters control the plasma anodization process, but the influence of these variables has not been fully clarified so far [Ref 12]. The purpose of this study is to develop and optimize a procedure for the generation of a stable oxide film during the plasma-anodizing process of AZ91D magnesium alloy. In

this chapter, effect of power mode of plasma anodization on the properties of formed oxide films were investigated.

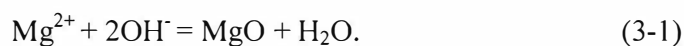
3.2. Results and Discussions

3.2.1 Evaluation of oxide films formed under DC and pulse voltage mode conditions

The effect of applied voltage on the formation of oxide film was evaluated in both DC and pulse modes at 50 °C. The treatment time was set to 15 min while the voltage applied to the specimen was changed from 50 to 200 V.

Figure 3-1 shows the cross-sectional structure and composition of the oxide films treated with DC and pulse modes at 150 V. In both EDS element mapping results showing the distribution of Mg, O and Si in the oxide film, Mg, O and Si are the main components of the oxide film and Mg, O and Si are uniformly distributed. In the pulse mode, the thickness of the cross section of the oxide film was relatively uniform, and a three-layer structure of the oxide film was recognized.

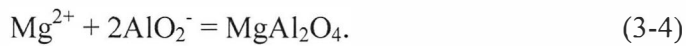
Figure 3-2 shows the XRD patterns of raw AZ91D and that treated with pulse plasma anodizing at 150 V. The results show clear differences in the peak intensities and crystal phases. After the plasma anodizing treatment, three ceramic phases, MgO, Mg₂SiO₄, and MgAl₂O₄, are identified on the AZ91D. The chemical species appearing during the anodization process are produced by various phenomena, such as the sample dissolution and electrolysis of the electrolyte solution, after which a ceramic phase is formed through a series of reactions. The MgO formation mechanism is similar to that observed in conventional Mg anodization techniques. As can be seen from equation (3-1), Mg²⁺ is transferred from the specimen to the oxidation layer/electrolyte solution interface, and OH⁻ ions are transferred from the electrolyte solution to the sample/oxidation layer interface. Therefore, MgO simultaneously forms at the oxidation layer/electrolyte solution interface and at the sample/oxidation layer interface,



Mg_2SiO_4 can be generated by the reaction of SiO_3^{2-} anions with Mg^{2+} . Na_2SiO_3 in the electrolyte solution dissociates to produce SiO_3^{2-} ions, which react with Mg^{2+} to form Mg_2SiO_4 ,



MgAl_2O_4 can also form via the reaction



Since AZ91D contains Al, the MgAl_2O_4 phase formed during the plasma anodization treatment has a stable spinel structure, which improves the corrosion resistance of the material by passivation. [Ref 2]

Figure 3-3 shows FESEM images of surface oxides treated in DC and pulse modes as a function of applied voltage. In the DC mode, surface of the oxide layer showed a non-uniform, porous morphology. Applying a high DC voltage of 200 V resulted in higher non-uniformity and larger pore size. The pores that appeared on the surface were formed by oxygen bubbles generated when a micro-arc formed on the surface during the plasma anodizing treatment. The size of the micro-arc is proportional to the magnitude of current [Ref 1], and thus, a higher applied voltage resulted in larger pores. In the pulse mode, the oxide surface showed a relatively constant pore size up to a 150 V voltage condition and a small amount of released material and microcracks or craters (sinkhole / pipe) were detected at 200 V. In both conditions, as the voltage increased, the pores became larger and non-uniform, but the pores of the oxidized surface in the pulse mode were relatively constant in size and less in defect. The non-uniform growth pattern of the oxide film and oxygen bubble trapping during the growth process resulted in the formation of a wider pore layer in the ceramic layer.

Figure 3-4 shows cross-sectional images of the specimen to observe the thickness of the oxide layer grown as a function of applied voltage. The thickness of the oxide layer

treated with DC and pulse modes increased from 8 to 36 μm depending on the anodization voltage. As the applied voltage increased in the plasma anodizing process, the oxide layer became thick. In addition, the oxide layer of the specimen treated at 200 V was 2 or 3 times thicker than that treated at 50 V. In the pulse mode, the growth rate of the thickness was relatively low. It is attributed to 500 ms (off-time) of the pulse mode. As the treatment voltage increases or the treatment time becomes longer, the oxide film grows thicker. In turn, as the oxide film becomes thicker, the electrical resistance increases, thus affecting generation of plasma. [Ref 3] Therefore, the current flowing on the specimen surface during the plasma anodizing treatment does not increase proportionately to the voltage level. Moreover, the higher applied voltage increases the strength of the plasma, thereby dissolving a greater amount of the material from the surface. Thus, a strong micro-arc is sustained for a long time with a voltage level that has exceeded the dielectric breakdown voltage.

Figure 3-5 shows optical microphotographs of the oxide films formed on the AZ91D material after plasma anodization at fixed voltages of 50 - 200 V in DC and pulse modes. The surface of the oxide film formed in all samples contains many products that generate crater traces, pores generated by secretions, and craters. This phenomenon is caused by the plasma explosion of the surface of the sample at a high temperature at which molten Mg reacts rapidly with the electrolyte and is cooled. The size of the pores produced by the plasma and the amount of product generated by the emission increases with increasing voltage.

Figure 3-6 shows the surface roughness of the AZ91D material as a function of plasma anodization voltage in DC and pulse modes, as indicated by R_a . As a result of controlling the voltage at 50 - 200 V in the pulse mode, the pore size in the oxide film was relatively constant and the surface roughness was in the range of R_a 0.1 to 0.4 μm . DC mode voltage control produced craters and microcracks and the surface roughness R_a ranged from 0.6 to 1.4 μm . Therefore, it is more preferable to perform voltage control in pulse mode rather than DC mode in order to obtain an oxide film having a uniform surface. These results are consistent with the trends observed in surface morphology (see Figure 3-5).

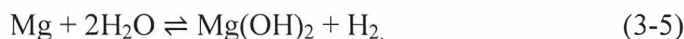
Figure 3-7 shows the corrosion resistance of the samples measured in a 3 mol dm^{-3} NaCl solution using EIS as a function of anodizing voltage. In this figure, corrosion resistance value is related to the magnitude of the AC impedance at 10 Hz, because the polarization resistance is usually dominant at this frequency. As expected, as the voltage of the plasma-anodization increased, corrosion resistance also increased. The corrosion

resistance was higher when pulse voltage was applied, which means that the oxide layer formed under pulse voltage condition is more protective.

Figure 3-8 shows the results of a salt spray test conducted for 72 hours in accordance with the ASTM standard to evaluate the corrosion properties of the plasma anodized Mg alloy specimens. The experiment was carried out using a 5 wt% NaCl solution and the temperature was maintained at 35 ° C. The corrosion properties were quantified by evaluating the average grade number (RN). The untreated AZ91D material and the plasma anodized material with DC mode at 150 and 200 V exhibited RN values of 3.5, 5 and 7, respectively, while the plasma anodized ones in pulse mode at 150 – 200 V showed a RN value of 9.5. These results mirror the trend observed in the surface roughness measurements and in the EIS data, shown in Figures 3-6 and 3-7.

Figure 3-9 shows the cross-sectional structure of the pulse anodized AZ91D after the salt spray test. The aggressive electrolyte, i.e. chloride, penetrates the oxide film cracks and promotes material corrosion. The final corrosion products, MgO and Mg (OH)₂, accumulate in the cracks of the oxide film and can interfere with the further progress of the corrosion process. [Ref 4] However, higher Cl⁻ ion concentrations at the interface accelerate corrosion. Figures 3-9 and 3-10 show that the entire oxide film is destroyed by Cl⁻ ion and the corrosion product spreads on the top surface of the oxide film and the protection of the oxide film is lost. Figure 3-10 shows that the corrosion products (a) consist of Mg, O and Cl⁻ ions and that Mg, O and Si are homogeneously distributed in the corrosion free region (b).

The corrosion of magnesium is the following oxidation-reduction reaction:



Magnesium in a neutral or alkaline solution is oxidized to Mg²⁺ and combines with OH⁻ ions formed by the simultaneous reduction of water to form Mg (OH)₂ on the magnesium surface.

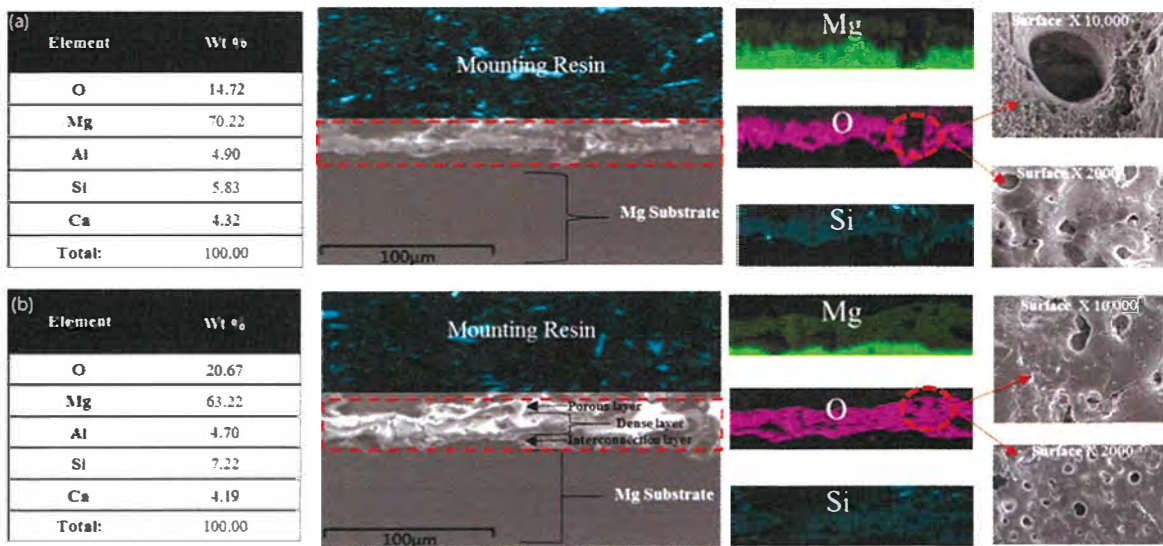


Figure 3-1. Cross-sectional view and EDS mapping of AZ91D after plasma anodization using (a) DC and (b) pulse at 150 V.

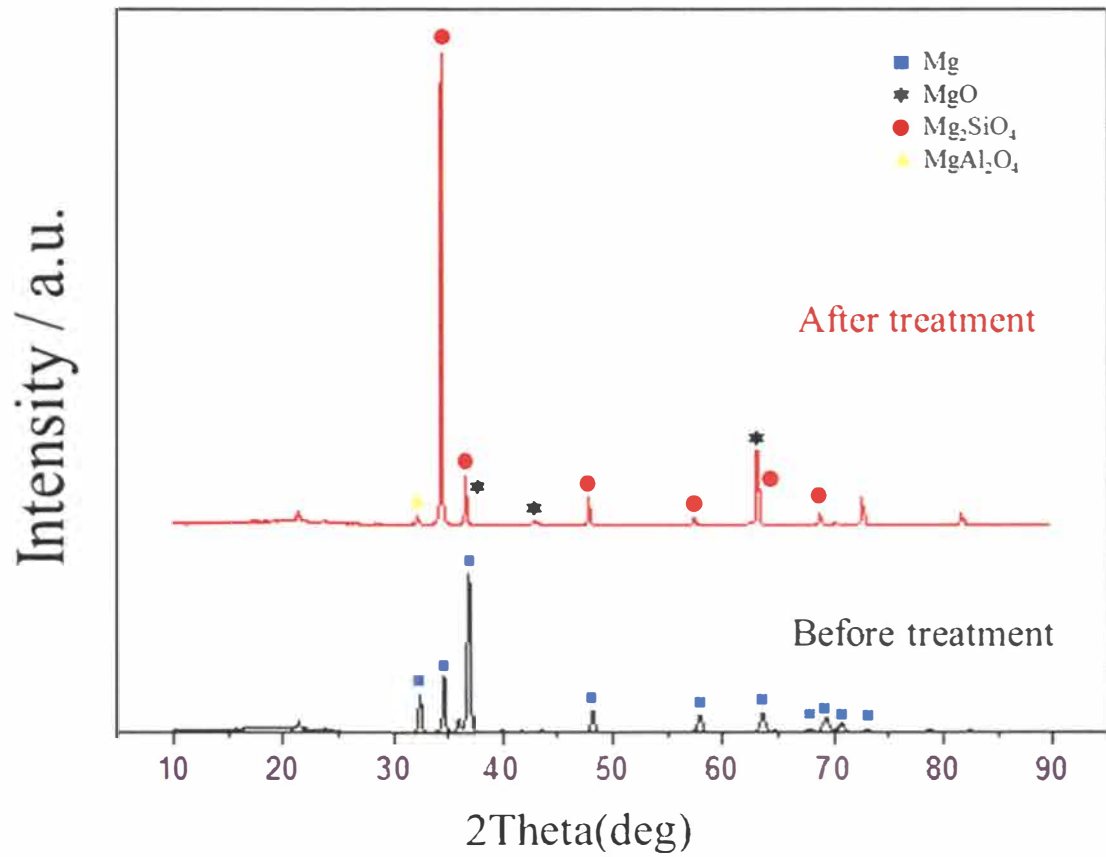


Figure 3-2. XRD patterns of AZ91D (a) before and (b) after plasma anodizing at (a) AZ91D (b) 150 V.

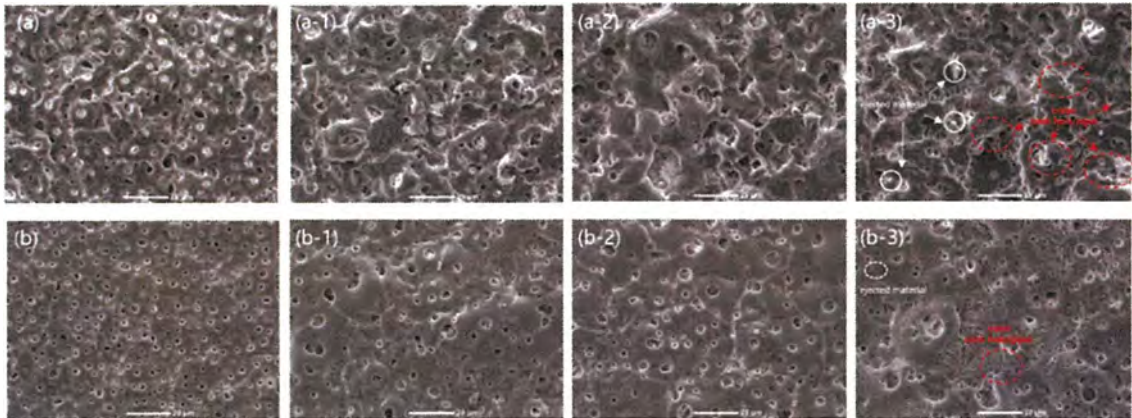


Figure 3-3. Surface morphologies of AZ91D after plasma anodizing using DC (a) and pulse (b) at (a, b) 50 V, (a-1, b-1) 100 V, (a-2, b-2) 150 V and (a-3, b-3) 200 V.

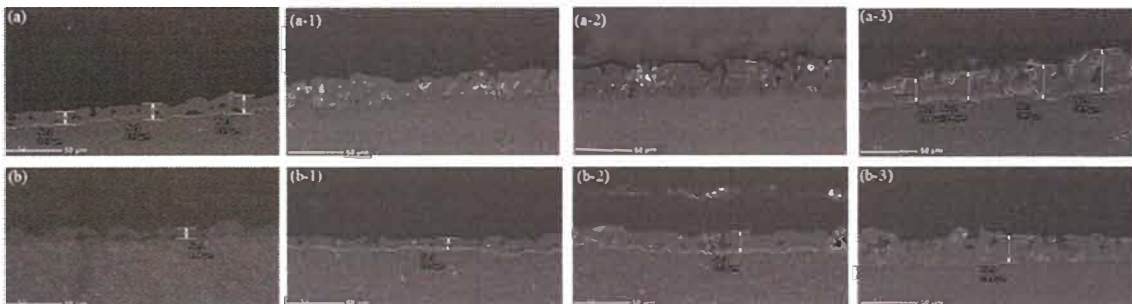


Figure 3-4. Cross sections of AZ91D after plasma anodizing using DC (a) and pulse (b) at (a, b) 50 V, (a-1, b-1) 100 V, (a-2, b-2) 150 V and (a-3, b-3) 200 V.

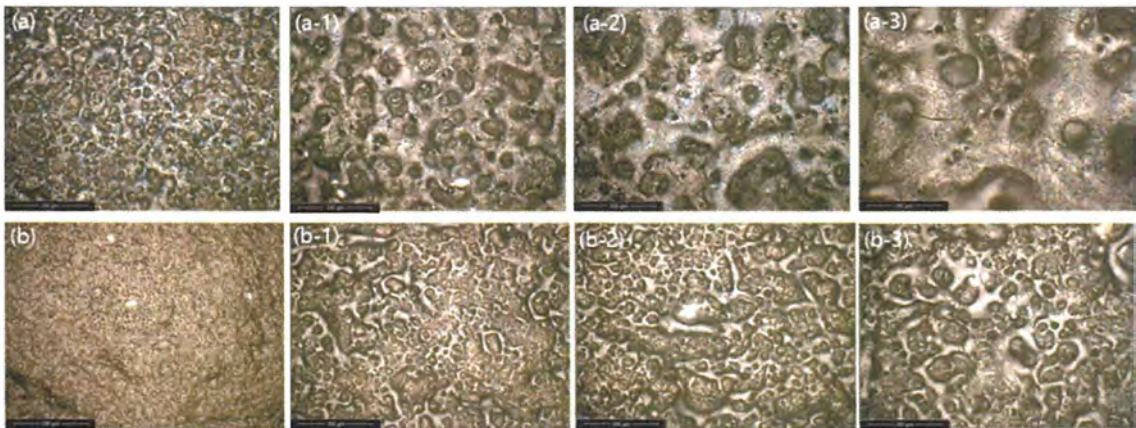


Figure 3-5. Digital microscope surface photographs ($1000\times$ magnification) of AZ91D after plasma anodizing using DC (a) and pulse (b) at (a, b) 50 V, (a-1, b-1) 100 V, (a-2, b-2) 150 V and (a-3, b-3) 200 V.

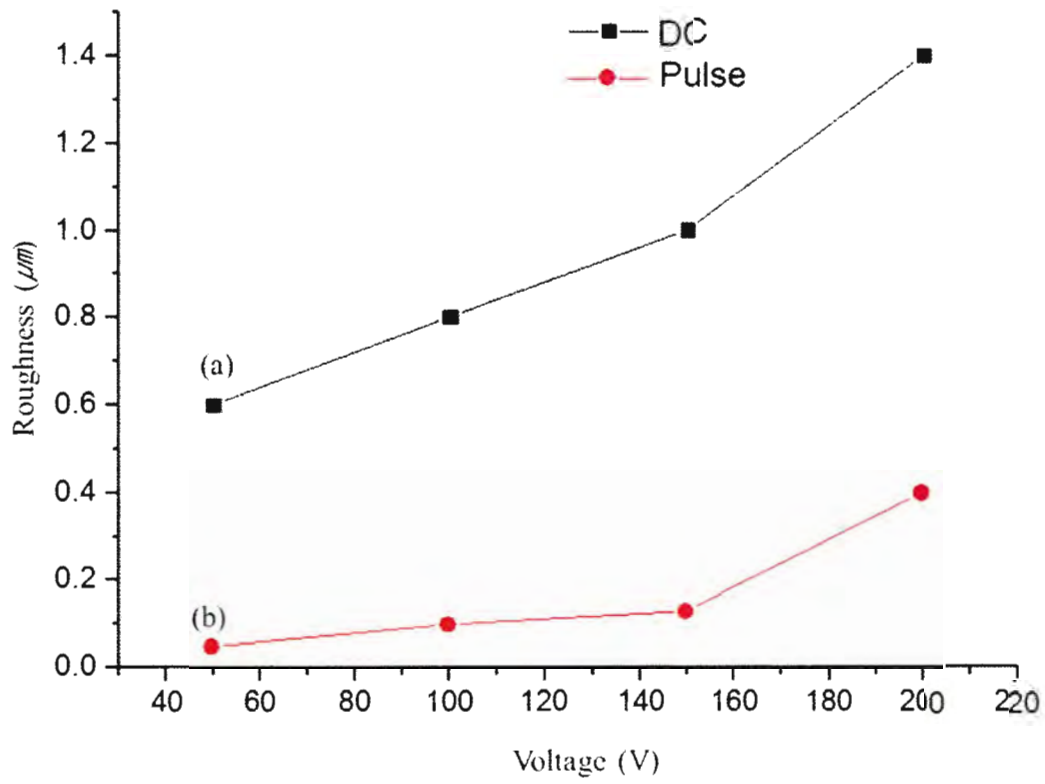


Figure 3-6. Effect of voltage on the surface roughness of the oxide film on the AZ91D surface after plasma anodization. DC (a) and pulse (b).

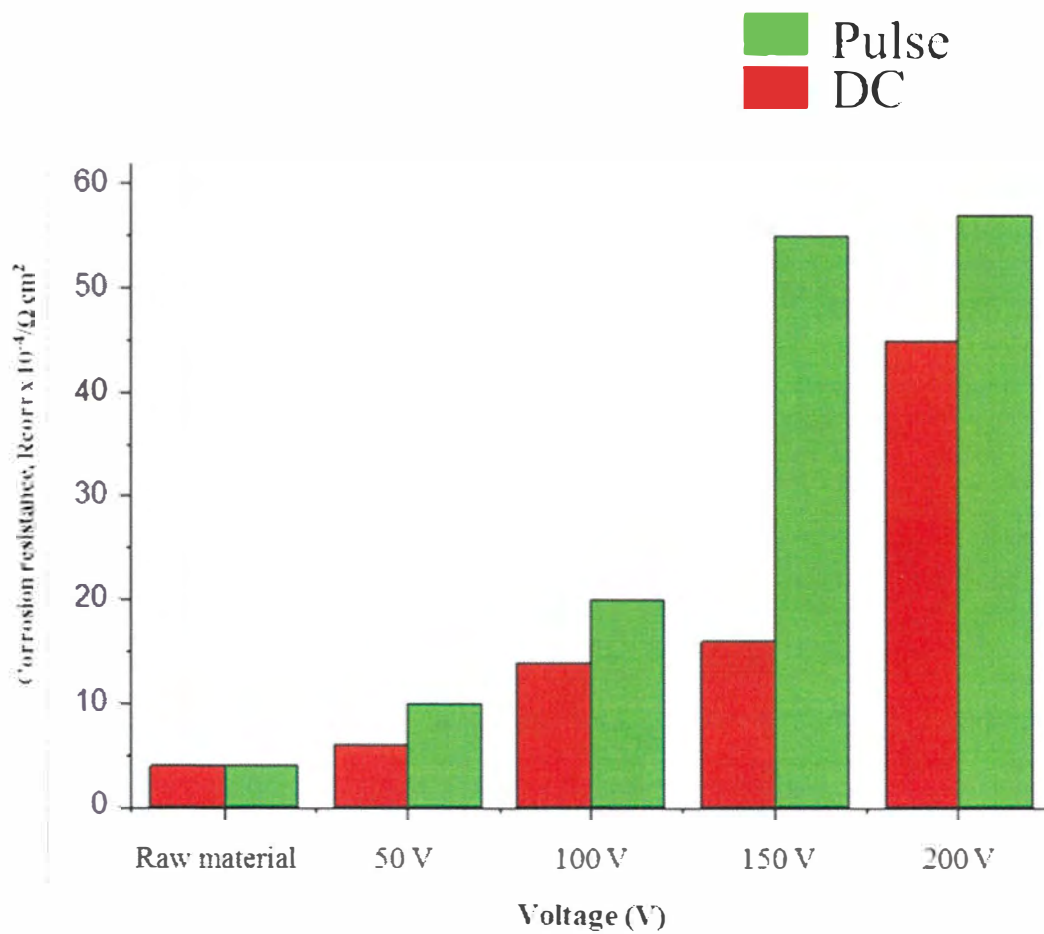


Figure 3-7. Effect of applied DC and pulse voltage for plasma anodizing on the corrosion resistance of AZ91D as evaluated by EIS in a 3 mol dm^{-3} NaCl solution at 25°C .


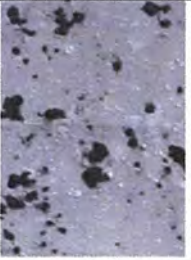


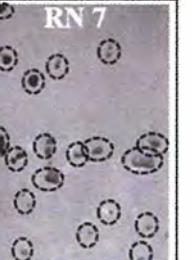

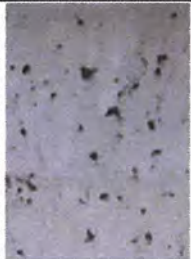

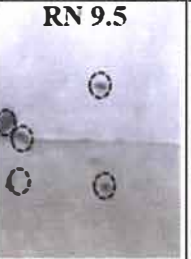
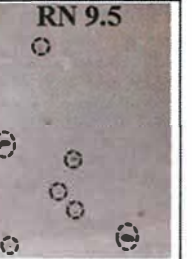
DC (V)		Raw material	50	100	150	200
Salt spray time (h)	72					
	72					

Figure 3-8. Effect of DC and pulse voltage for plasma anodizing of AZ91D on the corrosion behavior by 72 hours salt spray test.

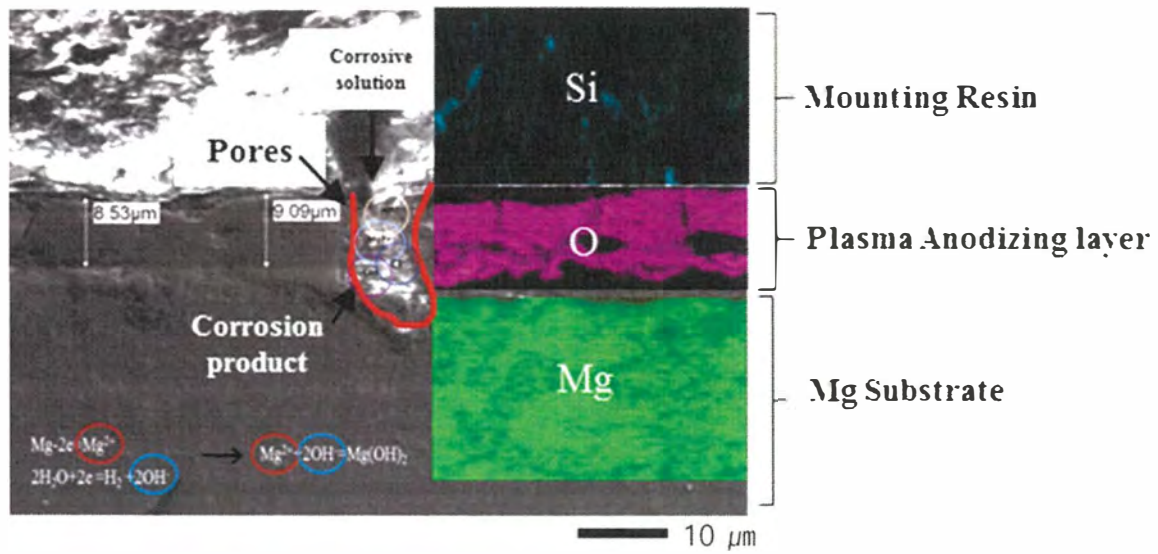


Figure 3-9. Cross-sectional micrograph of the corrosion site of pulse plasma anodized AZ91D at 150 V after the salt spray test.

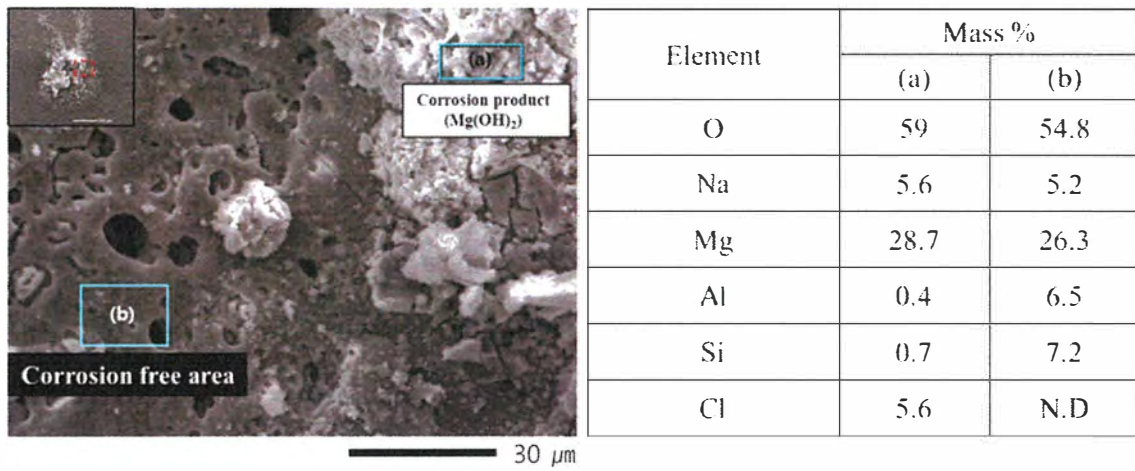


Figure 3-10. Surface micrograph and EDS analysis data for the pulse plasma anodized material at 150 V after the salt spray test.

3.2.2 Evaluation of oxide films formed under pulse current and pulse voltage mode conditions

In the previous section, it was concluded that better oxide films formed under pulse voltage mode. In this section, further examination is made focusing on the pulse mode.

Figure 3-11 shows the three-layer structure oxide film of plasma anodizing. The porous structure of the outermost layer may be advantageous to additional painting to have excellent coating adhesion. The dense middle layer is superior in mechanical properties (abrasion resistance) and corrosion resistance, and the interconnection layer is a very thin layer through which electricity passes from the material to the oxide film [Ref 1]. Various types of oxide pore / crack structures can be generated in the plasma anodization process. The roughness due to porosity and pore size can affect the durability characteristics.

Figure 3-12 shows FESEM images of raw material and that treated under 150 V voltage control and 10 A dm⁻² current control, where each power was applied in a pulse mode. When the voltage was controlled, the pores of the oxidized surface showed a relatively constant size and only a small amount of the ejected material was detected. Also, the surface pore size was relatively uniform and no micro cracks or crater (sinkhole/pipe) were observed. When the current was controlled, the surface void became uneven, and a lot of fine cracks and crater holes were observed.

Figure 3-13 shows of the cross-sectional plasma oxidation oxide formed under 10 A dm⁻² current control. A crater (sinkhole/pipe) is a pore created by the plasma at the material / oxide interface, and a sinkhole/pipe leads a porous coating with less durability. The reason of microcrack generation is that the temperature of the material metal rises due to the heat generated in the plasma electrolytic oxide film process and the tensile stress becomes larger than the thermal expansion coefficient of the oxide film. [Ref 5].

Figure 3-14 shows surface roughness of AZ91D material before and after the plasma anodizing treatment as indicated in *Ra*. As a result of controlling the voltage, it was observed that the pores on the surface of the oxide film were relatively constant and the surface roughness was in the range of *Ra* 0.2 to 0.3 μm. When the current was controlled, craters and micro cracks were generated, and the surface roughness was 0.45 to 0.6 μm in *Ra*. Therefore,

it is more preferable to control the voltage than to control the current to obtain a uniform oxide film.

Figure 3-15 shows the effect of pulse plasma anodizing on the anodic polarization behavior in 3.5 wt.% NaCl solution at 25 °C. It was found that specimen after plasma anodizing treatment showed higher breakdown potential than the original material. The breakdown potential was highest when 150 V pulse voltage was applied, which means that the oxide layer formed under constant voltage was more protective.

Figure 3-16 shows the results of salt spray test that was performed for 72 h in accordance with ASTM standards for assessing the corrosion characteristics of the magnesium alloy specimens treated with plasma anodization. Untreated AZ91D material and that treated with 10 A dm⁻² showed RN values of 3.5 and 7, respectively, while the specimens treated with 150 V plasma anodizing showed RN values of 9.

Figure 3-17 is the result of EDS element mapping showing the surface distribution of Mg, O and Si on the oxide film composition formed by plasma anodizing treatment with 150 V pulse voltage. Experimental results were obtained for both Mg, O and Si as the main film forming elements. Si and O are uniformly distributed. Mg and O account for 88.6% of the total atomic%. Chemical species that form such phases are generated by various phenomena such as specimen dissolution and electrolysis of the electrolyte solution, after which ceramic phases formed via various reactions, as indicated equations (3-1) ~ (3-4).

3.3 Conclusion

A plasma anodizing device suitable for the anodic oxidation of magnesium alloys has been developed and its applicability for AZ91D alloys has been demonstrated.

Anodization is controlled by voltage, which can be optimized to obtain a uniform oxide layer on the magnesium alloy surface. When the voltage was in the pulse mode of 150 V, the concentration of defects in the oxide layer was minimized. The surface roughness also decreased and the corrosion resistance increased from $RN = 3.5$ to $RN = 9.5$. Mg, Al, O and Si were uniformly distributed on the surface of the oxide film under optimized conditions. Cl⁻ ions, known to promote corrosion, were detected in the corroded oxide layer.

The roughness of the surface which is related to the size and shape of the pores and the resulting defects in the oxide film may have a greater effect on the durability of the material than the thickness of the oxide film. Also, the defect which appeared when the pulse current of 10 A dm^{-2} was employed did not form under the pulse voltage condition of 150 V and the number of pores was also smaller.

Corrosion resistance increased from $RN 3.5$ to 9 and it was confirmed that Mg, Al, O and Si were evenly distributed on the surface of the oxide film. The optimum oxide film was obtained at 150 V process pulse voltage.

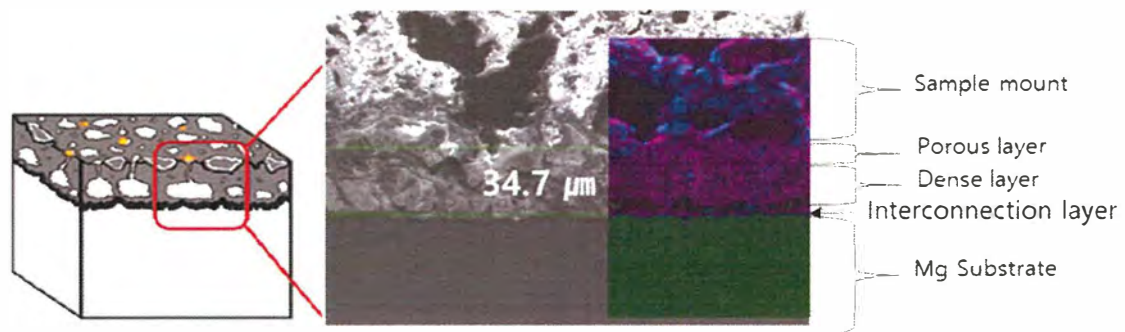


Figure 3- 11. Cross sectional view of AZ91D after plasma anodizing using pulse for at 150 V, 10 min.

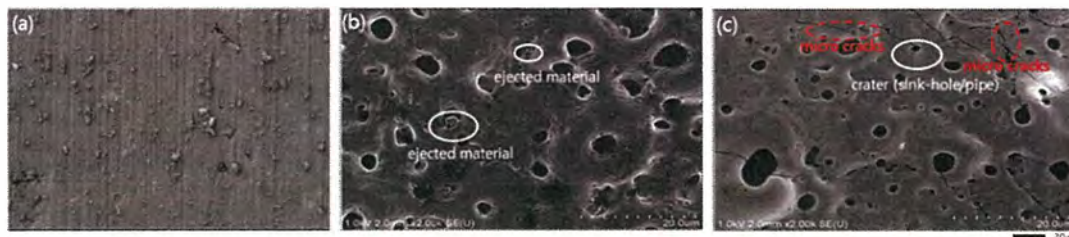


Figure 3-12. Surface morphologies of AZ91D before (a) and after pulse plasma anodizing for 30 min under (b) voltage control of 150 V and (c) current control of 10 A dm^{-2} .

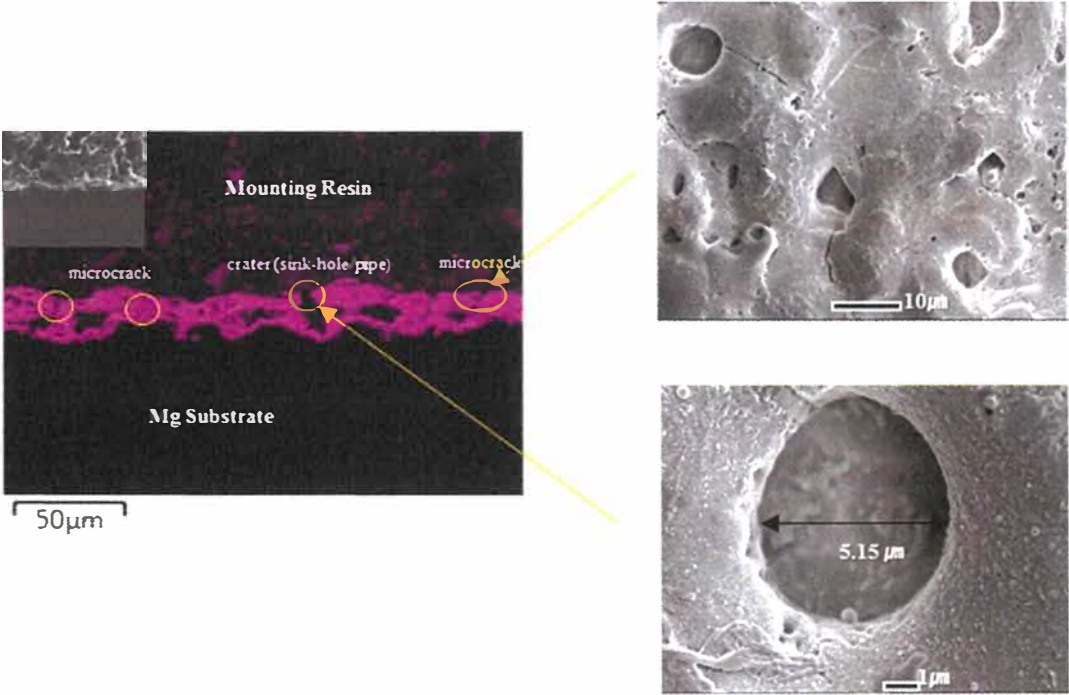


Figure 3-13. The structure of oxide film formed on AZ91D by the pulse plasma anodizing for 10 min under current control of 10 A dm^{-2} .

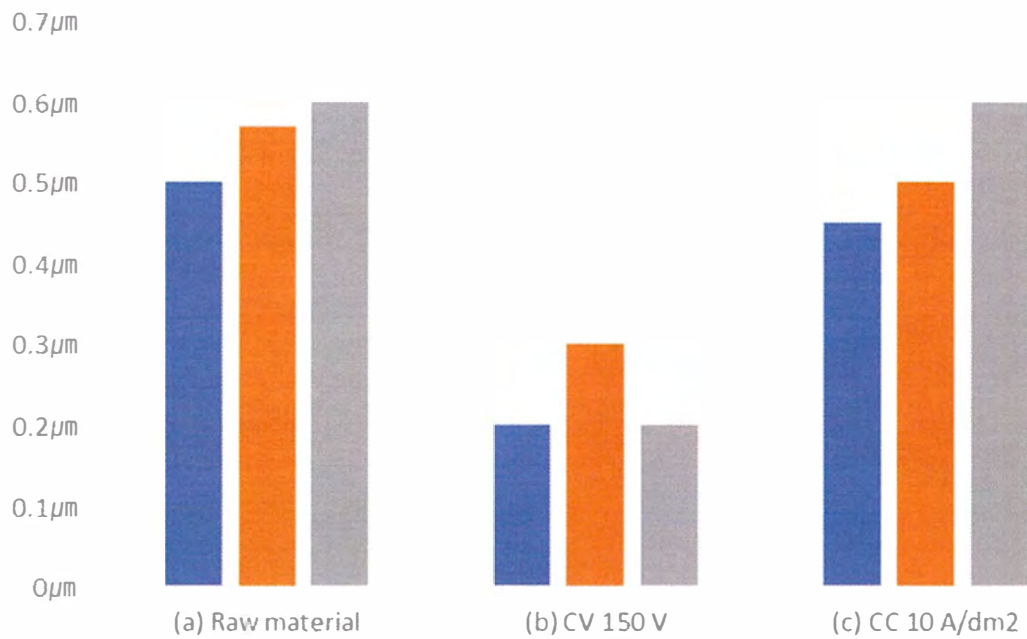


Figure 3-14. Surface roughness of AZ91D after pulsed plasma anodization for 10 min: (a) Raw material (b) Voltage control 150 V (c) Current control 10 A dm⁻².

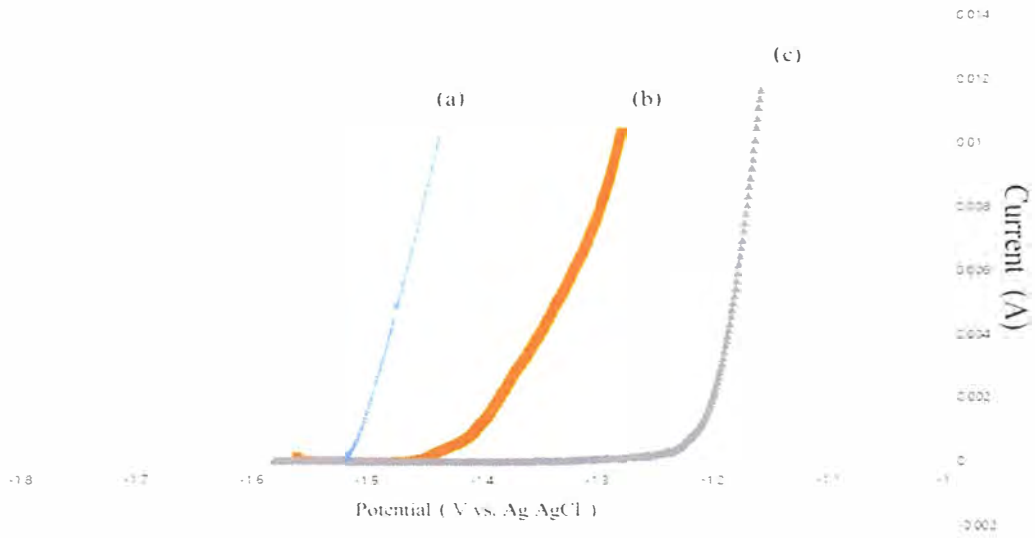


Figure 3-15. Anodic polarization curves of AZ91D in a 3.5 wt.% NaCl solution at 25 ° C (a) raw material, (b) plasma anodized under current control of 10 A dm⁻², (c) plasma anodized under voltage control of 150 V.

		RAW MATERIAL	10 A/dm ²	150 V
Salt spray time (h)	72			

Figure 3-16. Surface images of specimens after 72 hours salt spray test.

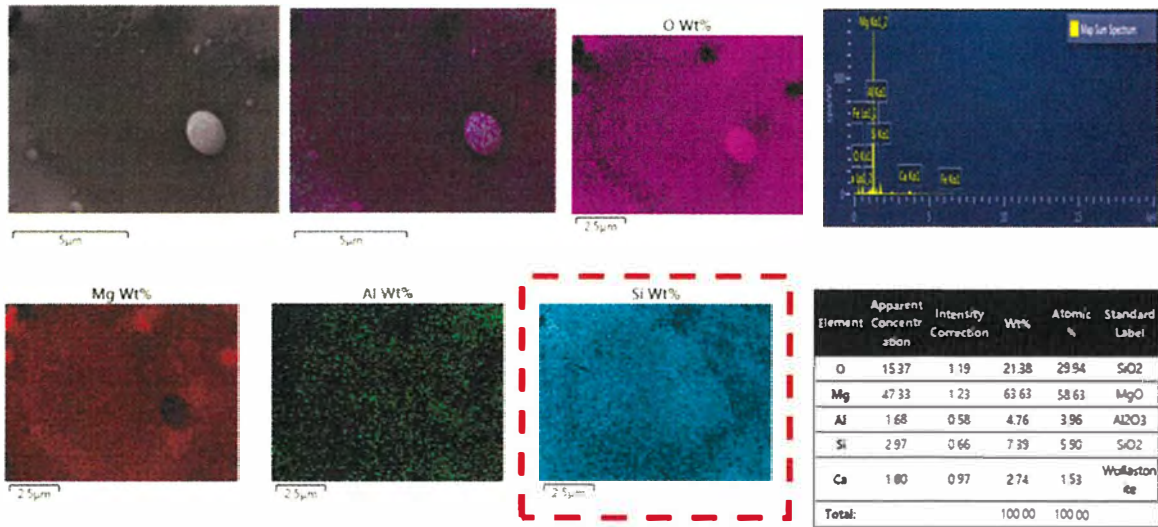


Figure 3-17. EDS elemental maps of the plasma anodizing films formed on AZ91D Mg alloy at 150 V for 30 min.

3.4 References

1. Lee, S. H., Yashiro, H., & Kure-Chu, S. Z., *J. Korean Inst. Surf. Eng.*, **50(6)** (2017) 432-438.
2. Mordike, B. L., & Ebert, T., *Materials Science and Engineering: A*, **302(1)** (2001) 37-45.
3. Song, G., Atrens, A., Stjohn, D., Nairn, J., & Li, Y., *Corrosion Science*, **39(5)** (1997) 855-875.
4. Ma, Y., Nie, X., Northwood, D. O., & Hu, H., *Thin Solid Films*, **494(1-2)** (2006) 296-301.
5. Gray, J., & Luan, B., *Journal of alloys and compounds*, **336(1-2)** (2002) 88-113.
6. Srinivasan, P. B., Blawert, C., & Dietzel, W., *Materials Science and Engineering: A*, **494(1-2)** (2008) 401-406.
7. Zhang, Y., Yan, C., Wang, F., Lou, H., & Cao, C., *Surface and Coatings Technology*, **161(1)** (2002) 36-43.
8. Duan, H., Du, K., Yan, C., & Wang, F., *Electrochimica Acta*, **51(14)** (2006) 2898-2908.
9. Narayanan, T. S., Park, I. S., & Lee, M. H., *Progress in Materials Science*, **60** (2014) 1-71.
10. Wang, L., Zhou, J., Liang, J., & Chen, *Surface and Coatings Technology*, **206(13)** (2012) 3109-3115.
11. Hussein, R. O., Northwood, D. O., & Nie, X., *Surface and Coatings Technology*, **237** (2013) 357-368.
12. Xia, S. J., et al. "Electrochemical studies of AC/DC anodized Mg alloy in NaCl solution." *J. Electrochem. Soc.*, **151.3**, (2004).

Chapter IV. Effect of electrolyte parameters on the corrosion resistance of plasma Anodized AZ91D magnesium alloy

Published in:

- S.H. Lee, H. Yashiro and S.-Z. Kure-Chu, Electrolyte Temperature Dependence on the Properties of Plasma Anodized Oxide Films Formed on AZ91D Magnesium Alloy. *Korean Journal of Materials Research*, **29(5)** (2019) 288-296.
- S.H. Lee, H. Yashiro and S.-Z. Kure-Chu, Effect of sodium hydroxide concentration of Plasma Anodic Oxidation on the properties of oxide film formed on AZ91D Magnesium Alloy, *IJARSET* **volume.6(4)** (2019) ISSN: 2350-0328.

4.1 Introduction

In chapter III, plasma anodization was introduced for surface treatment of AZ91D magnesium alloy and optimized in terms of power mode. Controlled voltage of 150 V in a pulse mode resulted in best performance in respect to corrosion resistance. However, there are many other process parameters to be optimized. Electrolyte temperature is one of those parameters which has not been studied systematically. Because plasma temperature reaches over 2000 °C, electrolyte has been paid little attention as an effective parameter. However, in an anodic oxidation process even with plasma discharge, films are formed through a reaction with the electrolyte; thus the process should be influenced by the electrolyte temperature. In this chapter, variables in electrolyte including electrolyte temperature and concentration are optimized in terms of corrosion resistance.

4.2 Results and Discussion

4.2.1 Effect of electrolyte temperature on the characteristics of oxide film for AZ91D magnesium alloy formed by plasma anodization

Figure 4-1 illustrates the change in current and plasma images generated on the surface during the anodization with pulsed voltage of 150 V. The plasma generation occurs via several stages, and other phenomena are also observed. Conventional anodic oxidation occurs in the stage A, during which substantial gas evolution is also observed. When a breakdown voltage is reached, fine and white micro discharges start at weak sites on the surface of the sample. The amount of plasma generated on the surface increases with time. The maximum orange plasma amount is generated during the stages B and C, whereas in the stage D, the volume occupied by the plasma increases. The current response characteristics over time were similar for 10 and 50 °C. However, the current response at 10 °C throughout all the stages was slightly slower than that at 50 °C. This appears to be related to the higher conductivity of the electrolyte at 50 °C.

Figure 4-2 shows the optical microscopic surface images of the oxide films formed on the AZ91D material after the plasma-anodizing treatment in which the temperature of the electrolyte was varied between 10 and 50 °C at a fixed voltage of 150 V for 15 min. The surface of the oxide film formed in all the samples included inhomogeneous products, which resulted in crater traces, pores produced by secretions, and craters. This phenomenon was attributed to plasma explosion at the surface of the sample at high temperature, with the molten magnesium reacting with the electrolyte rapidly, and subsequently cooling. It was observed that the size of the pores produced by the plasma and the amount of products generated by the emission decreased as the temperature of the electrolyte increased.

Figure 4-3 shows the roughness of the specimens as a function of the electrolyte temperature. The roughness of the raw material was 0.6 μm in R_a , and the surface roughness decreased from 0.7 to 0.15 μm as the temperature of the electrolyte increased from 10 to 50 °C. Cooling the electrolyte to a relatively low temperature (10 °C) caused larger pore size and higher surface roughness.

Figure 4-4 shows the FESEM images of the surface of the samples treated at 10 and 50 °C. The surface of the specimen treated at 10 °C exhibited uneven porosity, with several microscopic cracks and craters. A sinkhole/pipe is a hole created by the plasma at the

material/oxide interface, which leads to a porous coating with low durability [Ref 10]. The surface and cross-section of the oxidized specimen treated at 50 °C showed a relatively constant pore size, and only a small amount of exhaust material was detected on the surface. In addition, the number of microcracks appeared to be relatively small. Microcracks are considered to be generated because the temperature of the metallic material increases in response to the heat generated in the plasma electrolytic oxidation process, and the tensile stress becomes larger than the thermal expansion coefficient of the oxide film. The pores of the oxide film are generated by the evolution of oxygen during the plasma anodization process. As the arc discharge time during the process is very short (approximately 10 μ s), the oxygen generated during the process is trapped in the high-temperature and high-pressure molten oxide [Ref 11]. As the temperature of the electrolyte increases, the electrical conductivity of the electrolyte also increases. Increasing the electrical conductivity of the electrolyte reduces the breakdown voltage during plasma anodization coating and reduces the dielectric strength. Therefore, the arc discharge persists for a longer time and its intensity is amplified even if the plasma anodization progresses for the same time. The high-strength arc discharge on the surface of the material promotes oxide film sintering, and the temperature is thereafter decreased by the relatively cool electrolyte, to form a dense and uniform oxide film [Ref 12].

Figure 4-5 shows the results of the energy-dispersive X-ray spectroscopy (EDS) element mapping and distribution of Mg, O, and Si in the oxide films at the temperatures of 10 and 50 °C. Mg, O, and Si were the main components of the film and Mg, O, and Si were uniformly distributed within it. At 50 °C, the thickness of the cross-section of the oxide film was relatively uniform. As shown in Figs. 4-3, 4-4, and 4-5, the plasma-anodized oxide film tends to be uniformly formed as the electrolyte temperature increases.

Figure 4-6 shows the mean film thickness determined from the cross-section of the anodized film at 10–50 °C. The thickness of the oxide film tended to decrease as the temperature of the electrolyte increased. The thickness of the oxide film was 41–37 μ m at 10–20 °C and 28–24 μ m at 30–50 °C.

Figure 4-7 shows the EDS analysis results for the surface oxide films formed at 10–50 °C. As the temperature increased, Magnesium and other cations increased whereas oxygen

decreased in mass. This suggests that the oxide films formed at lower temperatures were highly hydrated and as the temperature increased, they became dehydrated, i.e.,



This may also explain the temperature dependence of the thickness of the oxide film, shown in Figure 4-6.

Figure 4-8 shows the corrosion resistance of the samples measured in a 3 mol dm^{-3} NaCl solution using EIS, as a function of the anodizing electrolyte temperature. As expected, the corrosion resistance increased with increase in temperature of the plasma-anodizing electrolyte. In this figure, the corrosion resistance value was related to the magnitude of the AC impedance at 10 Hz, because the Bode plot of the impedance indicated that the magnitude of the impedance was almost constant below 10 Hz.

Figure 4-9 shows the results of a brine spray test performed for 72 h in accordance with the ASTM standard, to evaluate the corrosion characteristics of the plasma-anodized magnesium alloy specimens. The experiment was performed using a 5 wt% NaCl solution and the temperature was maintained at 35 °C. The corrosion properties were quantified by evaluating the average grade number (RN). RN values of 3.5 and 6 were obtained at 10 and 20 °C, respectively, whereas the samples anodized at 30–50 °C showed RN values in the range 7–9. These results mirror the trend observed in the EIS data shown in Figure 4-8. The corrosion resistance is affected by pores in the oxide films, which are attributed to bubble generation during the plasma-anodizing process. In particular, it is important to verify the presence of open pores in order to assess the corrosion resistance of the film because the pores penetrating the oxide film become a passage through which corrosive substances can enter from the outside [Ref 13]. Oxide films formed via plasma anodization usually have a three-layer structure, where the middle layer is the densest and plays the most important role in corrosion resistance [Ref 14].

Figure 4-10 shows the cross-sectional structure of the oxide film, which had been plasma anodized at 10 °C (a) and 50 °C (b), after the salt spray test.

When the electrolyte temperature was 10 °C, as shown in Figure 10 (a), the outer layer had many pores through which aggressive ions could intrude easily and build up where defects were concentrated. This may have led to the eventual breakdown of magnesium substrate locally. In contrast, the film formed at 50 °C had a less porous outer layer. This layer and the middle dense layer appear to have effectively protected the substrate from corrosion.

Figure 4-11 shows that the aggressive Cl^- ions were accumulated in the oxide film cracks, where corrosion proceeded. It shows that the entire oxide film was destroyed by the Cl^- ion, the corrosion product spread over the upper surface of the oxide film, and the protection of the oxide film was lost. The worse surface roughness with more penetrating pores produced at lower temperatures is thus related to the poor durability of the material in a corrosive environment.

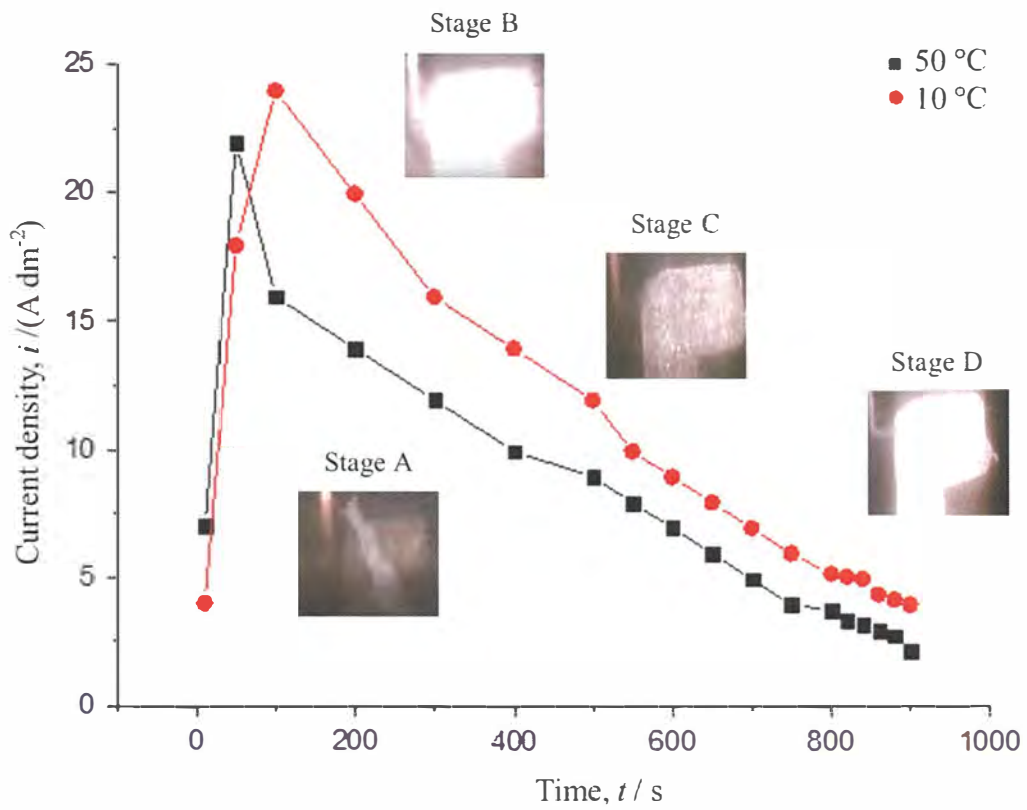


Figure 4-1. Effect of electrolyte temperature on the variation of current density in different stages of plasma anodization.

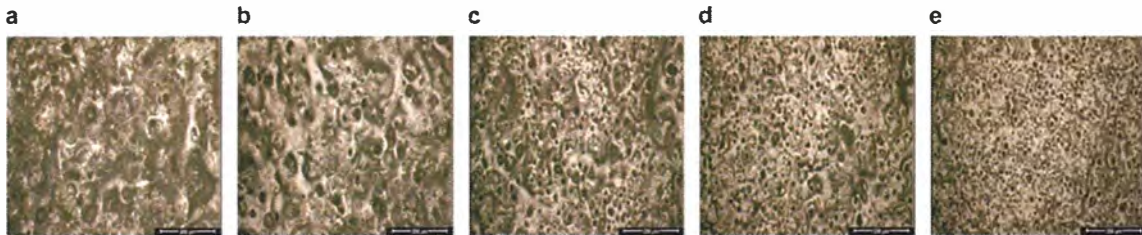


Figure 4-2. Digital microscope surface photographs of plasma anodized AZ91D under the electrolyte temperatures of (a) 10 °C, (b) 20 °C, (c) 30 °C, (d) 40 °C and (e) 50°C.

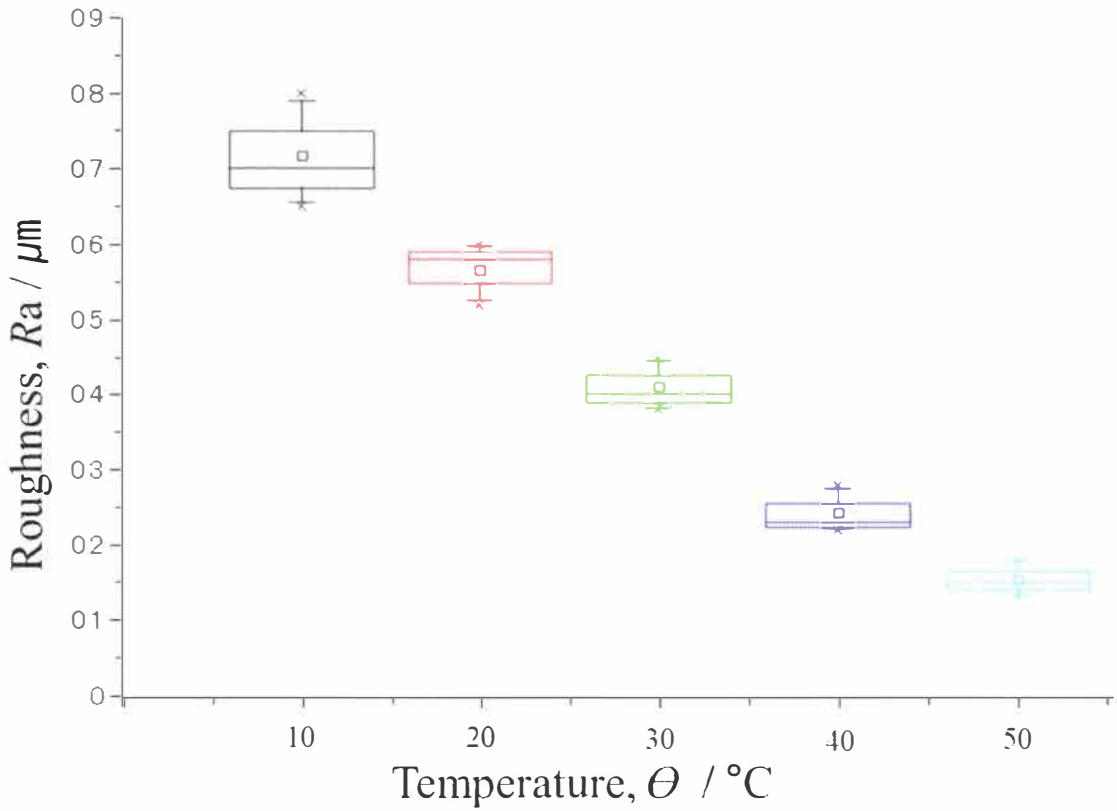


Figure 4-3. Effect of electrolyte temperature on the surface roughness of the AZ91D after plasma anodization.

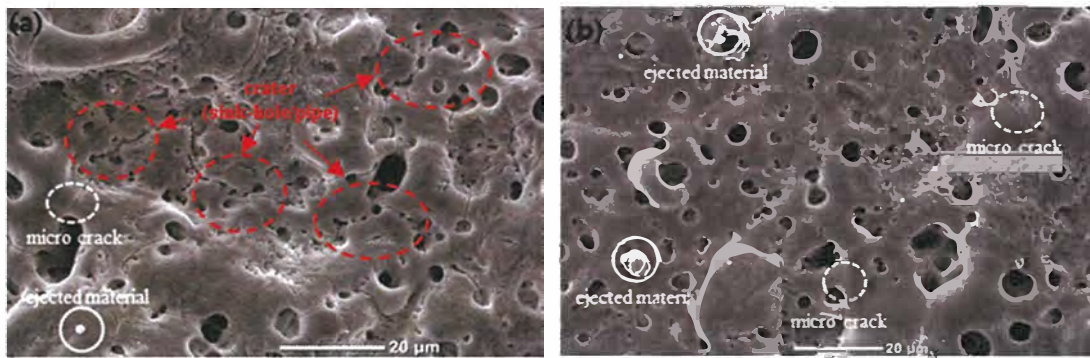


Figure 4-4. Surface morphologies of the AZ91D after pulse plasma anodization at (a) 10 °C and (b) 50 °C.

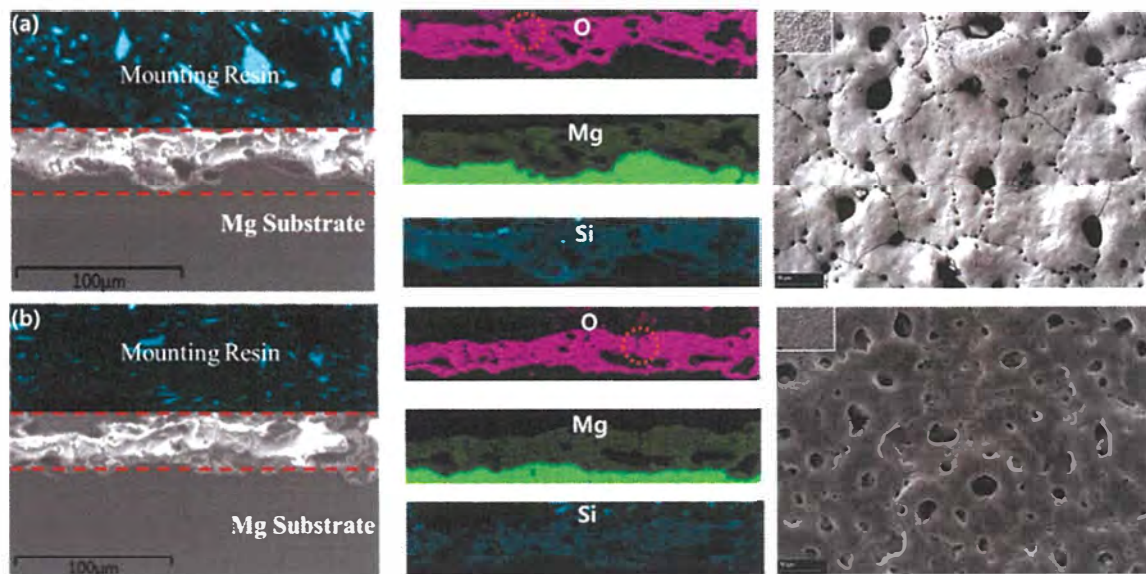


Figure 4-5. Cross-sectional view and EDS mapping of the AZ91D after plasma anodization at (a) 10 °C and (b) 50°C.

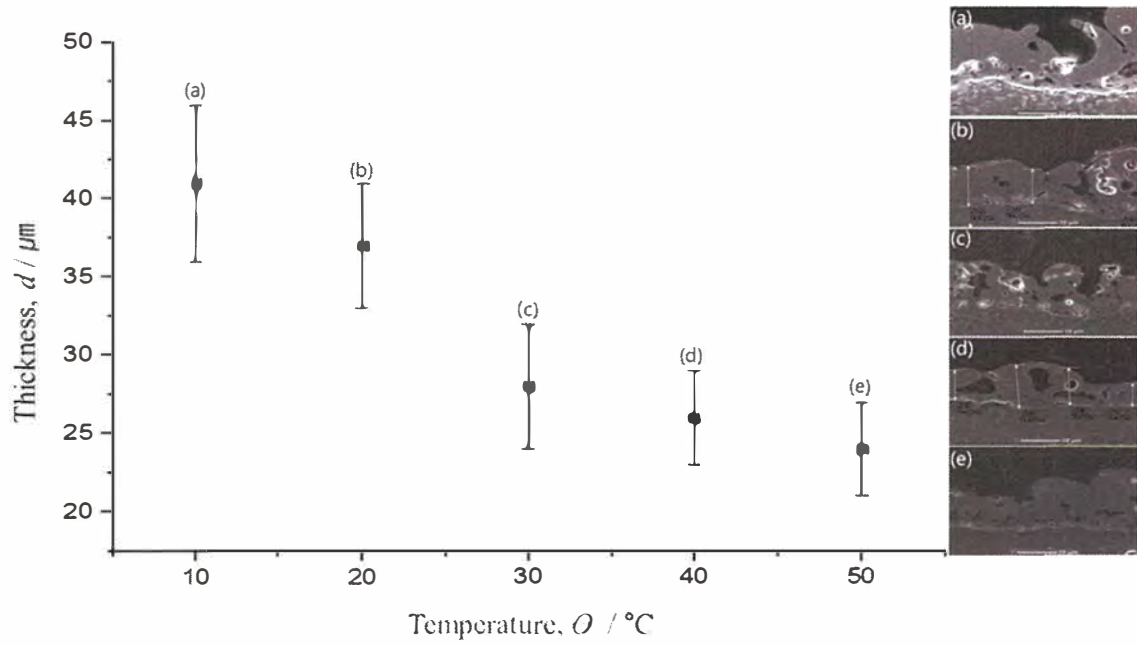


Figure 4-6. Effect of electrolyte temperature on the thickness of oxide film formed by plasma anodization of AZ91D.

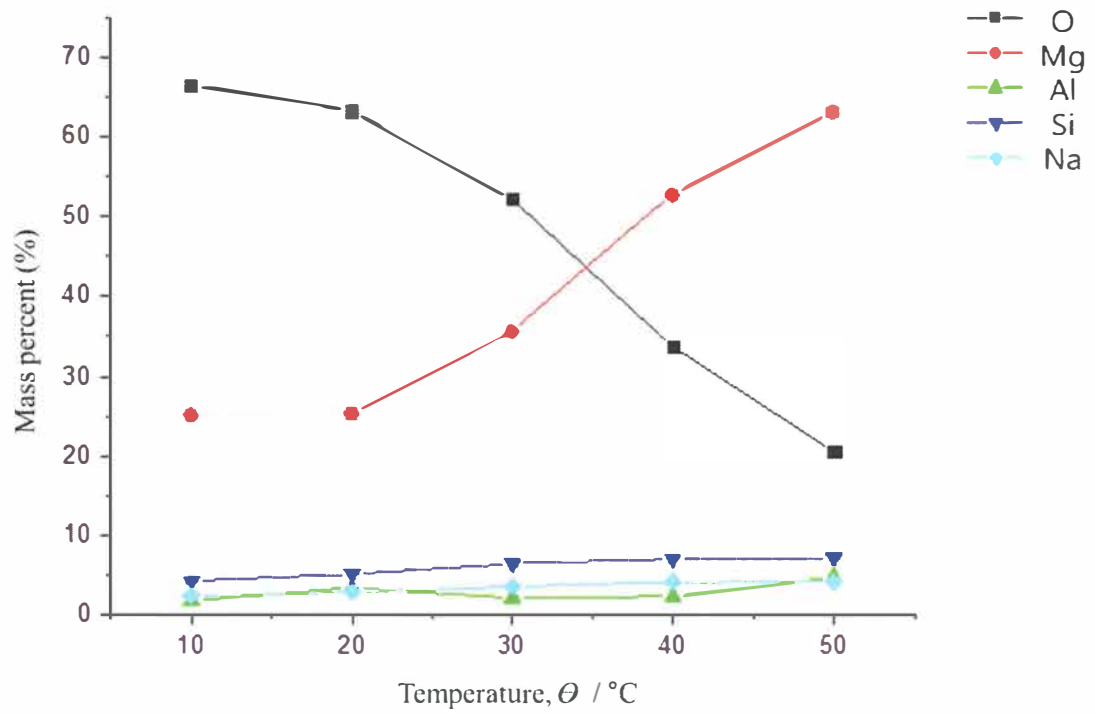


Figure 4-7. Effect of electrolyte temperature on the composition of oxide film formed by plasma anodization of AZ91D.

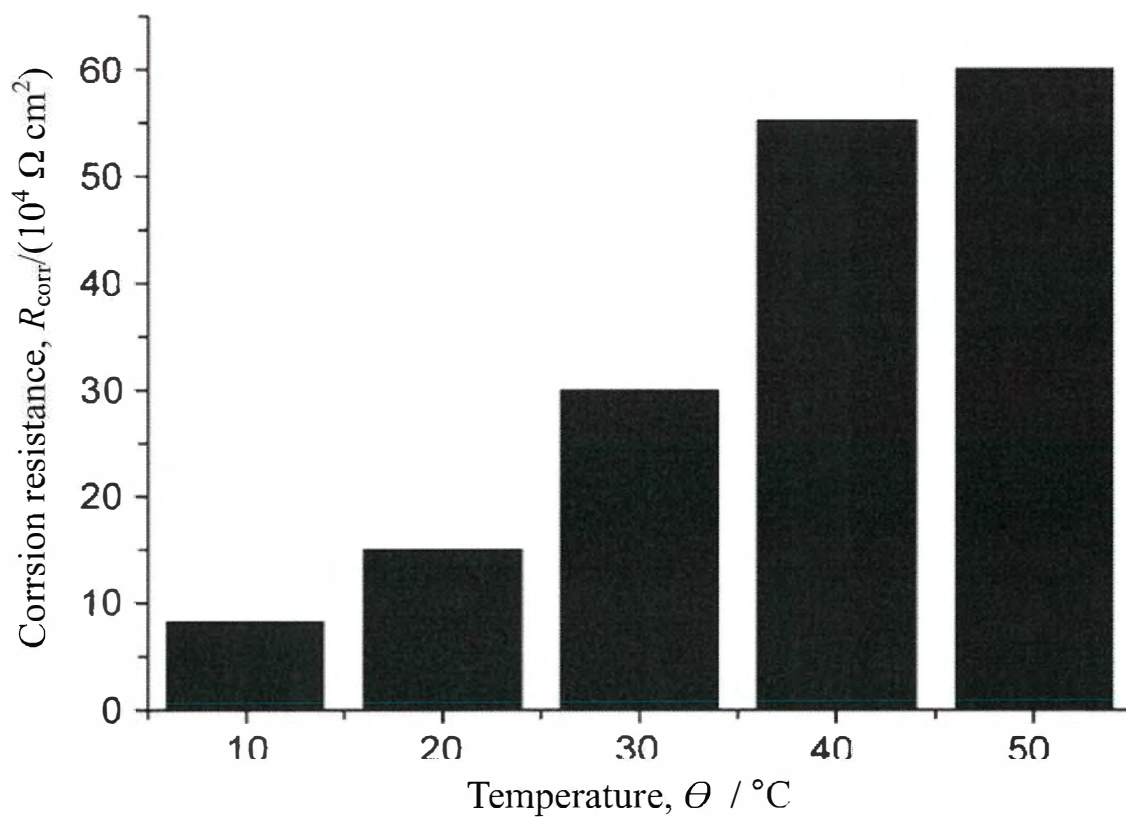


Figure 4-8. Effect of electrolyte temperature for plasma anodization on the corrosion resistance of the treated AZ91D. (Corrosion test solution: $3 \text{ mol dm}^{-3} \text{ NaCl}$, temperature: $25 ^\circ\text{C}$).

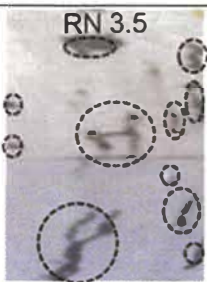
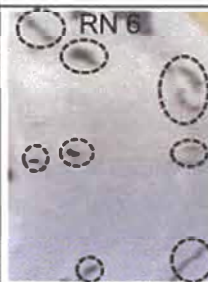
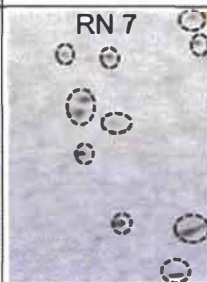
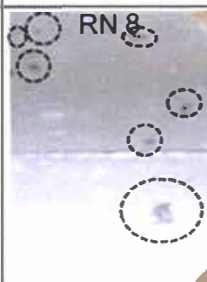
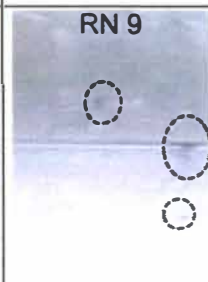
Temp $\theta / ^\circ\text{C}$	10	20	30	40	50
72 Hr	RN 3.5 	RN 6 	RN 7 	RN 8 	RN 9 

Figure 4-9. Effect of electrolyte temperature for plasma anodization of AZ91D on the surface images after the salt spray test (72 h).

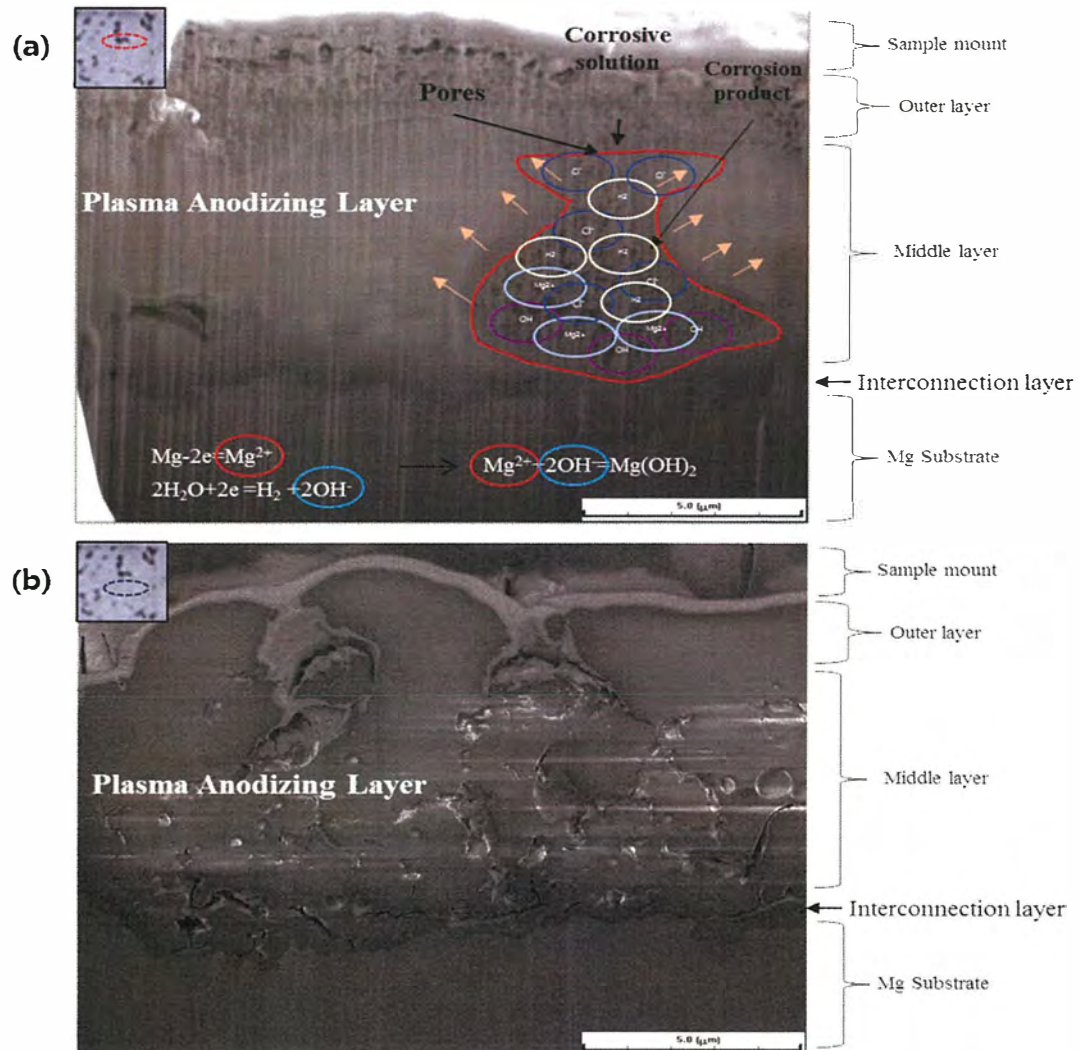


Figure 4-10. Cross-sectional micrographs of the corrosion site of the AZ91D after the salt spray test for 72 h. The oxide layer was formed by the plasma anodization for 15 min with electrolyte temperature of (a) 10 °C and (b) 50°C.

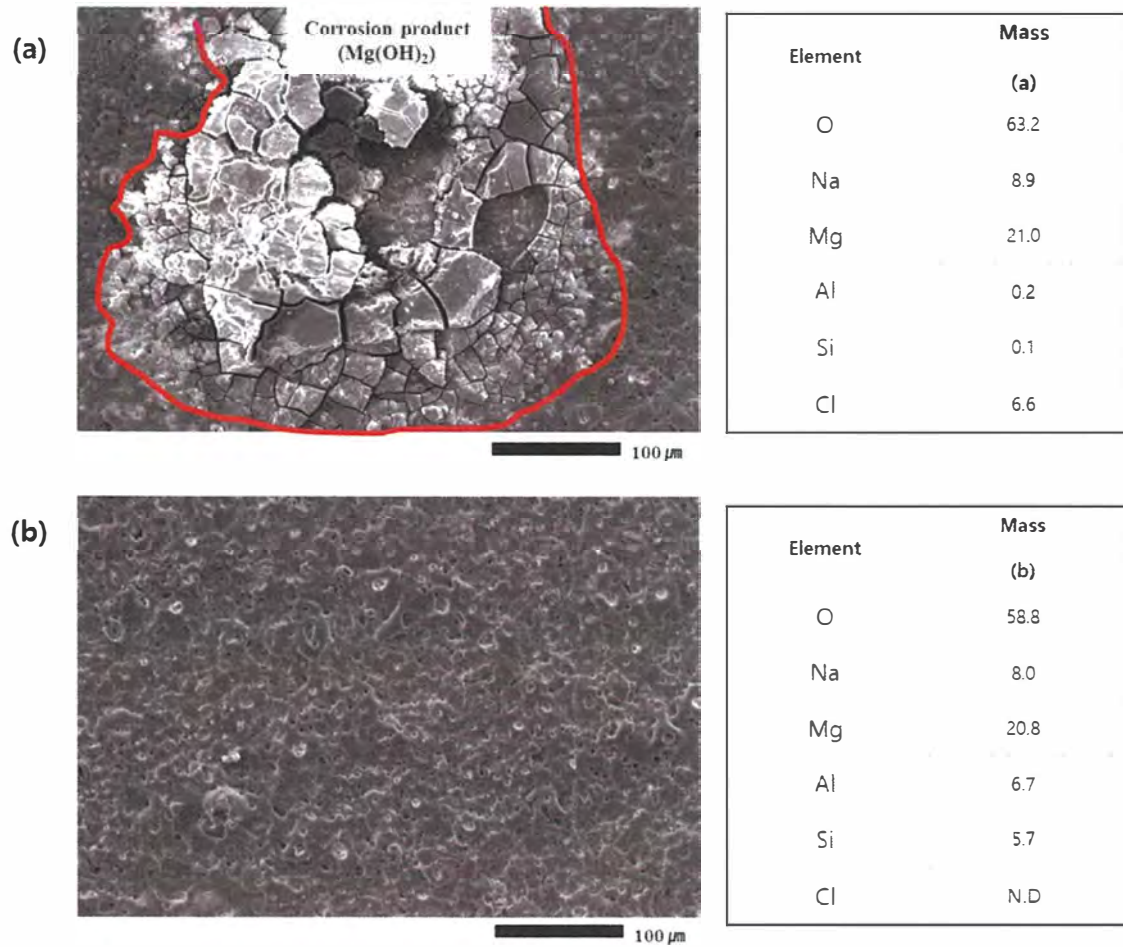


Figure 4-11. Surface micrographs of the corrosion area and EDS component analyses of the AZ91D after the salt spray test for 72 h. The specimens were plasma anodized with electrolyte temperature of (a) 10 °C and (b) 50°C.

4.2.2 Effect of sodium hydroxide concentration of plasma anodic oxidation on the properties of oxide film formed on AZ91D magnesium alloy

In order to investigate the influence of the NaOH concentration on the formation of the plasma oxide film, the pulse voltage was fixed at 150 V at 50 °C for 15 min, and the NaOH concentration was changed among 0.06 M, 0.13 M, and 0.25 M.

Figure 4-12 is an optical microscope image of the oxide film formed on the AZ91D material after plasma anodizing treatment, in which the concentration of the NaOH was changed from 0.06 M to 0.25 M at a fixed voltage of 150 V for 15 min. The surfaces of the oxide films formed in all samples contain crater traces, pores generated by secretions, and uneven products that generate craters. This phenomenon is caused by the plasma explosion of the surface of the sample at high temperature at which molten magnesium reacts rapidly with the electrolyte and is cooled. It was found that the size of the pores produced by the plasma and the amount of released product decreased with increasing NaOH concentration.

Figure 4-13 shows the roughness of the specimen with changes in NaOH concentration. As the NaOH concentration increased from 0.06 M to 0.25 M, the surface roughness decreased from 0.52 to 0.08 and 0.06 μm . The higher the concentration of the NaOH, the lower the surface roughness is.

Figure 4-14 shows the FESEM images of the sample surface treated at concentrations of NaOH of 0.06 M, 0.13 M, and 0.25 M. The surface of the specimen treated at 0.06 M showed uneven porosity and some eject material and microcracks, which are holes created by the plasma at the material/oxide interface, leading to a porous coating with low durability [Ref 11]. The surface of oxidized specimens treated at 0.13 M and 0.25 M showed a relatively constant pore size and only a small amount of eject material was detected on the surface. Also, the number of eject material and microcracks was relatively small. As the concentration of the electrolyte increases, the electrical conductivity of the electrolyte also increases. Increasing the electrical conductivity of the electrolyte lowers the breakdown voltage and reduces the dielectric strength during plasma anodization. Thus, the arc discharge forms a dense and uniform oxide film even if the plasma anode proceeds for the same time [Ref 7].

Figures 4-15, 16 and 17 show the average film thickness, structure, and composition determined from the cross section of plasma anodic oxide film formed in electrolytes with different NaOH concentrations. As seen from Figure 4-15, the thickness of the oxide film tends to decrease with increasing NaOH concentration. The thicknesses of the oxide films were 21–35 μm (0.06 M), 16.5–22.5 μm (0.13 M), and 7–18 μm (0.25 M). The plasma anodic oxide film had few defects and uniformly formed as the NaOH concentration increased, and the thickness was relatively low.

Figure 4-17 shows the EDS elemental mapping and distribution results for Mg, O and Si in the oxide film. Mg, O and Si were the main components of the film, and Si and O were uniformly distributed. As the concentration of NaOH increased, magnesium increased and oxygen decreased in mass. This can also explain the concentration dependence of the oxide thickness shown in Figures 4-16 and 17.

Figure 4-18 shows the corrosion resistance measured in a 3 mol dm^{-3} NaCl solution using EIS as a function of NaOH concentration. In this figure the corrosion resistance value is related to the magnitude of the AC impedance at 10 Hz. As expected, an increase in NaOH concentration improves corrosion resistance, among which corrosion resistance is the best at the concentration of 0.13 M.

Figure 4-19 shows the results of a brine spray test performed for 72 h in accordance with ASTM standards to evaluate the corrosion characteristics of plasma anodized magnesium alloy specimens in electrolytes with different NaOH concentrations. The RN values were 6 for NaOH concentration of 0.06 M and 9.5 and 8, for NaOH concentrations of 0.13 and 0.25 M, respectively. These results reflect the observed effects of surface roughness, thickness, and trends in EIS data.

Figures 4-18 and 4-19 show that the corrosion resistance is improved as the concentration of the NaOH increases and is the best at the concentration of 0.13 M.

Generally, the thicker the coating layer in the coating process such as plating, the better the corrosion resistance. However, in the case of the oxide coating process, i.e., plasma anodization, the corrosion resistance is not proportional to the thickness of the oxide coating. In this experiment, the concentration of NaOH affects the arc discharge time and the arc strength as shown in the cross-sectional image of the oxide film in Fig. 4-18 and 19, and ultimately affects the oxide microstructure. As a result, when the test pieces are

simultaneously treated at the same current density, the density of the oxide film becomes high as the concentration of the NaOH becomes high. High density oxide films significantly improve the corrosion resistance. The oxide film of high density with lower porosity cannot be penetrated easily by aggressive ions, hence the corrosion resistance is excellent.

Figures 4-19 and 4-20 show the surface and composition of the oxide film after the plasma anodization for 72 h with 0.06 M (a), 0.13 (b) and 0.25 M (c) of NaOH. Aggressive Cl^- ions accumulate in the oxidized film cracks that have undergone corrosion, indicating that the entire oxide film is destroyed by Cl^- ions and the corrosion products spread on the upper surface of the oxide film and the protection of the oxide film is lost. The deteriorated surface roughness with more defects and pores at 0.06 M is therefore associated with lower durability of the material in a corrosive environment.

4.3 Conclusion

The plasma anodization process for AZ91D alloy was evaluated with respect to the electrolyte temperature, which can be optimized by obtaining a uniform oxide layer with better corrosion resistance. The concentration of defects in the oxide layer decreased as the processing temperature was increased from 10 to 50 °C. The surface roughness also decreased, and the corrosion resistance increased from $RN = 3.5$ to 9. It was confirmed that Mg, Al, O, and Si were uniformly distributed on the surface of the oxide film in the optimized condition. As the electrolyte temperature increased, the oxygen content in the oxide film decreased because of dehydration of hydroxide. Cl^- ions were detected in the corroded area.

The anodizing process was also evaluated in relation to the NaOH concentration, and the NaOH concentration was optimized in terms of a uniform oxide layer and better corrosion resistance. As the concentration of treating NaOH increased from 0.06 M to 0.13 M and 0.25 M, the surface roughness decreased, the thickness of the oxide film decreased, and the oxide film defect on the surface and the cross section also decreased. The optimum NaOH concentration was 0.13 M and the corrosion resistance increased from $RN = 6.0$ to 9.

Based on the results of this study, a higher temperature of the electrolyte is favorable for plasma anodization of AZ91D to obtain a film with higher homogeneity and corrosion resistance, and the NaOH concentration of 0.13 M is favorable for plasma anodizing of AZ91D, where a film with excellent homogeneity and corrosion resistance is obtained.

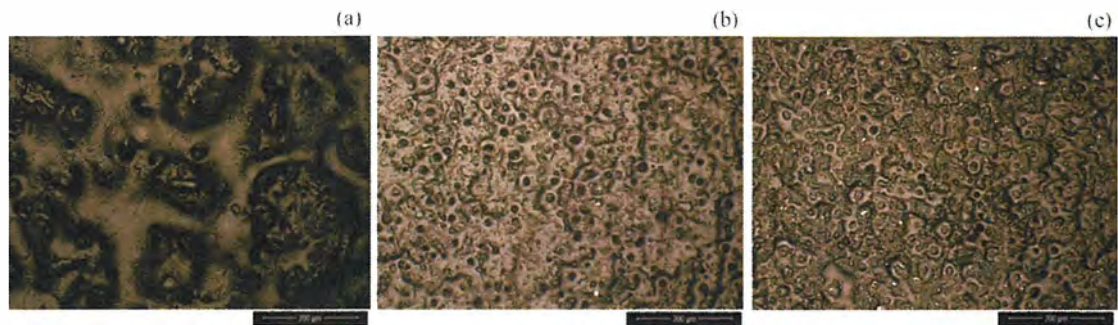


Figure 4-12. Digital microscope surface photographs of AZ91D plasma-anodized in electrolytes with NaOH concentrations of (a) 0.06 M, (b) 0.13 M, (c) 0.25 M.

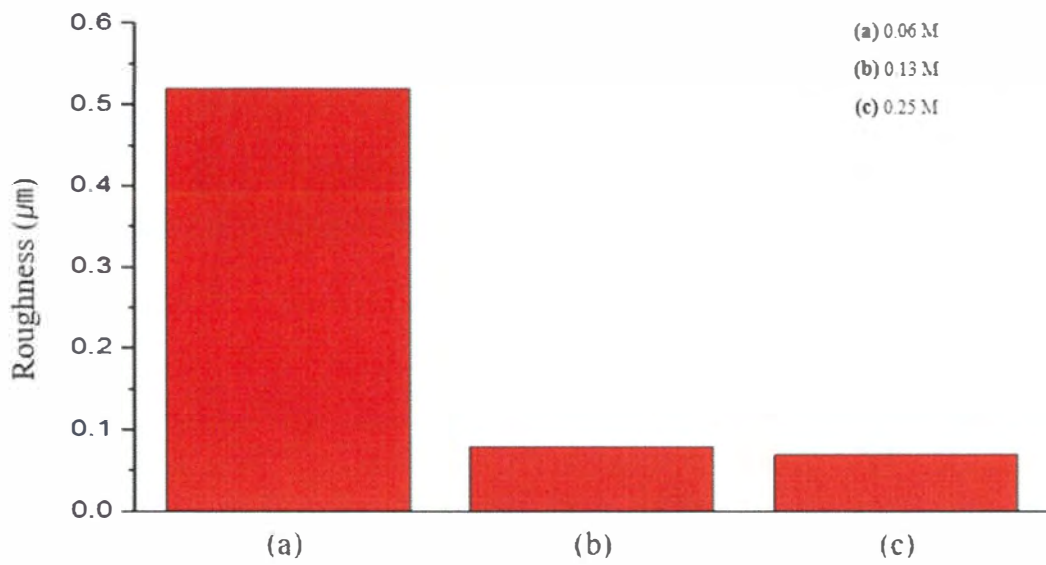


Figure 4-13. Surface roughness of the oxide film formed on AZ91D by the plasma anodization in electrolytes with NaOH concentrations of (a) 0.06 M, (b) 0.13 M, (c) 0.25 M.

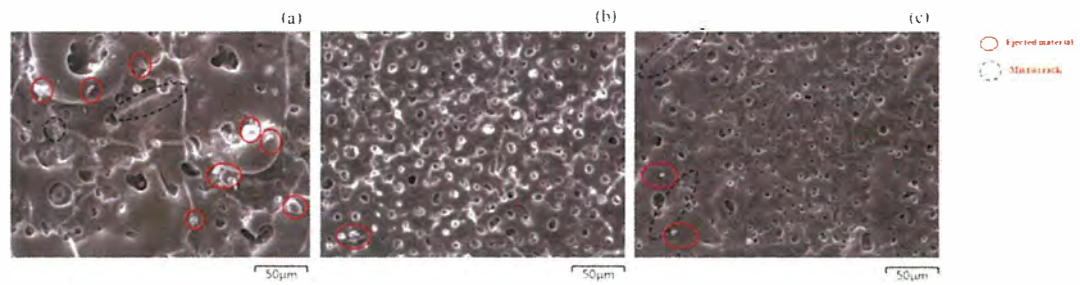


Figure 4-14. Surface morphologies of AZ91D after plasma anodization in electrolytes with NaOH concentration of (a) 0.06 M, (b) 0.13 M, (c) 0.25 M.

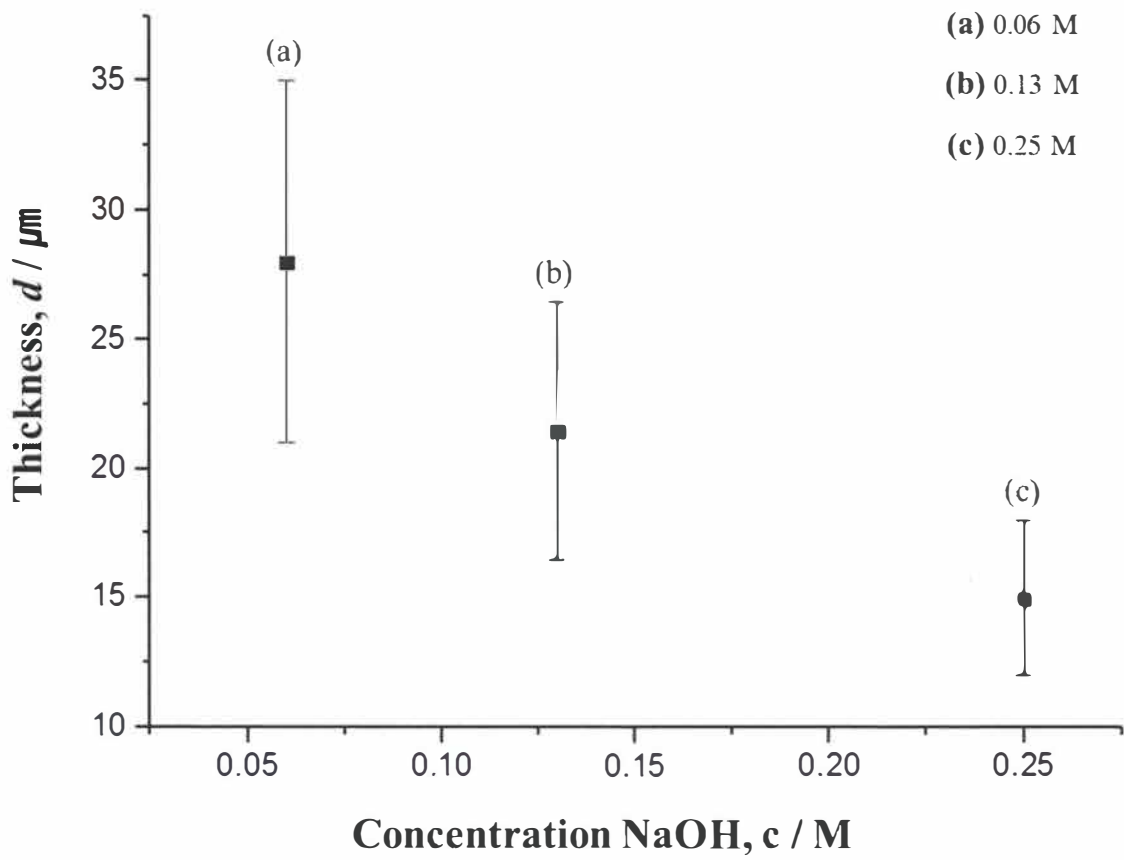


Figure 4-15. Thickness of oxide films formed on AZ91D by plasma anodization in electrolytes with NaOH concentrations of (a) 0.06 M, (b) 0.13 M, (c) 0.25 M.

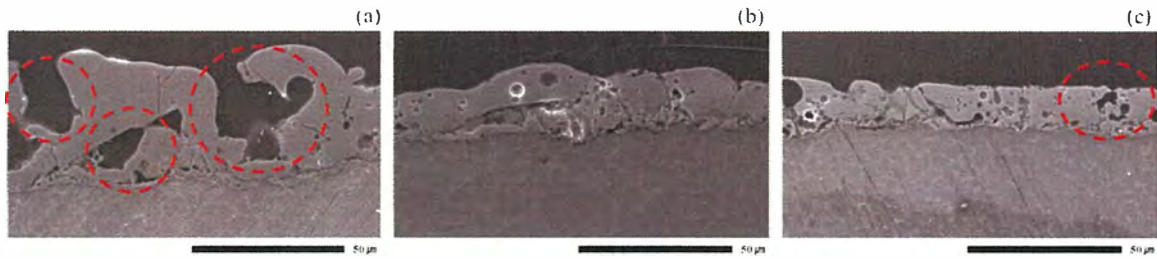


Figure 4-16. Cross-sectional views of AZ91D after plasma anodization in electrolytes with NaOH concentrations of (a) 0.06 M, (b) 0.13 M, (c) 0.25 M.

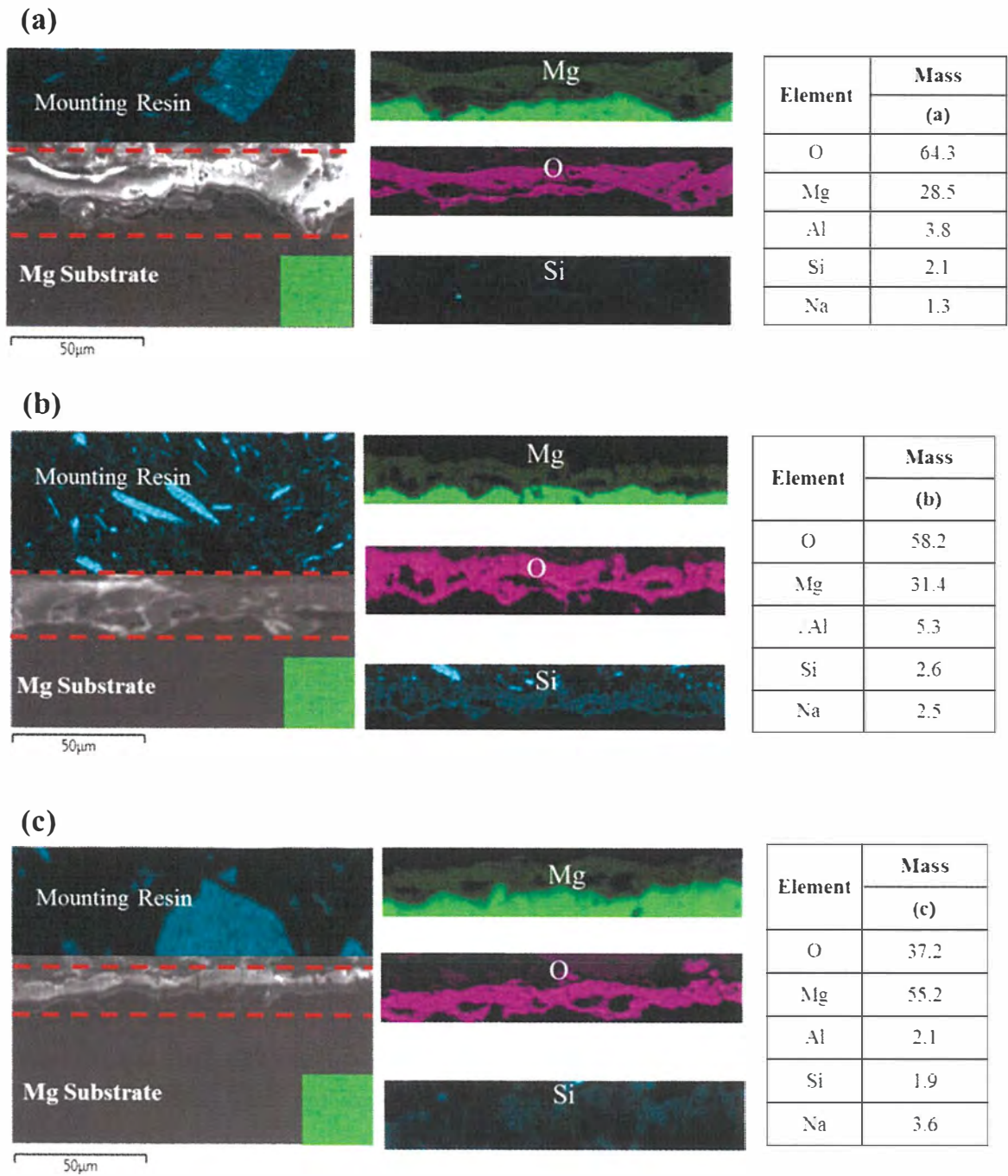


Figure 4-17. Cross sectional views of AZ91D after plasma anodizing in electrolytes with NaOH concentrations of (a) 0.06 M, (b) 0.13 M, (c) 0.25 M.

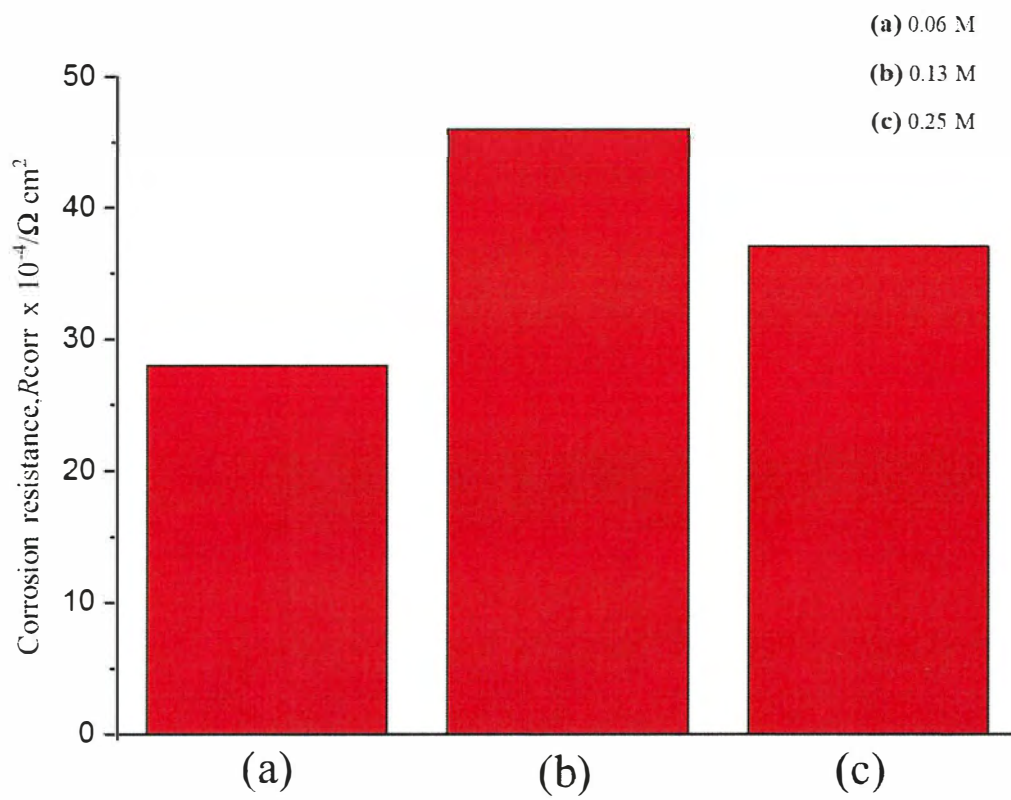


Figure 4-18. Effect of NaOH concentration for plasma anodization on the corrosion resistance of the treated AZ91D (Corrosion test solution: $3 \text{ mol dm}^{-3} \text{ NaCl}$, temperature: $25 \text{ }^\circ\text{C}$).

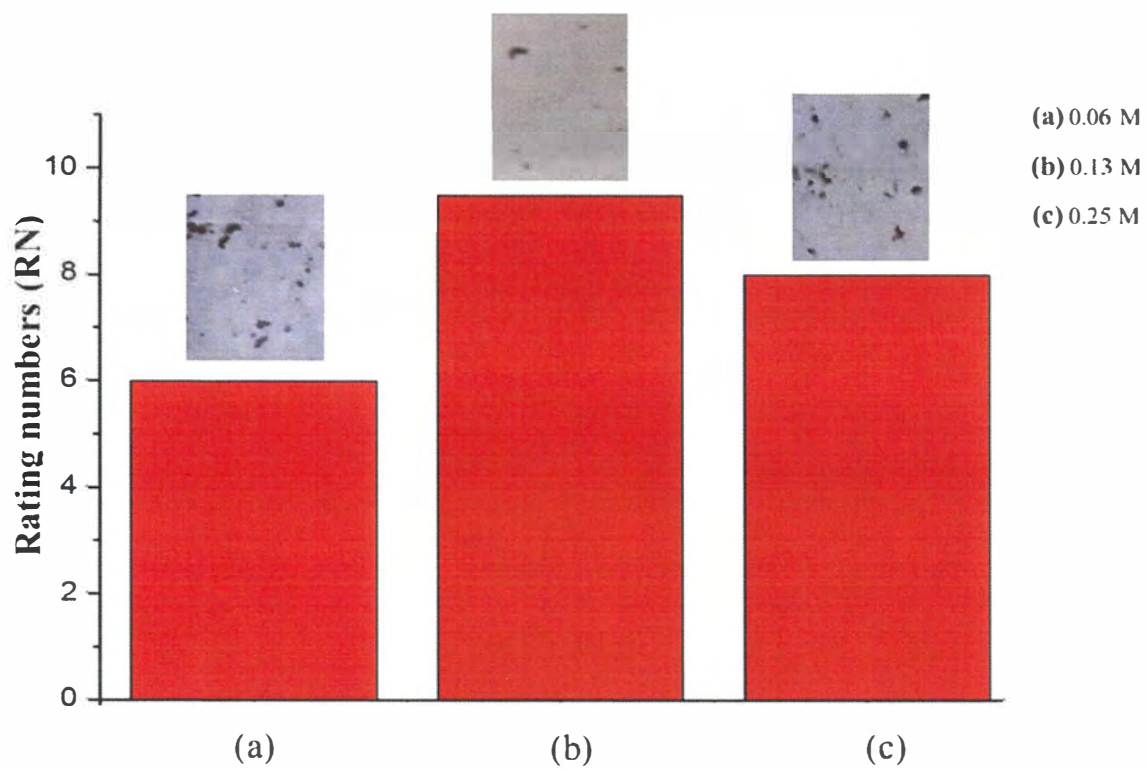


Figure 4-19. Surface images and RN values after the salt spray test (72 h) for the AZ91D plasma anodized in electrolytes with NaOH concentrations of (a) 0.06 M, (b) 0.13 M, (c) 0.25 M.

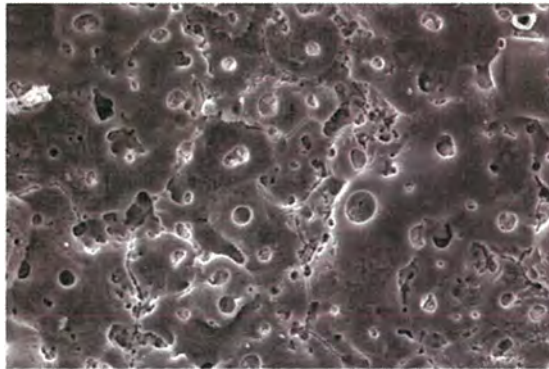
(a)



Element	Mass
	(a)
O	59.8
Mg	24.9
Al	4.2
Si	3.5
Na	3.4
Cl	4.2

50µm

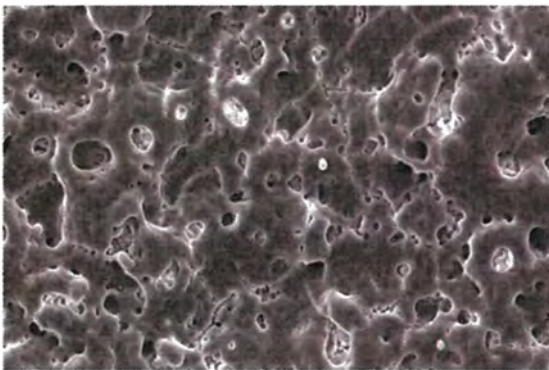
(b)



Element	Mass
	(b)
O	60
Mg	29.3
Al	5.2
Si	3.7
Na	1.8
Cl	N.D

50µm

(c)



Element	Mass
	(c)
O	44.2
Mg	48.7
Al	1.8
Si	1.5
Na	3.8
Cl	N.D

50µm

Figure 4-20. Surface micrograph of the corrosion area of AZ91 and EDS component analysis after the salt spray test (72 h) for the AZ91D plasma-anodized in electrolytes with NaOH concentration of (a) 0.06 M, (b) 0.13 M, (c) 0.25 M.

4.4 References

1. Lee, S. H., Yashiro, H., & Kure-Chu, S. Z., *J. Korean Inst. Surf. Eng*, **50(6)** (2017) 432-438.
2. S.H. Lee, H. Yashiro and S.-Z. Kure-Chu., Effect of Power Mode of Plasma Anodization on the Properties of formed Oxide Films on AZ91D Magnesium Alloy, *Korean Journal of Materials Research*, **28(10)** (2018) 544-550.
3. Mordike, B. L., & Ebert, T, *Materials Science and Engineering: A*, **302(1)** (2001) 37-45.
4. Song, G., Atrens, A., Stjohn, D., Nairn, J., & Li, Y, *Corrosion Science*, **39(5)** (1997) 855-875.
5. Ma, Y., Nie, X., Northwood, D. O., & Hu, H., *Thin Solid Films*, **494(1-2)** (2006) 296-301.
6. Gray, J., & Luan, B., *Journal of alloys and compounds*, **336(1-2)** (2002) 88-113.
7. Srinivasan, P. B., Blawert, C., & Dietzel, W., *Materials Science and Engineering: A*, **494(1-2)** (2008) 401-406.
8. Zhang, Y., Yan, C., Wang, F., Lou, H., & Cao, C., *Surface and Coatings Technology*, **161(1)** (2002) 36-43.
9. Duan, H., Du, K., Yan, C., & Wang, F., *Electrochimica Acta*, **51(14)** (2006) 2898-2908.
10. S. Moon and Y. Nam, Anodic Oxidation of Mg–Sn Alloys in Alkaline Solutions, *Corros. Sci.*, **65** (2012) 494-501.
11. E. Atar, C. Sarioglu, U. Demirler, W. Sabri Kayali, and H. Cimenoglu, Residual Stress Estimation of Ceramic Thin Films by X-ray Diffraction and Indentation Techniques, *Scripta Mater.*, **48(9)** (2003) 1331-1336.
12. Narayanan, T. S., Park, I. S., & Lee, M. H., *Progress in Materials Science*, **60** (2014) 1-71.
13. Kwon, D., & Moon, S., Effects of NaOH Concentration on the Structure of PEO Films Formed on AZ31 Mg Alloy in PO_4^{3-} and SiO_3^{2-} Containing Aqueous Solution, *Journal of the Korean institute of surface engineering*, **49(1)** 46-53(2016).
14. Y. Yan, Y. Han, D. Li, J. Huang, and Q. Lian, Effect of NaAlO_2 Concentrations on Microstructure and Corrosion Resistance of $\text{Al}_2\text{O}_3/\text{ZrO}_2$ Coatings Formed on Zirconium by Micro-arc Oxidation, *Appl. Surf. Sci.*, **256(21)** (2010) 6359-6366.

Chapter V. Physical properties of oxide films on AZ91D magnesium alloy formed by plasma anodization

Published in:

- Sung-Hyung Lee, Hitoshi Yashiro, Kazuki Aoki, Hidetaka Nanao, Song-Zhu Kure-Chu, Physical Properties of Oxide Films on Mg Alloy Formed by Plasma Anodization. *Korean Journal of Materials Research*, (11) Published November 2019.

5.1 Introduction

In the preceding chapters, magnesium alloy AZ91D was successfully treated by plasma anodization to enhance corrosion resistance. There are some additional demands for the magnesium alloy to be applied for commercial use. Tribological property is one of the most important criteria to be evaluated because such corrosion-resistant layer needs to be strong enough against wear.

Because magnesium alloys are not only light but excellent in heat conductivity, they are expected to be used as a heat sink in electric devices. However, scarce study is available on the thermal conductivity of the corrosion-resistance layer formed by plasma anodizing. In this chapter, the effect of electrolyte temperature for the plasma anodization on the heat conduction property, dielectric breakdown voltage and mechanical properties of the oxide film was investigated.

5.2 Results and Discussion

5.2.1 Film morphology

Figure 5-1 shows the top views and cross-sectional images of the samples treated at various temperatures and the energy-dispersive X-ray spectroscopy (EDS) element mapping of Mg, O and Si. The surface of the specimens treated at 10, 20 and 30 °C showed uneven porosity and some microcracks and craters. The surface and cross section of oxidized specimens treated at 40 and 50 °C showed a relatively constant pore size. The elements of Mg, O and Si in the oxide film are uniformly distributed within the film at every temperature. Plasma anodic oxide films tend to be formed uniformly with decreasing thickness of the oxide film as the electrolyte temperature is increased [Ref 1].

5.2.2 Dielectric breakdown voltage

Figure 5-2 shows the results of dielectric breakdown voltage measurements for the plasma anodized AZ91D alloy in electrolytes with different temperatures. The dielectric breakdown field of MgO is about 10 MV m^{-1} [Ref 2]. The specimen plasma-anodized at 50 °C had an oxide film with mean thickness of 24 μm . The breakdown voltage of 280 V corresponds to the breakdown field of 13 MV m^{-1} which is close to the value of MgO. On the contrary, the breakdown voltage was as high as 1080 V for the specimen plasma anodized at 10 °C, with oxide layer of about 40 μm . The breakdown field of the oxide layer was doubled to 26 MV m^{-1} as compared with the value at 50 °C [Ref 1]. The result may be attributed to that the oxide film formed at 10 °C had large pore and voids and that many micro cracks dispersed electricity.

5.2.3 Heat conducting property

Heat conducting property of the plasma anodized AZ91D was evaluated by the laser flash method. In this test, a laser energy pulse was applied to the AZ91D surface and the temperature change at the oxide surface was followed as shown in Fig 5-3. The temperature change is generally characterized by the half time $t_{1/2}$ in Fig 5-3, from which thermal diffusivity can be calculated according to the Parker formula:

$$\alpha = 0.1388d^2 / t_{1/2} \quad (5-1)$$

where α is thermal diffusivity ($\text{mm}^2 \text{K}^{-1}$) and d is the thickness of sample. In the case of AZ91D without anodized oxide layer, $t_{1/2}$ was 0.048 s giving the α value of $36 \text{ mm}^2 \text{K}^{-1}$.

As shown in Fig 5-4, $t_{1/2}$ increased as the surface of AZ91D was covered with oxide film. The largest value of $t_{1/2}$ was observed for the specimen plasma anodized at 10°C . There seems a correlation between the breakdown voltage and $t_{1/2}$; as the oxide layer becomes thinner or denser, the layer becomes less resistant against electric or thermal gradient. Although it is difficult to derive the thermal diffusivity value of the oxide layer from this experiment, pure MgO is known to have relatively high thermal diffusivity of $19 \text{ mm}^2 \text{s}^{-1}$ [Ref 2]. Thermal conductivity of MgO as calculated by the following equation [Ref 3,4] is $59 \text{ W m}^{-1}\text{K}^{-1}$:

$$\lambda = \alpha \times \rho \times C_p \quad (5-2)$$

where λ ($\text{W m}^{-1} \text{K}^{-1}$) is the thermal conductivity, ρ (g cm^{-3}) is the density and C_p ($\text{J g}^{-1} \text{K}^{-1}$) is the specific heat. On the other hand, the thermal conductivity of AZ91D as calculated from $\alpha = 36 \text{ mm}^2 \text{K}^{-1}$, $\rho = 1.65 \text{ g cm}^{-3}$ and $C_p = 0.90 \text{ J g}^{-1} \text{K}^{-1}$ is $53 \text{ W m}^{-1} \text{K}^{-1}$. This value shows a good agreement with the reported value of $51.2 \text{ W m}^{-1} \text{K}^{-1}$ [Ref 5]. Thus, the thermal conductivity of AZ91D is almost one-third of the pure magnesium ($160 \text{ W m}^{-1} \text{K}^{-1}$) because of the introduction of alloying element of Al, Zn and Mn.

The experimental result that $t_{1/2}$ increased by the plasma anodization indicates that the thermal conductivity of the plasma anodizing oxide layer is somewhat lower than the value of the raw material. A thermal conductivity value of about $8 \text{ W m}^{-1} \text{K}^{-1}$ was reported for the plasma anodizing oxide layer on the Mg alloy material [Ref 6,7].

The plasma anodizing oxide film acts as a thermal barrier and the thickness of the oxide film and the thermal conductivity are inversely proportional to each other. The thermal resistivity of the anodized AZ91D (R) is expressed according to:

$$R = \frac{L_1}{\lambda_1} + \frac{L_2}{\lambda_2} \quad (5-3)$$

where L_1 and L_2 are thickness of mother alloy and oxide layer, and λ_1 and λ_2 are thermal conductivity of mother alloy and oxide layer respectively. The thicker and less dense nature

of the oxide layer formed at lower temperature is thus disadvantageous for heat conducting property. The apparent thermal resistivity of a 3 mm thick plate of AZ91D would increase by 5 % by the plasma anodization at 50 °C assuming values $L_1 = 3$ mm, $\lambda_1 = 53$ W m⁻¹ K⁻¹, $L_2 = 24$ μm and $\lambda_2 = 8$ W m⁻¹ K⁻¹.

5.2.4 Tribological property

Figure 5-5 shows the surface hardness of the AZ91D plasma anodized at different temperatures of electrolyte. The surface hardness of the AZ91D raw material was 80 HV, while the value increased after the plasma anodizing treatment at the electrolyte temperatures of 10, 20, 30, 40 and 50 °C to 422, 578, 580, 628 and 634 HV, respectively. Compared to the AZ91D raw material, hardness increased 5-7 times by the plasma anodization.

It is believed that the reason for the difference in hardness by the electrolyte temperature is the resulting difference in film density depending on the growth rate of the film at different temperatures.

Figure 5-6 shows the results of the friction test under the condition of Table 2, in which the normal load was 50 (a), 10 (b) and 1 N (c), respectively.

As a result of the test, at the normal load of 50 N, the oxide film on the surface of the specimen was completely removed with formation of track width of 750 μm. The center of the upper ball (SUJ2 steel, Ø 10mm, 810 HV) is estimated to have sunk into AZ91D (80 HV) by 14 μm. At the normal load of 10 N, the bare track width became 580 μm corresponding to the maximum depth of 8 μm. At the normal load of 1 N, the oxide film remained present after the test and the wear width was about 350 μm. In order to evaluate the mechanical property of the oxide layer formed at different temperature, a normal load of 1 N was set under the condition of Table 2-2.

Figure 5-7 shows the result of friction test for the plasma anodized AZ91D at 20, 30, 40, and 50 °C. The results showed that the worn width was about 850 μm for the films formed at 20 and 30 °C. In the case of films formed at 40 and 50 °C, the wear scar was about 350 μm in width. This result is due to the higher surface hardness of the films formed at 40 and 50 °C, as shown in Fig. 5-5. As shown in Fig 4-3, the surface roughness at 40, 50 °C was much smoother with less defects.

Figure 5-8 shows SEM images of the surface of the films formed at 20 and 50 °C after the friction test. There is no pore shape in the film formed 20 °C after the friction test. On the other hand, the film formed at 50 °C had a pore shape which was crashed after the

friction test. These results are related to the hardness of the surface. The oxide layer formed at 20 °C is relatively soft and easy to be deformed on contact with the steel ball. This is why a wide scar formed as show in Fig 5-7 (a). The oxide layer formed at 50 °C is rather hard and deformed area is limited to cause a narrow scar as show in Fig 5-7 (d). It was confirmed that the oxide film was crushed and broken during the friction test.

It is apparent that the scar width decreases with increase of electrolyte temperature for plasma anodization as summarized in Fig 5-9. The above results are consistent with the results in Figure 5-7.

5.3 Conclusion

In this chapter, the physical and mechanical properties of AZ91D magnesium alloy were evaluated as a function of electrolyte temperature for plasma anodization. As the temperature of the electrolyte increased from 10 °C to 50 °C, the breakdown voltage became lower because the formed oxide layer became thinner with less defect at high temperature. The oxide layer formed by the plasma anodization were evaluated how they block heat conducting property of AZ91D by a laser flash method. The results indicated that heat resistivity became smaller as the electrolyte temperature became higher because of the same reason for decreasing of breakdown voltage. According to the results of friction test, the surface hardness increased and the wear amount of the oxide film decreased as a result of increase of electrolyte temperature for plasma anodizing. These results are due to that as the temperature of the electrolyte increases, the surface hardness increases, the surface and cross-sectional defects decrease, the density decreases, and the surface roughness decreases. Based on the results of this study, the higher the temperature of the electrolyte for plasma anodizing, the better the physical and mechanical properties of the formed oxide layer on AZ91D.

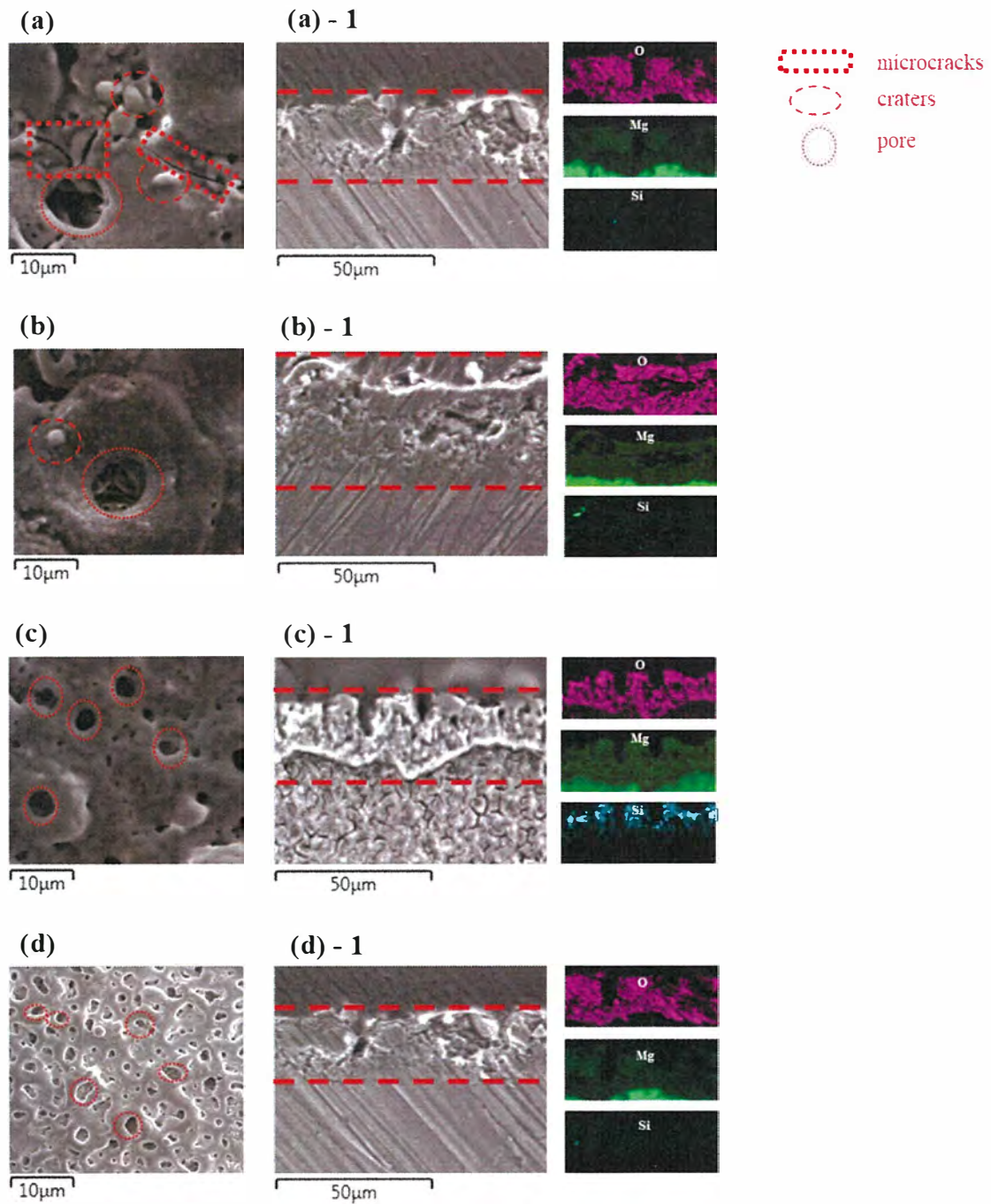


Figure 5-1. Surface and cross-section morphologies and EDS element mapping of the AZ91D after plasma anodization at (a) 20 °C, (b) 30 °C, (c) 40 °C and (d) 50 °C.

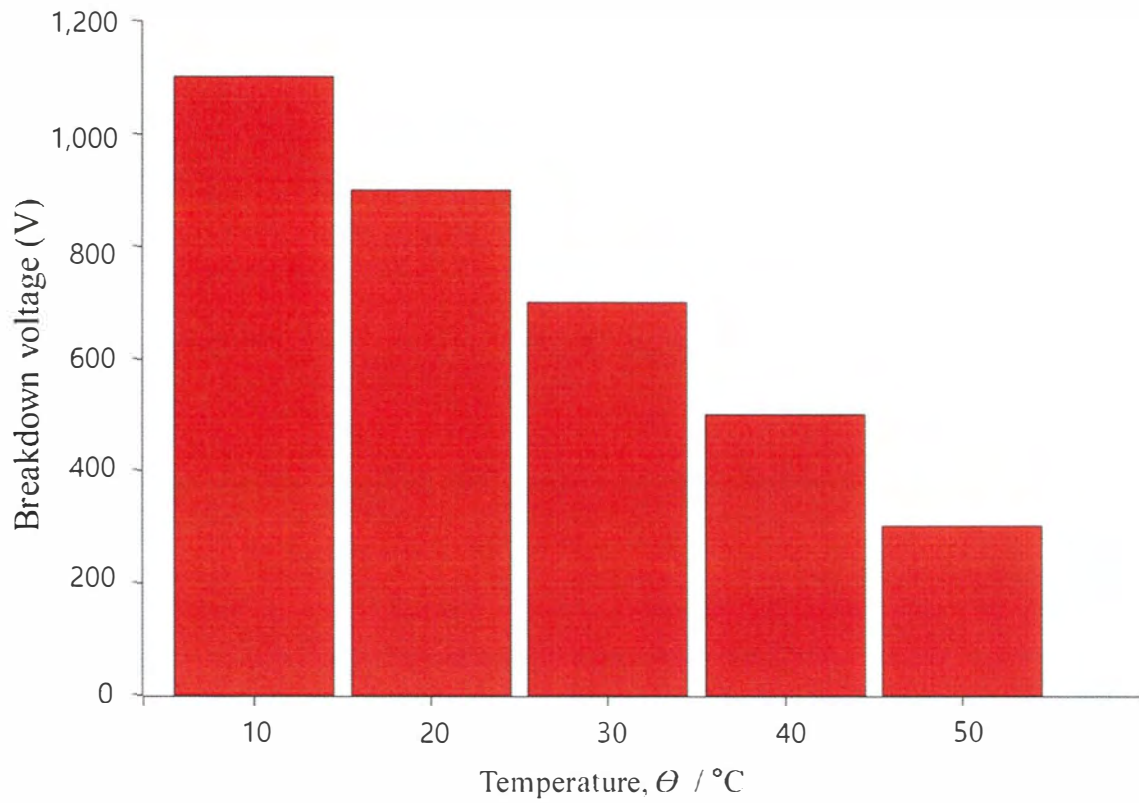


Figure 5-2. Effect of electrolyte temperature on the breakdown voltage of the AZ91D after plasma anodization.

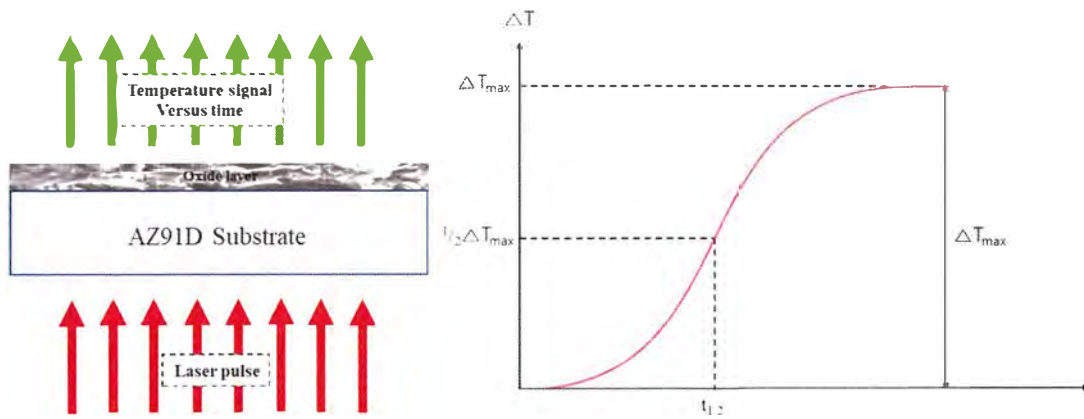


Figure 5-3. Thermal diffusion measurement by laser flash method on AZ91D magnesium alloy material.

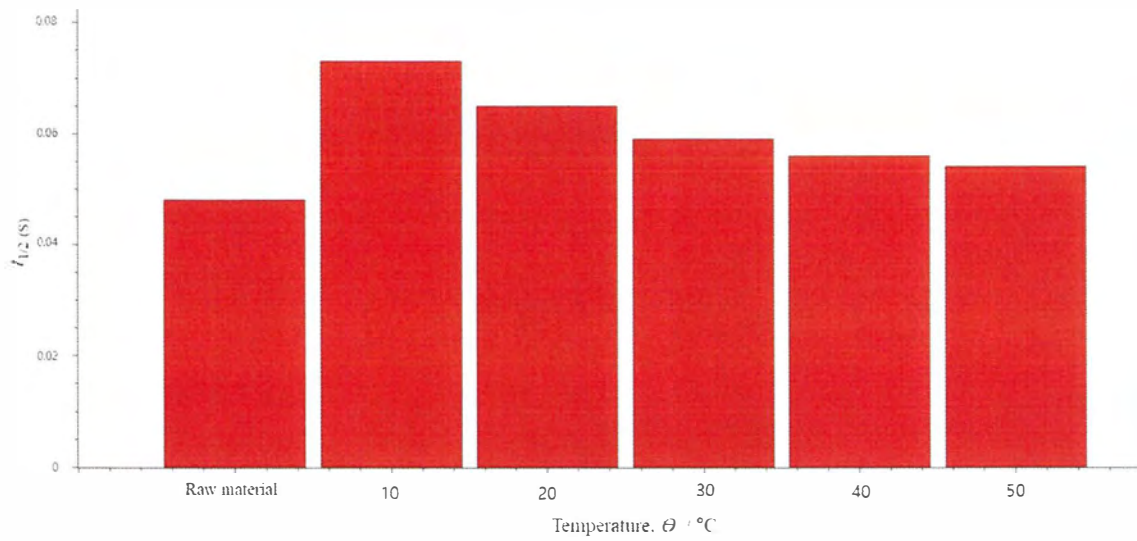


Figure 5-4. The half time ($t_{1/2}$) determined from the laser flash method for the AZ91D after plasma anodization in the electrolyte of different temperatures.

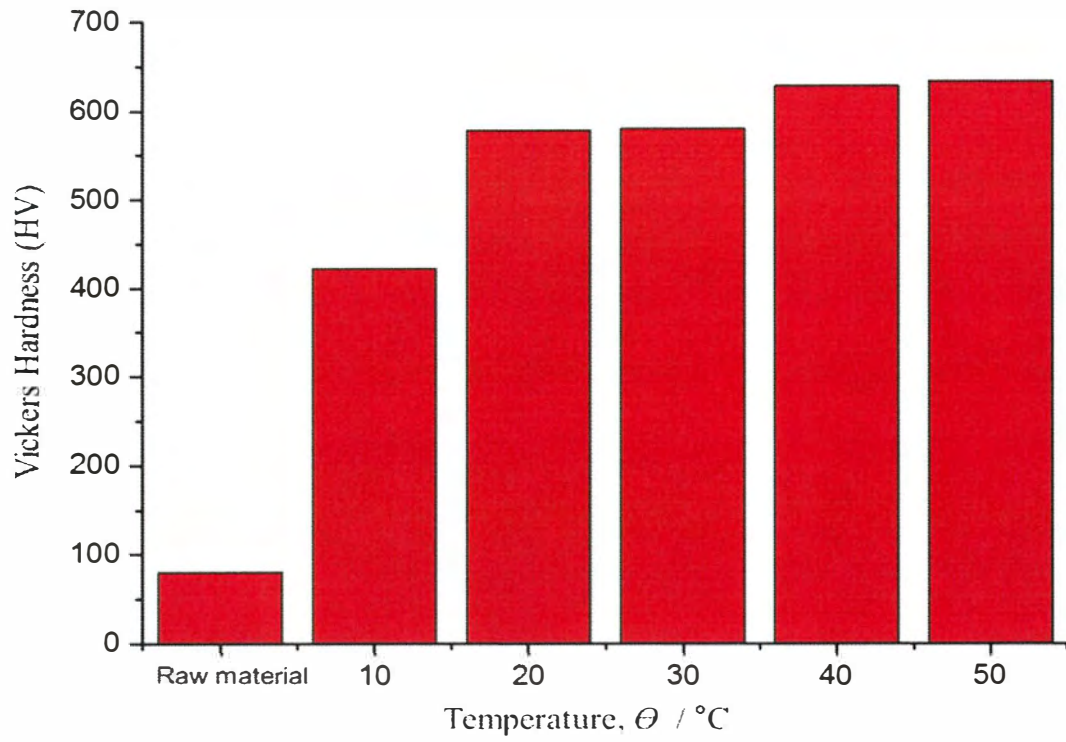


Figure 5-5. Effect of electrolyte temperature on the Vickers hardness of the AZ91D after plasma anodization.

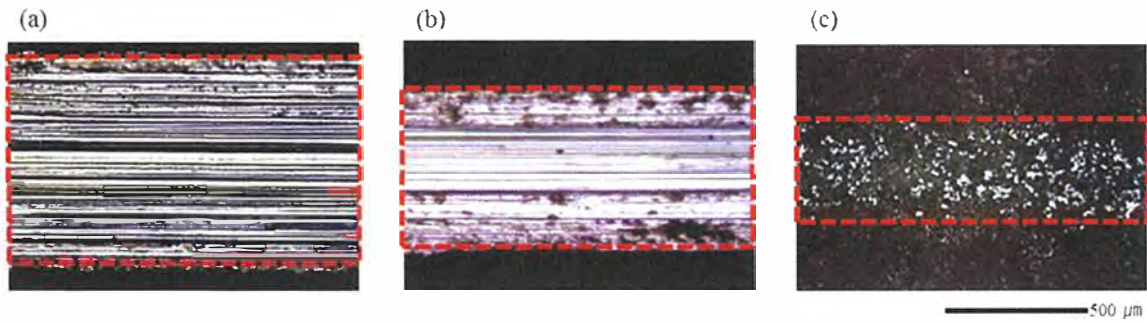


Figure 5-6. Digital microscope surface photograph of AZ91D magnesium alloy after the surface friction test under the applied load of (a) 50 N, (b) 10 N and (c) 1 N. Specimens were plasma anodized by pulsed voltage of 150 V for 15 min at 50 °C.

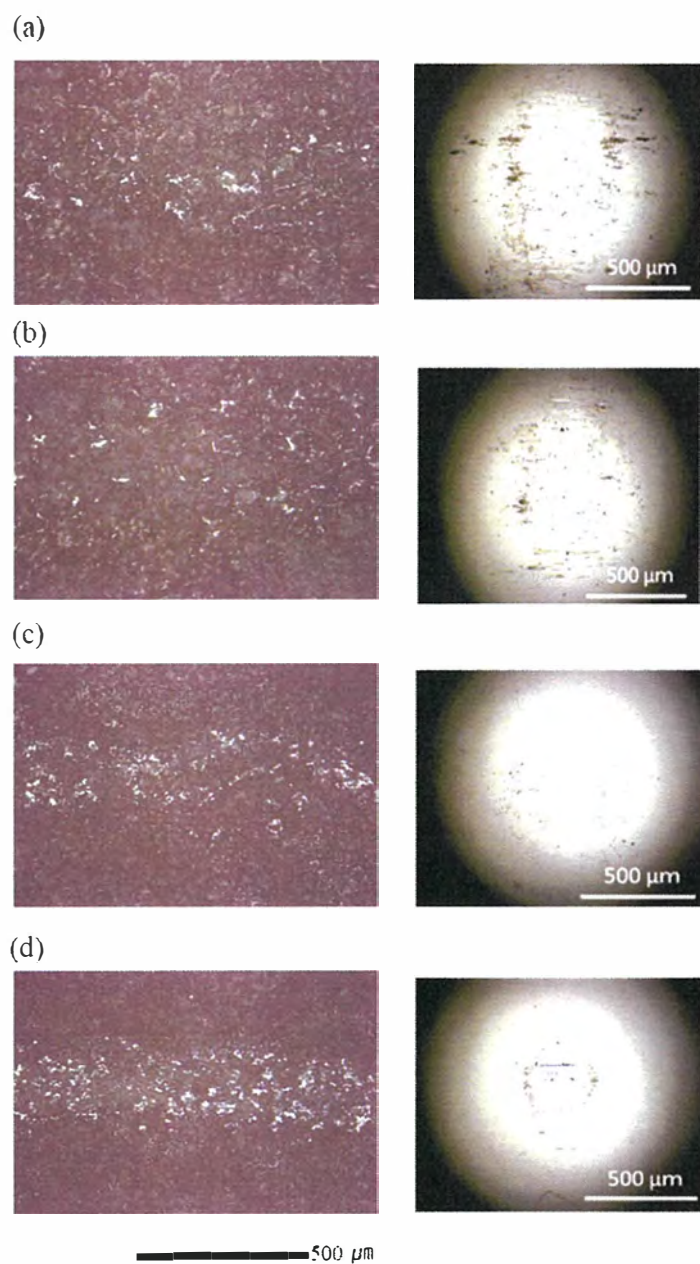


Figure 5-7. Digital microscope surface photographs of AZ91D and SUJ2 steel ball after surface friction test after plasma anodization of AZ91D at (a) 20 °C, (b) 30 °C, (c) 40 °C and (d) 50 °C.

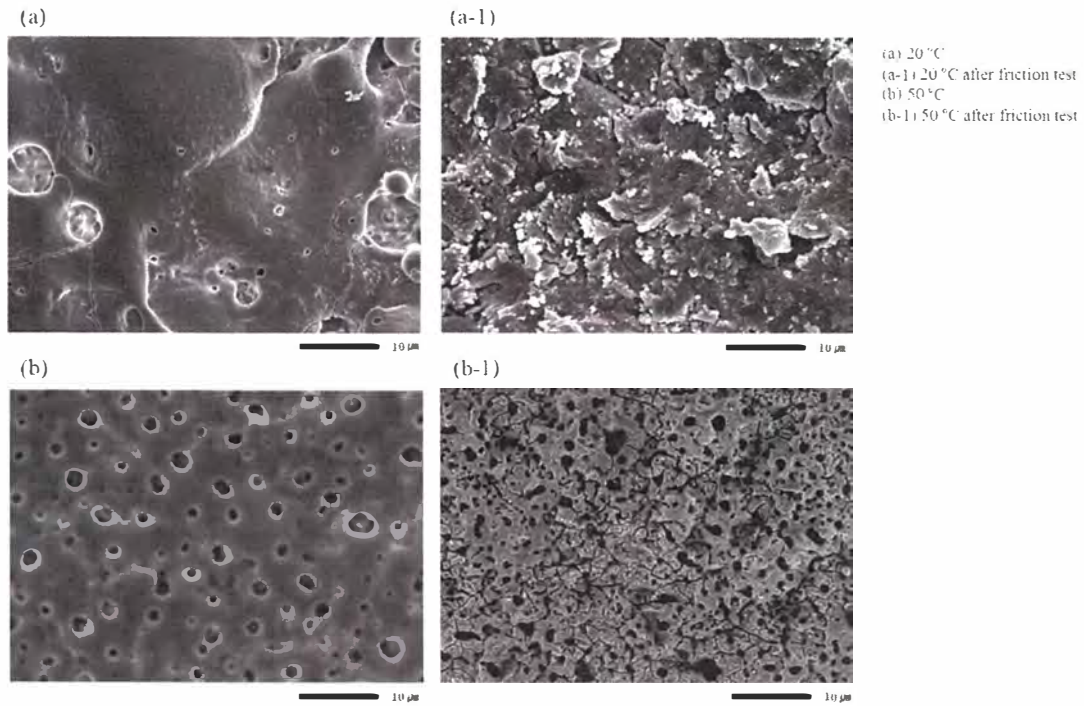


Figure 5-8. Surface comparison of AZ91D before (left) and after (right) the surface friction test. Specimens were plasma anodized under the electrolyte temperature of (a) 20 °C and (b) 50 °C.

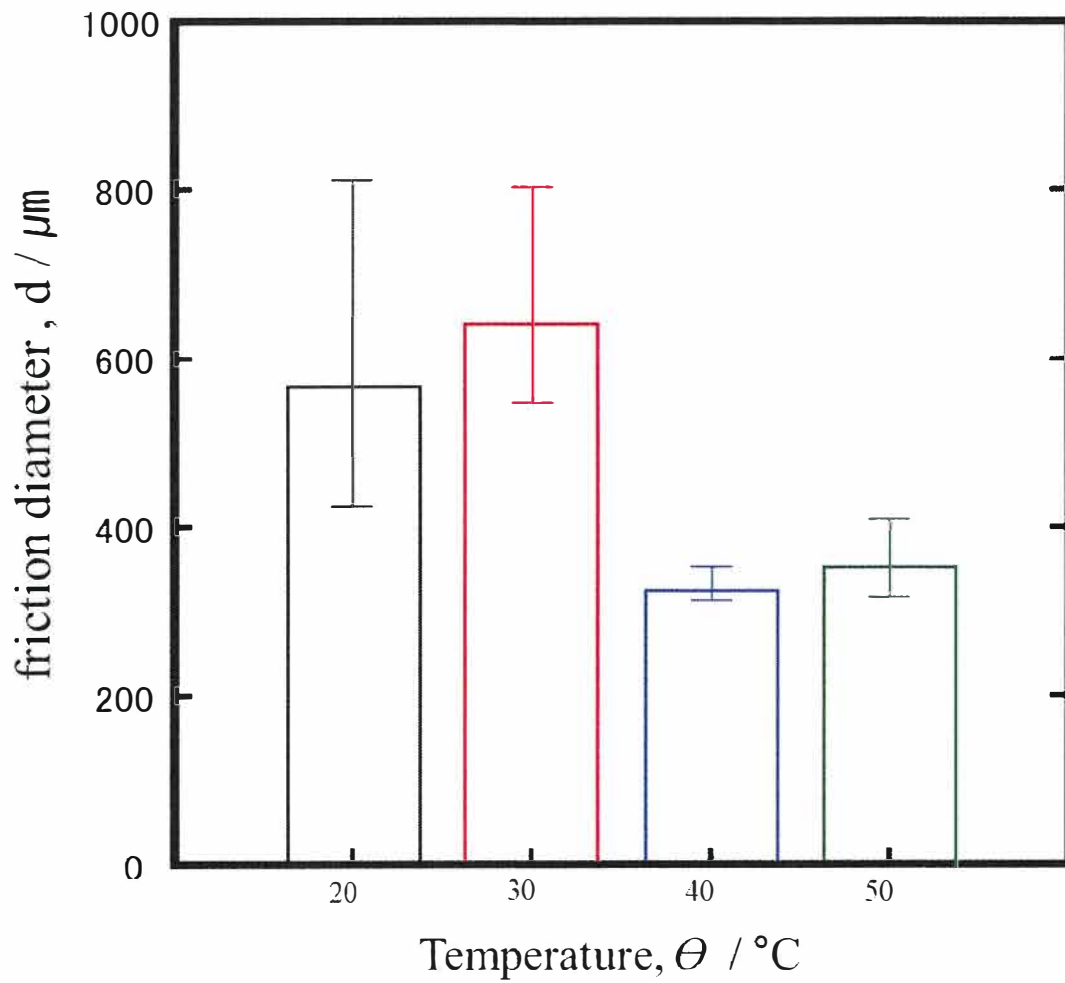


Figure 5-9. Comparison of wear diameter of SUJ2 steel balls after friction test with AZ91D plasma anodized at different electrolyte temperatures.

5.4 References

1. S.H. Lee, H. Yashiro and S.-Z. Kure-Chu, Electrolyte Temperature Dependence on the Properties of Plasma Anodized Oxide Films Formed on AZ91D Magnesium Alloy, *Korean Journal of Materials Research*, **29.5** (2019) 288-296.
2. Beauchamp, E. K. "Effect of microstructure on pulse electrical strength of MgO, *Journal of the American Ceramic Society*, **54.10** (1971) 484-487.
3. Humrickhouse-Helmreich, Carissa J., Rob Corbin, and Sean M. McDeavitt, "Measurement of thermal diffusivity of depleted uranium metal microspheres. *Journal of Nuclear Materials* **446.1-3** (2014) 100-105.
4. Kuniya, Keiichi et al., *Thermal conductivity, electrical conductivity and specific heat of copper-carbon fiber composites*, *Transactions of the Japan institute of metals*, **28.10** (1987) 819-826.
5. Yuan, Guangyu et al., "Effects of heat treatment on the thermal properties of AZ91D magnesium alloys in different casting processes, *Journal of Alloys and Compounds*, **766** (2018) 410-416.
6. J.A. Curran, T. W. W. T. Clyne, Thermo-physical properties of plasma electrolytic oxide coatings on aluminium, *Surf. Coatings Technol.*, **199** (2005) 168–176.
7. J.A. Curran, H. Kalkanci, Y. Magurova, T.W. Clyne, Mullite-rich plasma electrolytic oxide coatings for thermal barrier applications, *Surf. Coatings Technol.*, **201** (2007) 8683–8687.

Chapter VI. Comparative evaluation of the surface treatment effect of AZ91D alloy material

Published in:

- Lee, Sung-Hyung, Hitoshi Yashiro, and Song-Zhu Kure-Chu. "Comparative Evaluation of Surface Treatment Effect of AZ91D Alloy Material." *Ijasre* **5(5)** (2019) DOI: 10.31695/IJASRE.2019.33213.

6.1 Introduction

A new plasma anodizing process for AZ91D alloy has been developed in the previous chapter. In this chapter, the new plasma anodization method is compared with conventional surface treatment methods, i.e. non – chromate and anodizing.

As shown in Tables 6-1 and 6-2, non-chromate and anodizing are currently used as surface treatment methods for magnesium alloys, especially for AZ91D alloy, as a proven surface treatment method that eliminates environmental problems such as the use of chromic acid and fluoride poisonous materials [Ref 1,2]. In order to select the best surface treatment method to improve the performance of the AZ91D alloy, various factors such as the surface treatment process and the characteristics of the oxide film must be considered This study compares the characteristics, structure and corrosion resistance of AZ91D alloy treated by non-chromate, anodizing and plasma anodizing processes.

6.2 Results and Discussion

Figure 6-1 shows the change in current and surface image during the plasma anodizing and conventional anodizing of the AZ91D material. The plasma anodizing method proceeds from the step A to the steps B-C where the maximum plasma is generated starting from the generation of gas, and to the step D where the volume of the plasma is increased [Ref 3]. In the anodizing process, a fine plasma is generated along with gas generation in step A, and a step B is performed in which only a minute amount of gas is generated over time. The anodizing process is a lower-voltage process compared to the plasma anodizing process.

Figure 6-2 shows the surface structure and composition of the AZ91D after non-chromate, anodization and plasma anodization. It was confirmed that Mg, O and P were uniformly distributed in the result of the EDS element mapping showing the distribution of the oxide film component in the phosphate coating of the non-chromate. Since it is an electroless surface treatment method, the pores of the surface are not visible and the thin oxide layer is uniformly present.

In the case of anodization and plasma anodization, Mg, O and Si were uniformly distributed as the main components of the oxide film in all the EDS element mapping. In the plasma anodizing, the surface of the oxide layer showed a larger size of the pore. Applying a pulse voltage of 200 V resulted in more pronounced non-uniformity and a larger pore size. The voids appearing on the surface are formed by the oxygen bubbles generated when microscale arcs are formed on the surface during the plasma anodizing process. Since the size of the microscale arc is proportional to the magnitude of the current, the higher the applied voltage, the larger the pore size [Ref 4]. The non-uniform growth pattern of the oxide film and the oxygen bubble trapping during the growth process lead to the formation of a wider porous layer in the ceramic layer.

Figure 6-3 shows cross-sectional images of each specimen for indicating the thickness of each oxide layer. The thickness of the non-chromate oxide film layer was confirmed to be 1 μm or less. The anodized product had oxide thickness of 5–10 μm and a plasma anodized product of 10–20 μm thickness. The thickness of the oxide film of the specimen treated with a 200 V voltage in the plasma anodizing surface treatment process is two or three times larger than that of the specimen treated at 50 V. In addition, the size of the

pores in the plasma anodized product was large and voids were recognized in the cross section.

Figures 6-4 and 5 show the results of laser flash response as characterized by $t_{1/2}$ and breakdown voltage of oxide films formed by three treatments on AZ91D alloy material. In the results of the $t_{1/2}$, the value is lower in the order of non-chromate, anodization and plasma anodization. In addition, the results of the dielectric breakdown voltage measurements were inversely related. The results mainly reflect the difference in thickness of the oxide films.

Figure 6-6 shows the surface microhardness of AZ91D alloy material specimens with different surface treatments. The surface hardness of the non-chromate treated surface was 80 HV, which is the same as that of the AZ91D alloy raw material, and this result was confirmed to be caused by the too thin oxide film of 1 μm or less. The surface hardness of the specimens treated under anodization and plasma anodization conditions were 230 and 620 HV, respectively. Therefore, the surface hardness of the sample subjected to anodic oxidation was 3 to 8 times higher than that of the AZ91D alloy material and the non-chromate treated specimen. The reason for the difference in surface microhardness of such specimens under the conditions of anodization and plasma anodization is that the conductivity of the electrolyte is different due to the concentration of the electrolyte. It is suspected that a difference in the density of the oxide film due to the release of the oxygen gas has occurred due to the growth rate of the oxide film generated at different voltage and current density differences therebetween.

Figure 6-7 shows the corrosion resistance of the samples with surface treatments in a 3 mol dm⁻³ NaCl solution as evaluated by EIS. As expected, the corrosion resistance of the plasma anodizing method was the best.

Figure 6-8 shows the results of a salt spray test carried out for 72 h in accordance with ASTM standards to evaluate the corrosion characteristics of AZ91D alloy specimens treated by non-chromate, anodization and plasma anodization. The experiment was carried out using a 5 wt% NaCl solution, and the temperature was maintained at 35 °C. Corrosion properties were quantified by evaluating the average grade number (RN). The RN value of the non-chromate and anodizing surface treatment method was 3.5–7, while the plasma anodizing surface treatment gave RN value of 9. These results coincide with the trends observed in EIS data (see Figure 6-7). The oxide film formed by plasma anodization

Chapter VI

generally has a three-layer structure, among which the intermediate layer is the densest and most important in corrosion resistance [Ref 5].

6.3 Conclusion

Mg, O, and P were detected in the non-chromate film, and Mg, O and Si were uniformly distributed in the anodizing process and the plasma anodization process. In addition, there were no pores in the non-chromated surface and the thickness of the oxide layer was less than 1 μm . The anodizing process and the plasma anodization process produced thicker oxide layer of 10–20 μm with some pores. The thermal barrier was the least for non-chromate films, and plasma anodizing gave the highest dielectric breakdown voltage. In the measurement of surface microhardness, the values of non-chromate were 80 HV, while anodizing and plasma anodizing increased the value to 230 and 620 HV, respectively. Based on this research, a surface treatment method that is optimized for a AZ91D can be selected.

Table 6-1. Comparison of surface treatment processes of AZ91D alloy materials.

Surface Treatment	Non-chromate Treatment	Anodizing	Plasma Anodizing
Process	Degreasing ↓ Activation ↓ Cleaning ↓ Etching ↓ Rinse ↓ Non-chromate	Degreasing ↓ Activation ↓ Cleaning ↓ Etching ↓ Rinse ↓ Anodizing	Degreasing ↓ Activation ↓ Plasma anodizing

Table 6-2. Comparison of characteristics of surface treatment process of AZ91D alloy materials.

Surface Treatment	Non-Chromate	Anodizing	Plasma Anodizing
Cell voltage (V)	-	20-80	120-300
Current density, $I/(A\ dm^{-2})$	-	<10	<30
Substrate Pretreatment	Critical	Critical	Less critical
Common electrolytes	Sulfuric acid. Phosphoric acid	Alkaline	Alkaline
Thickness, $d / \mu m$	~ 0.5	~ 10	~ 200
Adhesion to substrate	Moderate	Moderate	Very high
Temperature control	Critical	Critical	Less critical

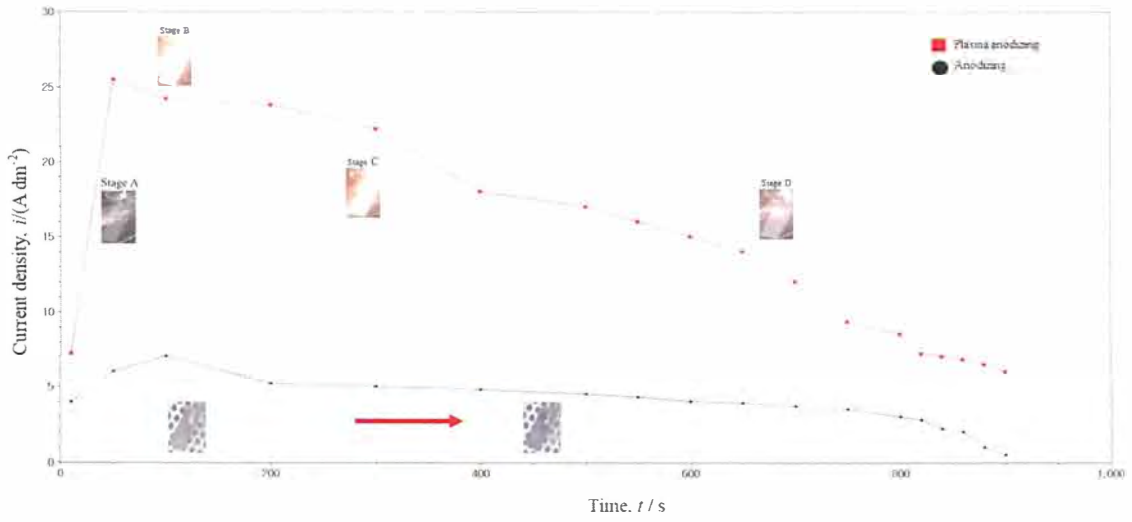


Figure 6-1. Typical variation of current density showing different stages of AZ91D surface treatment.

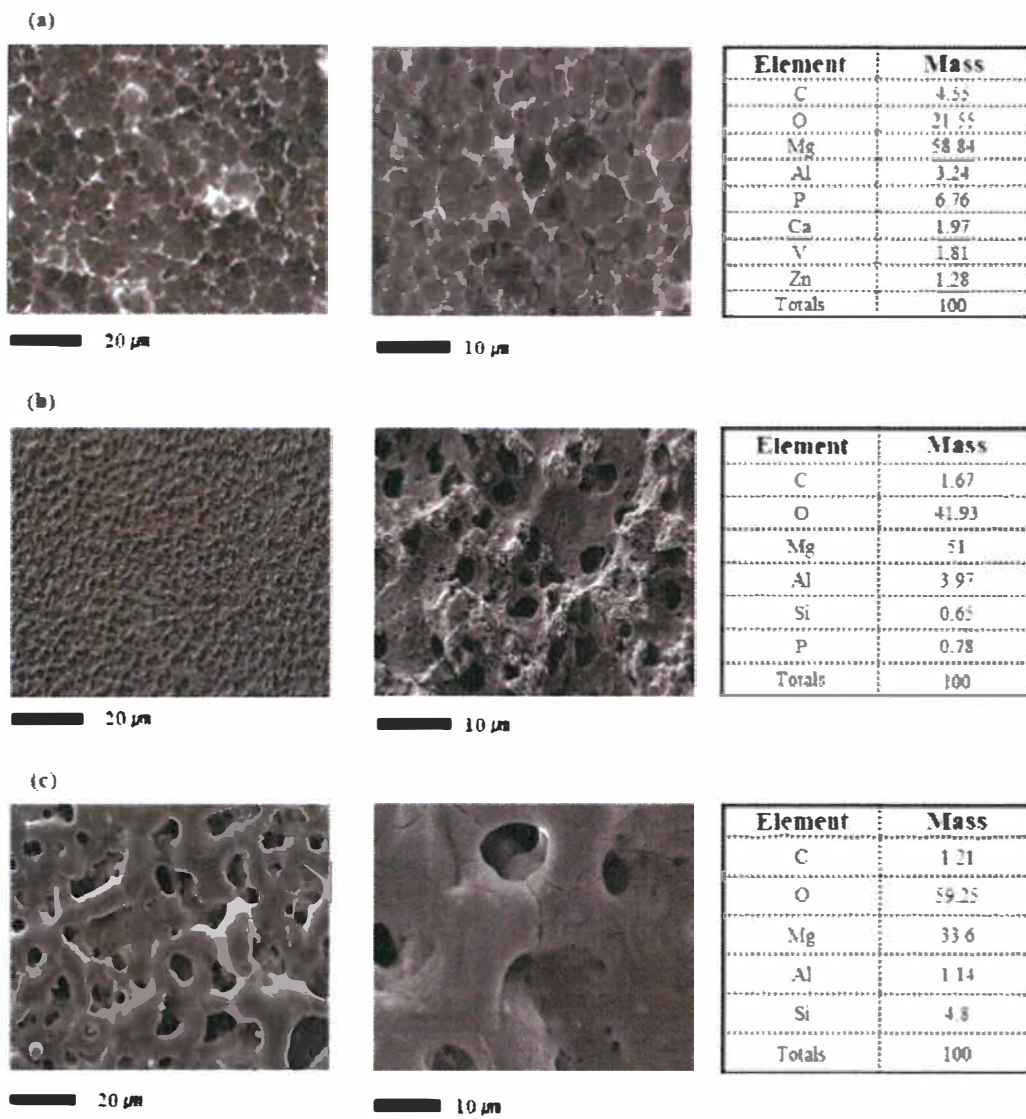


Figure 6-2. Surface morphologies and composition of AZ91D alloy materials after Non-chromate (b) Anodizing (c) Plasma anodizing.

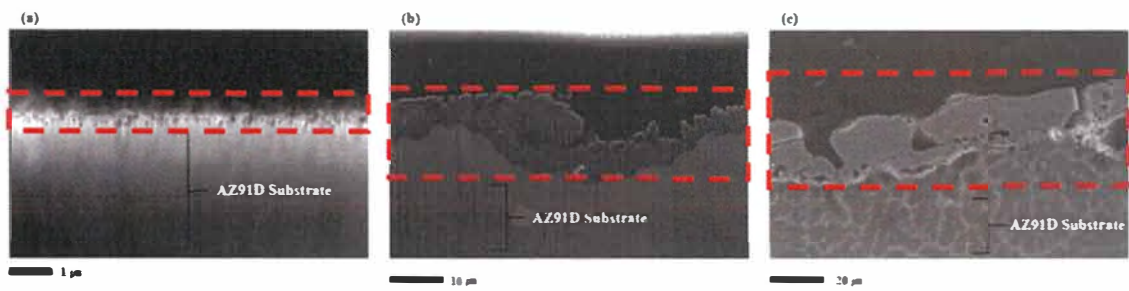


Figure 6-3. Cross sections of AZ91D alloy materials after Non-chromate (b) Anodizing (c) Plasma anodizing.

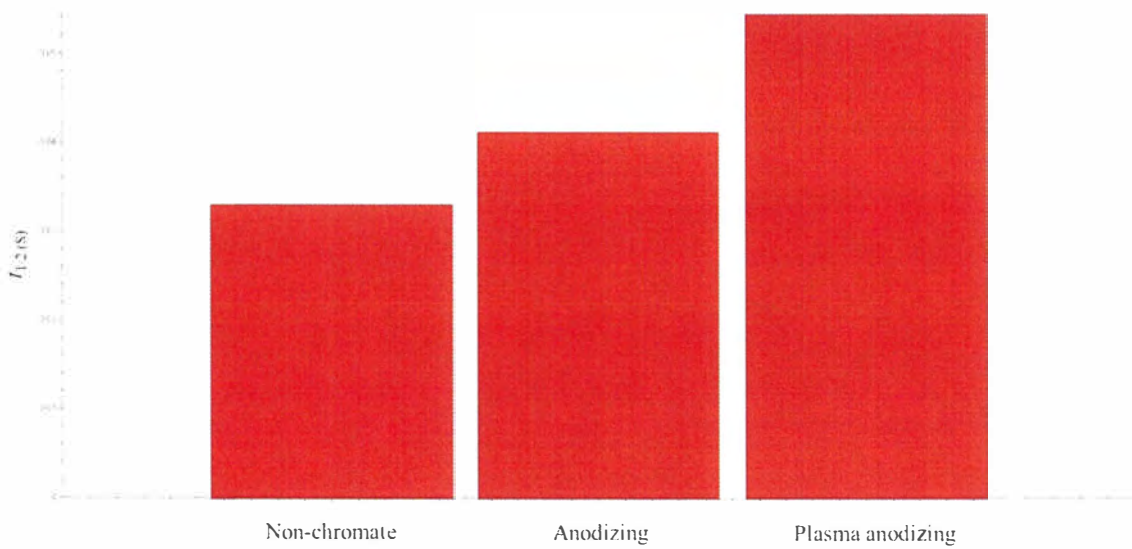


Figure 6-4. Effect of AZ91D alloy materials surface treatment method on the $t_{1/2}$ value in the laser flash test.

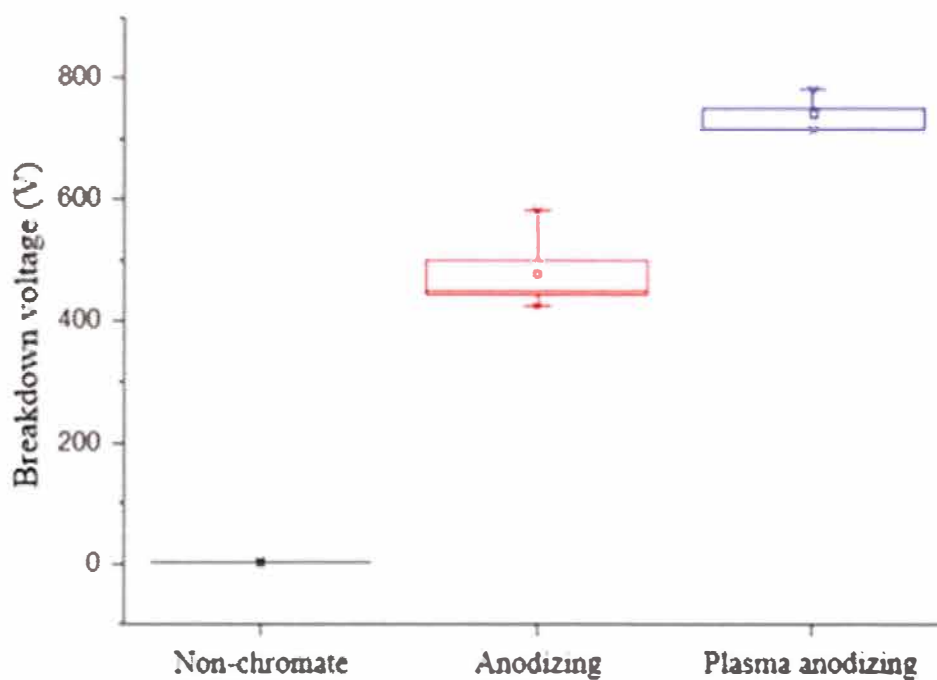


Figure 6-5. Effect of AZ91D alloy materials surface treatment method on breakdown voltage.

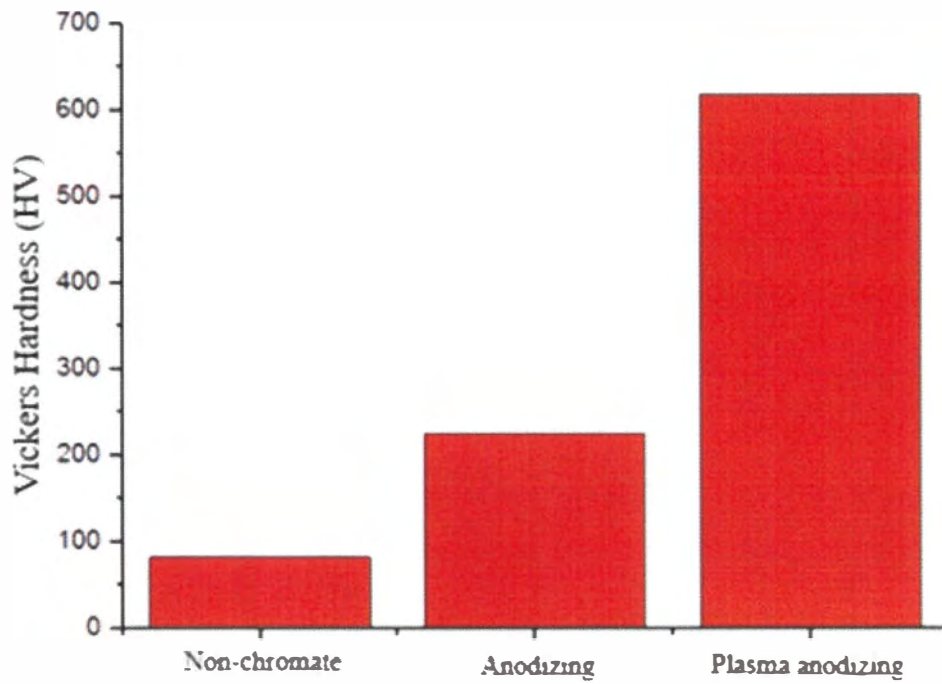


Figure 6-6. Effect of AZ91D alloy materials surface treatment method on the Vickers hardness.

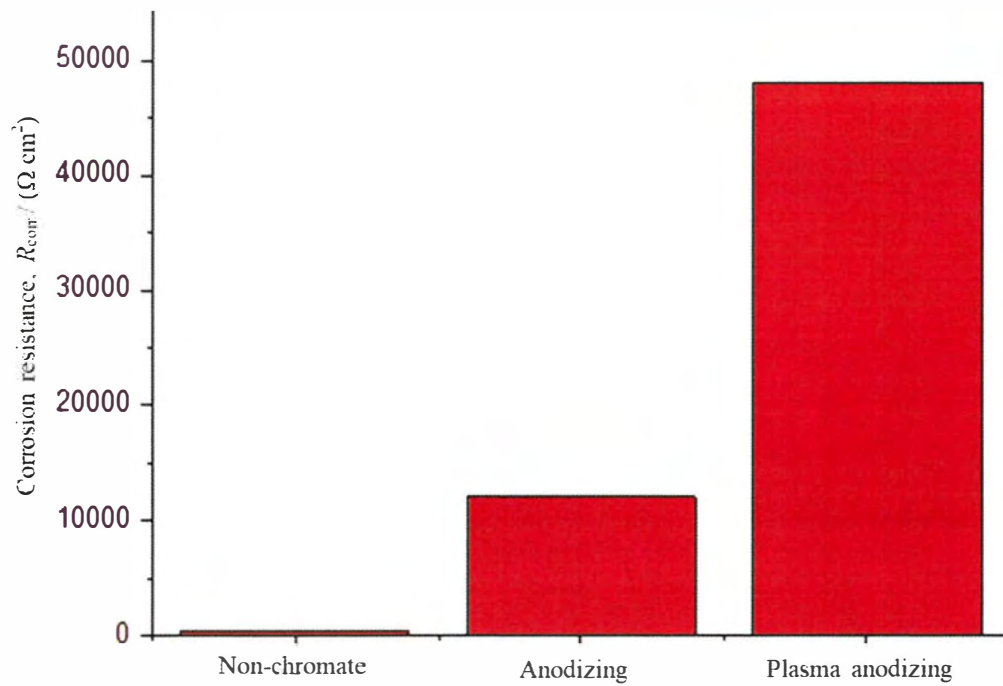


Figure 6-7. Effect of surface treatment method on the corrosion resistance of the treated AZ91D alloy materials. (solution: $3 \text{ mol dm}^{-3} \text{ NaCl}$, temperature: $25 \text{ }^\circ\text{C}$).



Surface Treatment	Non-chromate	Anodizing	Plasma Anodizing
72 h	 <p>RN 3.5</p>	 <p>RN 7</p>	<p>RN 9</p>

Figure 6-8. Surface images of the AZ91D alloy materials surface treatment method after the salt spray test (72 h).

6.4 References

1. MAKAR, G. L.; KRUGER, JI. *Corrosion of magnesium. International materials reviews*, **38.3** (1993) 138-153.
2. EMLEY, E. F. *Principles of Magnesium Technology Pergamon Press. New York, London*, 1966.
3. S.H. Lee, H. Yashiro and S.-Z. Kure-Chu, Electrolyte Temperature Dependence on the Properties of Plasma Anodized Oxide Films Formed on AZ91D Magnesium Alloy, *Korean Journal of Materials Research*, **29.5** (2019) 288-296.
4. Narayanan, T. S., Park, I. S., & Lee, M. H. *Progress in Materials Science*, **60** (2014) 1-71.
5. Y. Yan, Y. Han, D. Li, J. Huang, and Q. Lian, Effect of NaAlO₂ Concentrations on Microstructure and Corrosion Resistance of Al₂O₃/ZrO₂ Coatings Formed on Zirconium by Micro-arc Oxidation, *Appl. Surf. Sci.*, **256(21)** (2010) 6359-6366.

Chapter VII. General Conclusion

The interest in the structural applications of lightweight materials has increased significantly due to their importance in the environmental pollution and energy saving problems. The consumption of magnesium alloys has particularly increased in the automobile and electronic industries during the past decade due to their low density, high specific strength and recyclability. Even so, the application field of magnesium alloys has been rather limited because of their poor corrosion resistance. In recent years, the modification of alloy composition and heat treatments has been attempted to improve the corrosion resistance of magnesium alloys. However, there is a growing need for better surface treatment techniques for magnesium alloys in order to significantly improve the corrosion resistance which required in a wide range of applications. A number of surface treatment techniques such as electroplating, conversion coating, gas-phase deposition and anodizing have been developed to prevent the corrosion of magnesium alloys. Plasma anodization process is a relatively new surface treatment technique which offers a number of distinct advantages compared to other traditional process. In this study, plasma anodization process is introduced to AZ91D alloy to improve its corrosion resistance. Specific objectives are as follows: Firstly, a study on the structure of an oxide film formed by plasma anodizing treatment on AZ91D alloy. Second, a study on the chemical characteristics of the oxide film formed by the plasma anodizing treatment on the AZ91D alloy. Third, the physical properties of the oxide film formed by the plasma anodizing process on the AZ91D alloy. Fourth, a comparison of the effect of surface treatment method on AZ91D alloy. The important results obtained during the course of this work are summarized below.

Effect of power mode of plasma anodization on the properties of formed oxide films on AZ91D magnesium alloy

Effect of power condition for plasma anodization of AZ91D on the pore formation, surface roughness, and corrosion resistance were investigated. The layer thickness was found to increase linearly with voltage. The surface roughness, R_a , ranged from 0.2 μm to 0.3 μm , and the corrosion resistance increased from 3.5 to 9.5 in rating number (RN) as evaluated

according to the 72-h salt spray test. In the DC plasma anodization mode, the thickness of the electrolytic oxide film of the AZ91D alloy was uneven. In the pulse mode, the thickness was relatively uniform with formation of a three-layer structure. The pulse mode caused less roughness, uniform thickness and improved corrosion resistance. The change in power mode from DC to pulse at 150 V decreased the surface roughness (R_a) from 0.9 μm to 0.1 μm and increased the corrosion resistance in RN from 5 to 9.5. In the following experiments, pulsed voltage of 150 V was adopted as a power mode.

Corrosion Resistance of Plasma Anodized AZ91D magnesium Alloy

The dependence was studied of the thickness, composition, pore formation, surface roughness, and corrosion resistance of the formed films on temperature of the electrolyte in which anodization was performed. The higher electrolyte temperature resulted in the lower surface roughness, the smaller oxide film thickness, and the better corrosion resistance. More specifically, as the electrolyte temperature increased from 10 to 50 °C, the surface roughness (R_a) decreased from 0.7 to 0.15 μm , and the corrosion resistance increased from 3.5 to 9 in RN according to the salt spray test. The temperature increase from 10 to 50 °C also caused an increase in magnesium content in the film from 25 to 63 wt% and a decrease in oxygen from 66 to 21 wt%, indicating dehydration of the film. As the concentration of NaOH increased, from 0.06 M to 0.13 M and 0.25 M, the thickness of the oxide layer decreased, and the surface roughness (R_a) decreased from 0.52 to 0.08 and 0.06 μm . Corrosion resistance increased from (RN) 6 to 8 and 9. As the concentration of NaOH increased, the oxide of the magnesium component in the oxide film increased and the oxygen component decreased.

Physical Properties of Oxide Films on Mg Alloy Formed by Plasma Anodization

The higher the electrolyte temperature for the formation of oxide films by the plasma anodization, the lower the breakdown voltage, probably because the films formed at higher temperatures were thinner and denser. Moreover, an increase in electrolyte temperature played an important role on the physical properties of the films. As the electrolyte temperature increased from 20 to 50 °C, hardness of the oxide layer increased. The friction test against steel ball indicated that the wear scar became narrower for the films formed at higher temperatures because the films became harder as indicated by the Vickers

hardness. The thinner and denser nature of the oxide film formed at 50 °C would be also advantageous for heat transfer in use as a heat sink. A laser flash test showed faster heat transfer for AZ91D with plasma anodized oxide layer formed at higher temperatures.

Comparative Evaluation of the Surface Treatment Effect of AZ91D alloy material

The comparative evaluation among non-chromate, anodization and plasma anodization were conducted in respect of surface components, oxide thickness, heat diffusivity, dielectric breakdown voltage, hardness, and corrosion resistance. More specifically, the least thermal barrier of the formed layer is recognized in non-chromate, and the breakdown voltage and Vickers hardness are the highest in the case of plasma anodization. In the salt spray test, the corrosion resistance rating number is shown as 3.5 for the non-chromate test, 7 for the anodizing test, and 9 for the plasma anodizing test. Thus, the plasma anodization treatment has a remarkable advantage over conventional process.

ACKNOWLEDGEMENTS

I would like to express my whole-hearted gratitude to Prof. Hitoshi Yashiro and Prof. Song-Zhu Kure-Chu for their encouragement throughout this study.

I also thank to Prof. Tatsuya Takeguchi and Prof. Hidetoshi Hirahara for their kind reviewing my thesis.

I would also like to thank Mr. Tetsuya Fujimura and Mr. Shigeaki Kikuchi for their experimental support.

Last but not least, I convey my love and gratitude to my companion Shizuka, my beloved Sumin and Surim, Forest and my parents in Korea.